Initial characterization of mouse Syap1 in the nervous system: Search for interaction partners, effects of gene knockdown and knockout, and tissue distribution with focus on the adult brain

Erste Charakterisierung des Maus-Syap1 im Nervensystem: Suche nach Interaktionspartnern, Auswirkungen von Gen-Knockdown und-Knockout sowie Untersuchungen über die Verteilung im Gewebe mit Fokus auf das adulte Gehirn

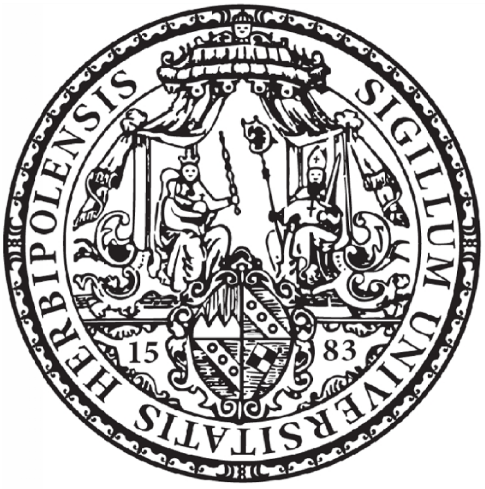

Doctoral thesis for a doctoral degree at the Institute for Clinical Neurobiology, University Hospital Wuerzburg and Graduate School of Life Sciences, Julius-Maximilian-University Wuerzburg

Section: Neuroscience

Submitted by

Dominique Schmitt

from

Lichtenfels

Wuerzburg, January 2017

Submitted on:…….

Members of the *Promotionskomitee:*

Chairperson:	Prof. Dr. Thomas Dandekar
Primary Supervisor:	Prof. Dr. Michael Sendtner
Supervisor (Second):	Prof. Dr. Erich Buchner
Supervisor (Third):	Prof. Dr. Markus Sauer

Date of Public Defence:……..

Date of Receipt of Certificates:……..

Table of contents

Table of contents ..... **III**
List of figures ..... **VI**
List of tables ..... **VIII**
Abbreviations ..... **IX**
Zusammenfassung **13**
Abstract **15**
1. Introduction **17**
1.1 Sap47 - the *Drosophila* homologue of mammalian Syap1 17
1.2 The mammalian synapse associated protein 1 18
1.3 Akt/Protein kinase B - a multifunctional cellular interface 19
1.4 TBCE and its important function in tubulin folding 21
1.5 Vesicular trafficking and protein sorting 23
1.6 The *Syap1* knockout mouse: Stem cell selection and mouse production 27
1.7 Aims of the thesis 29
2. Materials and Methods **30**
2.1 Materials 30
2.1.1 Animals 30
2.1.2 Cell lines: 30
2.1.3 Buffers and solutions 32
2.1.4 Suppliers for media, solutions and supplements 34
2.1.5 Kits 35
2.1.6 Antibodies 35
2.1.7 Programs 37
2.2 Methods 38
2.2.1 *Syap1* knockout mouse genotyping 38
2.2.2 DNA purification from agarose gel 39
2.2.3 DNA sequencing 39
2.2.4 RNA isolation 39
2.2.5 cDNA synthesis 40
2.2.6 RT-PCR 40
2.2.7 Production of *Syap1* knockdown and control lentiviruses 40
2.2.8 Protein extraction from mouse tissue 41
2.2.9 Protein isolation from mouse fat 42

2.2.10 Crude subcellular fractionation of NSC34 cells 42
2.2.11 Synaptic vesicle isolation 42
2.2.12 Immunocytochemistry 43
2.2.13 Immunohistochemistry of vibratome sections 44
2.2.14 Immunohistochemistry of neuromuscular junctions 45
2.2.15 SDS-polyacrylamide gel electrophoresis and Western blot analysis 45
2.2.16 Western blotting 47
2.2.17 Cell culture 47
2.2.18 Microtubule fractionation 50
2.2.19 Stimulation experiments 51
2.2.20 Brefeldin A treatment of cultured primary motoneurons 51
2.2.21 Co-immunoprecipitation 52
2.2.22 Protein cross-linking 53
2.2.23 Microscopy 53
2.2.24 Statistical analysis 53
3. Results 54
3.1 Syap1 antibody specificity test 54
3.1.1 Validation of antibody specificity for biochemical analysis 54
3.1.2 Validation of antibody specificity for immunofluorescence analysis 56
3.2 Subcellular localization of Syap1 protein 58
3.2.1 Syap1 accumulates in close proximity to organelles of the secretory pathway 58
3.2.2 Brefeldin A treatment disrupts Golgi association of Syap1 66
3.2.3 Syap1 is found in cytosolic and membranous fractions 68
3.2.3 Syap1 is present in axonal growth cones and synaptic vesicles 69
3.3 Syap1 protein is not restricted to synapses 73
3.4 Functional analysis of Syap1 protein 74
3.5 *Syap1* knockdown does not affect Akt phosphorylation in primary motoneurons 79
3.6 Possible interaction partners of Syap1 87
3.6.1 Possible interaction of Syap1 and TBCE protein 87
3.6.2 Possible interaction of Syap1 and Akt protein 91
3.7 Initial characterization of the first *Syap1* knockout mouse 93
3.7.1 Changing the genetic background 93
3.7.2 Establishment of a genotyping protocol 93
3.7.3 Phenotypic characterization of the *Syap1* knockout mouse 95
3.7.4 Syap1 protein distribution *in vivo* 98

3.8 Verification of *Syap1* knockdown data and functional analysis from isolated *Syap1*$^{-/-}$ motoneurons 116

3.8.1 Subcellular distribution of Syap1 protein in *Syap1*$^{-/-}$ motoneurons 116

3.8.2 Morphological and functional analysis of Syap1 protein in *Syap1*$^{-/-}$ cultured motoneurons 118

3.8.3 Akt-phosphorylation is not altered in *Syap1*$^{-/-}$ motoneurons and *in vivo* 120

4. Discussion 123

4.1 Generation of the first *Syap1* knockout mouse 123

4.2 Syap1 antibody specificity 124

4.3 Subcellular distribution of Syap1 *in vitro* 125

4.4 Syap1 expression 127

4.5 Syap1 distribution in the mouse nervous system 128

4.6 Syap1 and its interaction partners 129

4.7 Functional analysis 131

4.8 Conclusion 135

5. References 136

6. Appendix 150

6.1 Syap1 overexpression vector 150

6.2 Genotyping and qRT-PCR primer sequences 150

6.3 Nuclear/cytosolic fractionation of NSC34 cells 150

6.4 sh-Syap1 sequence BLAST 151

Affidavit/Eidesstattliche Erklärung 152

Curriculum vitae 153

Acknowledgements 155

List of figures

Figure 1: Proposed model of BSTA/Syap1 influencing Akt1 phosphorylation 19
Figure 2: Scheme of transport from the ER to the Golgi apparatus and associated membranes 24
Figure 3: Scheme of the targeted-mutation-1a allele (*Syap1*$^{tm1a(EUCOMM)Hmgu}$) and conditional strategies 28
Figure 4: Centrifugation protocol for crude synaptic vesicle isolation 43
Figure 5: Validation of Syap1 antibody specificity in Western blot analysis 55
Figure 6: Validation of antibody specificity for immunofluorescence 57
Figure 7: Co-stainings of Syap1 with GM130 in HEK293T cells 58
Figure 8: Co-stainings of Syap1 with GM130 in NSC34 cells 59
Figure 9: Co-stainings of Syap1 with acetylated tubulin/γ-adaptin and GM130 in motoneurons. 61
Figure 10: Co-stainings of Syap1 with COPI in motoneurons 63
Figure 11: Co-staining of Syap1 with COPI in motoneurons with high PMT voltage 64
Figure 12: Co-stainings of Syap1 with GM130 and TGN38 in motoneurons 65
Figure 13: Co-stainings of Syap1 with Calnexin and γ-adaptin in motoneurons 66
Figure 14: Localization of Syap1 protein after Golgi fragmentation 67
Figure 15: Crude subcellular fractionation of NSC34 cells 69
Figure 16: Syap1 is present in the axonal growth cone of motoneurons 70
Figure 17: Crude synaptic vesicle fractionation from mouse brain 71
Figure 18: Syap1 protein expression several mouse tissues 74
Figure 19: Functional effects of *Syap1* knockdown *in vitro* 75
Figure 20: Microtubule fractionation with cultured primary motoneurons 78
Figure 21: Akt phosphorylation kinetics in primary motoneurons 79
Figure 22: *Syap1* knockdown does not influence Akt phosphorylation at Ser^{473} and Thr^{308} in BDNF stimulated motoneurons 81
Figure 23: *Syap1* knockdown does not influence Akt phosphorylation at Ser^{473} and Thr^{308} in motoneurons 82
Figure 24: Compartment specific Akt phosphorylation in motoneurons after BDNF stimulation 84
Figure 25: Compartment specific Akt phosphorylation in motoneurons without stimulation 86
Figure 26: Co-immunoprecipitations testing for an interaction of Syap1 and TBCE 89
Figure 27: Co-immunoprecipitations for analysis of a possible Syap1-Akt interaction 92
Figure 28: Localization of *Syap1* genotyping primers 94
Figure 30: Example of a genotyping result 95
Figure 29: Gradient PCR 94

Figure 31: Pictures of *Syap1* wild type and *Syap1* knockout littermates 96
Figure 32: Verification of *Syap1* knockout by qRT-PCR and Western blot analysis. 97
Figure 33: Antibody specificity and *Syap1* knockout confirmation 98
Figure 34: Overview of Syap1 protein distribution in the mouse cerebrum and cerebellum ... 99
Figure 35: Syap1 antibody specificity exemplified in cortical brain sections 101
Figure 36: Syap1 distribution in the olfactory bulb 102
Figure 37: Syap1 distribution in the thalamus 104
Figure 38: Syap1 seems to be rarely expressed in astrocytes and other non-neuronal cells of the thalamus 106
Figure 39: Syap1 distribution in the hippocampus 108
Figure 40: Syap1 distribution in the cerebellum 110
Figure 41: Syap1 and vGlut1 overlap in the cerebellum 111
Figure 42: Syap1 distribution in the spinal cord 113
Figure 43: Syap1 localization at neuromuscular junctions 114
Figure 44: *Syap1* knockout does not influence the Golgi morphology 115
Figure 45: Syap1 distribution in wild type and *Syap1* knockout motoneurons 117
Figure 46: Influence of Syap1 on survival, axon length, dendritic outgrowth and soma size . 119
Figure 47: *Syap1* knockout does not decrease total Akt phosphorylation at Ser^{473} and Thr^{308} 120
Figure 48: Akt^{Ser473} phosphorylation *in vivo* seems not to be affected by *Syap1* knockout 122
Figure 49: FLAG-Syap1 pGJ3 overexpression vector 150
Figure 50: Crude nuclear/cytosolic fractionation of NSC34 cells 150
Figure 51: Nucleotide BLAST of sh-Syap1 sequence 151

List of tables

Table 1: Buffers and solutions 34
Table 2: Primary antibodies 36
Table 3: Secondary antibodies 37
Table 4: PCR protocol for *Syap1* knockout mouse line genotyping 38
Table 5: Composition of resolving gels 46
Table 6: Composition of the stacking gel 46
Table 7: Frequencies of offspring genotypes 96
Table 8: Genotyping and qRT-PCR primer sequences 150

Abbreviations

%	Percent
°C	Degree Celcius
aa	Amino acid
Akt/PKB	Akt kinase / protein kinase B
ALS	Amyotrophic lateral sclerosis
AP-1	Adaptor protein 1
APS	Ammonium peroxodisulfate
ARF	ADP-ribosylation factor
ATP	Adenosine 5'-triphosphate
BCA	Bicinchoninic acid assay
BDNF	Brain derived neurotrophic factor
BFA	Brefeldin A
bp	Base pair
BSA	Bovine serum albumin
BTX	Bungarotoxin
CCT	Cytosolic chaperonin containing TCP-1
CNTF	Ciliary neurotrophic factor
COP	Coat protein
DAPI	4',6-diamidino-2-phenylindole dihydrochloride
ddH_2O	Double-distilled water
DIV	Days *in vitro*
DMEM	Dulbecco's modified essential medium
DMSO	Dimethyl sulfoxide
DNA	Deoxyribonucleic acid
dNTP	Deoxynucleotide triphosphate
DTT	Dithiothreitol
E	Eluate
E13.5/14	Embryonic day 13.5/14
EAAT2	Excitatory amino acid transporter 2
ECL	Enhanced chemiluminescence
EDTA	Ethylene-diamin-tetraacetic acid

EGF	Epidermal growth factor
EGTA	Ethylene-glycol-tetraacetic acid
ER	Endoplasmic reticulum
ERES	ER-exit sites
Ergic	ER-Golgi intermediate compartment
FCS	Fetal calf serum
g	Gram
GAPDH	Glyceraldehyde-3-phosphate-dehydrogenase
GDP	Guanosine diphosphate
GEF	Guanine exchange factor
GFAP	Glial fibrillary acidic protein
GFP	Green fluorescent protein
GM130	Golgi matrix protein of 130 kDa
GTP	Guanosine-5'-triphosphate
HBSS	Hanks' balanced salt solution
HEK	Human embryonic kidney
HRD	Hypoparathyroidism-retardation-dysmorphism syndrome
HRP	Horseradish peroxidase
HS	Horse serum
I	Input
IC	Immunocytochemistry
IF	Immunofluorescence
IP	Immunoprecipitation
IP3	Inositol 1,4,5-trisphosphate
kDa	Kilodalton
KO	Knockout
L	Liter
M	Molar
mA	Milliampere
MAB	Monoclonal antibody
mM	Millimolar
mRNA	messenger ribonucleic acid

MT	Microtubule
MTOC	Microtubule organizing center
mV	Millivolt
NB medium	Neurobasal medium
NeuN	Neuronal nuclear protein
NP40	Nonident P-40
PAGE	Polyacrylamide gel electrophoresis
PBS	Phosphate buffered saline
PCR	Polymerase chain reaction
PFA	Paraformaldehyde
pH	pH-value
PH	Pleckstrin homology
PI3K	Phosphatidylinositol 3-kinase
PIP2	Phosphatidylinositol 4,5-bisphosphate
pmn	Progressive motor neuronopathy
PMT	Photomultiplier tube
PORN	Poly-DL-ornithine
rcf	Relative centrifugal force (multiples of "g")
RIPA buffer	Radioimmunoprecipitation assay buffer
RNA	Ribonucleic acid
RNAi	Ribonucleic acid interference
RT	Room temperature
S	Supernatant
SAP47	Synapse-associated protein of 47 kDa
SAR1	Secretion-associated and RAS-related protein 1
SDS	Sodium dodecyl sulfate
SDS-PAGE	Sodium dodecyl sulfate-polyacrylamide-gel-electrophoresis
SEM	Standard error of the mean
sh	Short-hairpin
SIM	Structured illumination microscopy
Syap1	Synapse-associated protein 1
TAE	Tris acetate EDTA

TBC A-E	Tubulin-specific chaperone A-E
TBST	Tris-buffered saline Tween-20
TEMED	N, N, N', N'-tetramethylethylenediamine
TGN	*trans*-Golgi network
Tris	Tris (hydroxymethyl)-aminomethan
TTL	Tubulin tyrosine ligase
VTC	Vesicular and tubular shaped clusters
WB	Western blot
Wt	Wild type
µg	Microgram

Zusammenfassung

Das Synapsen-assoziierte Protein von 47 kDa (Sap47) in *Drosophila melanogaster* ist das Gründungsmitglied einer phylogenetisch konservierten Proteinfamilie von unbekannter molekularer Funktion. Sap47 ist im gesamten Neuropil des adulten und larvalen Gehirns lokalisiert und mit glutamatergen, präsynaptischen Vesikeln in larvalen Motoneuronen assoziiert. Fliegen, denen das Protein fehlt, sind lebensfähig und fruchtbar und weisen keine schwerwiegenden strukturellen oder ausgeprägten verhaltensbezogenen Defizite auf, was darauf hinweist, dass Sap47 für eine basale synaptische Funktion entbehrlich ist beziehungsweise das Fehlen seiner Funktion durch andere, eventuell verwandte Proteine, kompensiert werden kann.

Über Syap1 - das Säugetierhomolog von Sap47 - wurde berichtet, dass es in verschiedenen nicht-neuronalen Zellen eine essentielle Rolle in der Akt1 Phosphorylierung spielt, indem es die Assoziation von mTORC2 und Akt1 begünstigt, welche für den nachgeschalteten Signalweg bei der Adipogenese essentiell ist. Die Funktion von Syap1 im Vertebraten-Nervensystem ist dagegen bislang unbekannt.

Die vorliegende Studie liefert die Erstbeschreibung von neuronalem Syap1 über die subzelluläre Lokalisation des Proteins in kultivierten Motoneuronen sowie die Verteilung in ausgewählten Strukturen des adulten Nervensystems der Maus und beschreibt initiale funktionelle Experimente. Allen beschreibenden Experimenten voran, wurden kommerziell erhältliche Syap1 Antikörper auf ihre Spezifität und Tauglichkeit für diese Studie getestet. Einer der Antikörper, der gegen das humane Protein hergestellt wurde, erkennt spezifisch sowohl das humane, als auch das murine Syap1 Protein und stellt somit ein unentbehrliches Werkzeug für alle biochemischen, immunzytochemischen und immunhistochemischen Untersuchungen dar.

Im Zuge der Arbeit wurde eine *Syap1*-Knockout Maus untersucht, welche vital und fruchtbar ist und keine offensichtlichen Veränderungen in ihrem morphologischen Phänotyp aufweist. Wie auch Sap47 in Fliegen, ist Syap1 im synaptischen Neuropil weit verbreitet, insbesondere in Regionen, die reich an glutamatergen Synapsen sind, aber es wurde auch in einer deutlichen, Golgi-assoziierten Akkumulation in bestimmten Gruppen neuronaler Zellkörper

beobachtet. In Motoneuronen wurde das Protein besonders in ähnlichen perinukleären Strukturen detektiert, welche zum Teil mit Golgi Markern überlappen und zudem in Axonen, Dendriten und Wachstumskegeln detektiert. Wie biochemische und immunhistochemische Untersuchungen ergaben, zeigt das Syap1 Protein eine weit verbreitete Expression im zentralen Nervensystem mit Regionen-spezifischem Verteilungsmuster wie es beispielsweise im Kleinhirn, dem Hippocampus oder dem olfaktorischen Bulbus beobachtet wurde. Neben der Expression in Neuronen wurde Syap1 auch in nicht neuronalen Geweben wie der Leber, Niere und im Muskel detektiert. Nicht-neuronalen Zellen im Gehirn fehlte dagegen die typische perinukleäre Akkumulation in immunhistochemischen Färbungen. Erste funktionelle Studien mit kultivierten primären Motoneuronen über entwicklungsbezogene, strukturelle und funktionelle Gesichtspunkte ergaben keinen Einfluss einer *Syap1* Depletion auf das Überleben oder morphologische Merkmale wie Axon- oder Dendritenlänge. Entgegen den Erwartungen, wurde nach *Syap1* Knockdown oder Knockout in neuronalem Gewebe oder kultivierten Motoneuronen keine Reduktion in der Akt1 Phosphorylierung an Ser^{473} oder Thr^{308} detektiert.

Abstract

The **s**ynapse-**a**ssociated **p**rotein of 47 kDa (Sap47) in *Drosophila melanogaster* is the founding member of a phylogenetically conserved protein family of hitherto unknown molecular function. Sap47 is localized throughout the entire neuropil of adult and larval brains and closely associated with glutamatergic presynaptic vesicles of larval motoneurons. Flies lacking the protein are viable and fertile and do not exhibit gross structural or marked behavioral deficiencies indicating that Sap47 is dispensable for basic synaptic function, or that its function is compensated by other related proteins.

Syap1 - the mammalian homologue of Sap47 - was reported to play an essential role in Akt1 phosphorylation in various non-neuronal cells by promoting the association of mTORC2 with Akt1 which is critical for the downstream signaling cascade for adipogenesis. The function of Syap1 in the vertebrate nervous system, however, is unknown so far.

The present study provides a first description of the subcellular localization of mouse Syap1 in cultured motoneurons as well as in selected structures of the adult mouse nervous system and reports initial functional experiments. Preceding all descriptive experiments, commercially available Syap1 antibodies were tested for their specificity and suitability for this study. One antibody raised against the human protein was found to recognize specifically both the human and murine Syap1 protein, providing an indispensable tool for biochemical, immunocytochemical and immunohistochemical studies.

In the course of this work, a *Syap1* knockout mouse was established and investigated. These mice are viable and fertile and do not show obvious changes in morphology or phenotype. As observed for Sap47 in flies, Syap1 is widely distributed in the synaptic neuropil, particularly in regions rich in glutamatergic synapses but it was also detected at perinuclear Golgi-associated sites in certain groups of neuronal somata. In motoneurons the protein is especially observed in similar perinuclear structures, partially overlapping with Golgi markers and in axons, dendrites and axonal growth cones. Biochemical and immunohistochemical analyses showed widespread Syap1 expression in the central nervous system with regionally distinct distribution patterns in cerebellum, hippocampus or olfactory bulb. Besides its expression in

neurons, Syap1 is also detected in non-neuronal tissue e.g. liver, kidney and muscle tissue. In contrast, non-neuronal cells in the brain lack the typical perinuclear accumulation.

First functional studies with cultured primary motoneurons on developmental, structural and functional aspects reveal no influence of *Syap1* depletion on survival and morphological features such as axon length or dendritic length. Contrary to expectations, in neuronal tissues or cultured motoneurons a reduction of Akt phosphorylation at Ser^{473} or Thr^{308} was not detected after *Syap1* knockdown or knockout.

1. Introduction

1.1 Sap47 - the *Drosophila* homologue of mammalian Syap1

The **S**ynapse **a**ssociated **p**rotein of **47** kDa gene (Sap47) was initially identified and characterized in 1995 by screening a *Drosophila* cDNA expression library with the monoclonal antibody nc46 (MAB nc46). In immunohistochemical preparations this antibody selectively labels most but not all of the synaptic terminals of the *Drosophila* nervous system (Reichmuth et al. 1995; Hofbauer et al. 2009). Electron micrographs of immunogold labeled Sap47 revealed that the protein is concentrated in synaptic boutons in close proximity to synaptic vesicles in *Drosophila* neurons (Saumweber et al. 2011). When homogenates from fly brain are analyzed by Western blot, the antibody recognizes a protein of 47 kDa but also cross-reacts with proteins of similar size from other insects or species indicating evolutionary conservation (Reichmuth et al. 1995). Indeed, various genome projects found homologues in insects, frogs, fish, and mammals (Doerks et al. 2002). The gene is located in 89A8-B3 region on chromosome 3R, coding for ten annotated polypeptides produced by alternative splicing (annotation symbol: CG8884; flybase.org). Sap47 is a member of a protein family containing the BSD domain which was first described in Doerks et al. (2002) and is present in functionally diverse proteins like **B**TF2 transcription factors, **s**ynapse associated proteins and **D**OS2-like proteins. The domain is about 60 amino acids in length and predicted to form three α-helices. Although the BSD domain is also found in various species and therefore assumedly being important, only one role in protein-protein interaction is suggested so far by Yao et al. (2013).

To obtain first indications on the function of the Sap47 protein, knockout flies were generated. Those null mutants were viable and fertile showing no gross structural or behavioral deficits, and therefore Sap47 is unlikely to have an essential basic synaptic function (Funk et al. 2004). The results achieved by Saumweber et al. (2011) indicate an involvement of Sap47 in short term synaptic plasticity at neuromuscular junctions by patch clamp current recordings during high frequency stimulation. Furthermore, at the behavioral level Sap47 null mutant larvae exhibit a defect in learning and memorizing the association of an odorant with

a rewarding tastant (Saumweber et al. 2011). Very recently, Kleber et al. (2016) reported for *Drosophila* larvae up-regulated Synapsin phosphorylation upon the lack of Sap47. However, although the lack of either Sap47 or Synapsin results in defects in the associative learning, no additive effect was observed in Synapsin/Sap47 double mutant larvae. This suggests a functional interdependence of Synapsin and Sap47 (Kleber et al. 2016).

1.2 The mammalian synapse associated protein 1

Little information about Syap1 protein is available in the literature so far. In mouse, the Syap1 gene maps to the X-chromosome coding for two predicted transcripts; of these only one is known to be protein coding (2,087 bp, 365 aa), whereas the other one retaining an intron (720 bp), is not (ensemble ENSMUSG00000031357).

Similarly, the human *Syap1* gene, located also on the X-chromosome, is predicted to result in two transcripts of which only one is coding for a 352 amino acid long protein (ensemble ENST00000380155). Human and murine Syap1 protein - similar as their homologue in *Drosophila melanogaster* - contain the BSD-domain as well (Doerks et al. 2002).

Chang et al. (2001) detected *Syap1* mRNA in most human tissues and report a down-regulation in the mRNA expression in human hepatocellular carcinoma. Furthermore, Syap1 is thought to be differentially regulated by tamoxifen in human breast cancer cells (Al-Dhaheri et al. 2006). Recently, Syap1/BSTA (**B**SD domain-containing **s**ignal **t**ransducer and **A**kt interactor) was described to play a crucial role in context of adipocyte differentiation from embryonic stem cells by promoting Akt1 phosphorylation at Serine^{473} via mTORC2-mediation upon stimulation (Figure 1, left side).

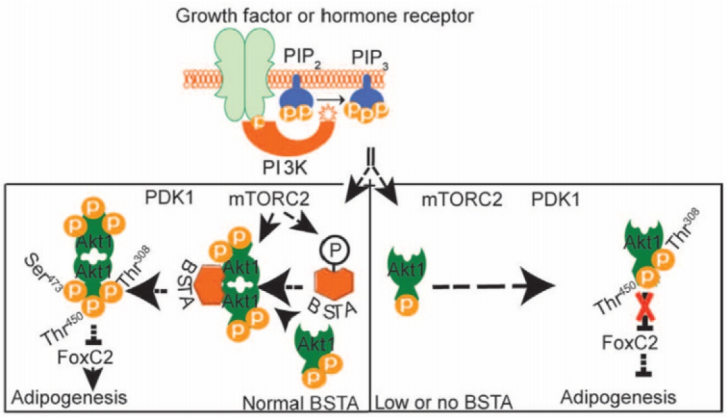

Figure 1: Proposed model of BSTA/Syap1 influencing Akt1 phosphorylation

The scheme shows the model hypothesized by Yao et al. (2013) of Syap1 function in growth factor-induced Akt1 phosphorylation at Ser^{473} via mTORC2-mediation in the context of adipocyte differentiation. When normal levels of Syap1 protein are available, the interaction of Syap1 with Akt1 – triggered by mTORC2 – accomplishes the phosphorylation of the kinase at Ser^{473} which then in turn activates a downstream signaling cascade promoting adipogenesis (left side). When Syap1 is depleted Akt1 phosphorylation is reduced leading to an inhibition (right side) of adipocyte differentiation (Yao et al. 2013).

This stimulation then results in a suppression of the FoxC2 transcription factor gene resulting in the activation of downstream signaling cascades which promote adipogenesis (Figure 1, left side). This study further showed that the Akt/Syap1 interaction in dividing cells is accomplished by the BSD domain requiring a preceding interaction between the mTORC2 complex and Syap1 in which Syap1 itself is phosphorylated (Yao et al. 2013). This is so far the first reported function of the mammalian Syap1 protein.

1.3 Akt/Protein kinase B - a multifunctional cellular interface

Akt kinases represent a central signaling node regulating many cellular functions such as cell survival, proliferation, metabolism and cellular growth responses (Manning and Cantley 2007). This family of kinases comprises three highly conserved isoforms Akt1, Akt2 and Akt3 (also referred to as PKAα, β and γ, respectively) all of which are functional (Brodbeck et al. 1999; Cheng et al. 1992; Jones et al. 1991). Although the three Akt isoforms are encoded by separate genes, they possess a conserved structure consisting of an N-terminal pleckstrin homology (PH) domain, attached to a central catalytic domain and a C-terminal regulatory domain (Auguin et al. 2004; Thomas et al. 2001; Milburn et al. 2003).

Accumulating evidence gained over the last few years of research demonstrates the existence of isoform-specific regulation considering the unique localization and function of each Akt

isoform. With isoform specific Akt antibodies, Santi and Lee (2010) determined the subcellular distribution of Akt1, 2 and 3. In MDA-MB231 cells Akt1 and Akt2 were mainly found in the cytoplasm whereas Akt2 also showed a clustered punctate staining pattern in the perinuclear region. By contrast, Akt3 was predominantly observed in the nucleus and nuclear membrane. These findings were largely consistent in several other cell lines (e.g. HeLa, HepG2, LNCaP, MCF-7) except in HEK293T (human embryonic kidney 293) cells. There, Akt1 was found to spread throughout the entire cell while Akt2 and 3 were dominantly observed in the nucleus. Nevertheless, solely the presence of T-antigen in this human embryonic cell line seemed to change the subcellular distribution of Akt1 which was then restricted to the cytoplasm.

Based on *in vivo* and *in vitro* data obtained from transgenic mouse models or cell studies using various knockout combinations of Akt isoforms it was demonstrated that the three Akt isoforms are functionally not redundant (Toker and Marmiroli 2014; Toker 2012; Gonzalez and McGraw 2009; Irie et al. 2005; Stambolic and Woodgett 2006). Thus, for instance, Akt1 and Akt2 which are the predominant isoforms in most cell types, are reported to regulate growth/survival (Chen et al. 2001; Cho et al. 2001b) and insulin-dependent metabolic signaling (Cho et al. 2001a; Garofalo et al. 2003). Akt3 by contrast, is mainly expressed in brain and testes and at lower levels in adipose tissue, mammal gland, lung and skeletal muscle (Brodbeck et al. 1999; Dummler and Hemmings 2007). Akt3 genetic ablation experiments show that this isoform seems to be of particular importance for neuronal and brain development since the deletion results in smaller brain size (Tschopp et al. 2005; Easton et al. 2005).

The Akt signaling pathway is activated by extracellular effectors like growth factors or cytokines. Upon binding to the respective transmembrane receptor including tyrosine kinase or G-protein coupled receptors, PI3K (phosphatidylinositol 3-kinase) - the major downstream effector - is recruited to the plasma membrane binding to the activated receptor. Once activated, PI3K phosphorylates the membrane phospholipid phosphatidylinositol (4,5)-diphosphate (PIP_2) and thereby generating phosphatidylinositol (3,4,5)- triphosphate (PIP_3). PIP_3 accumulation in turn promotes the translocation of the pleckstrin homology domain

containing proteins Akt and phosphoinositide-dependent kinase 1 (PDK1) to the membrane. This results in the phosphorylation of the activation loop of Akt at Thr^{308}. Maximal activity is achieved by an additional phosphorylation at Ser^{473} in the regulator domain via mTORC2 (Alessi et al. 1996; Anderson et al. 1998; Sarbassov et al. 2005; Jacinto et al. 2006). Upon full activation Akt isoforms exert their functions by phosphorylation of a wide array of downstream targets at different subcellular compartments reviewed by Manning and Cantley (2007). Akt for example is very well known for its role in regulating apoptosis either directly by phosphorylation of proteins regulating the cell cycle (Datta et al. 1997; Qi et al. 2006) or indirectly via phosphorylation of transcription factors (Brunet et al. 1999; Kane et al. 1999; Romashkova and Makarov 1999; Zhou et al. 2015). Besides this function, PI3K/Akt signaling was also reported to be implicated in neuronal differentiation (Park et al. 2012) and the regulation of neurite outgrowth, including branching, elongation and caliber control (reviewed by Read and Gorman 2009). There are further indications that Akt is also involved in synaptogenesis (Znamensky et al. 2003; Akama and McEwen 2003) and synaptic transmission (Wang et al. 2003).

1.4 TBCE and its important function in tubulin folding

Besides TBCE, prefoldin, the cytosolic chaperonin (CCT) and four other conserved chaperones TBC A-D are participating in the process leading to polymerizable tubulin heterodimers (Tian et al. 1996; Tian et al. 1997). After translation, the nascent, unfolded α- and β-polypeptide chains are directly captured by the chaperone prefoldin and subsequently transferred the cytosolic chaperonin (Lewis et al. 1996). Via ATP-hydrolysis chaperonin then facilitates a proper formation of the tertiary structure of α- and β-tubulin subunits (Gao et al. 1992; Gao et al. 1993). The β- and α-monomers are then bound by the tubulin-specific co-factors A and B, respectively, and forwarded to the co-factors D and E. Correctly folded and stabilized tubulin subunits are joined together by a complex formation of TBCE/α-tubulin and TBCD/β-tubulin. In the presence of TBCC, GTP-hydrolysis by β-tubulin forms a GDP α-β-tubulin dimer, which is finally released (Lewis et al. 1997). The newly synthesized heterodimers are assembled end to end forming a linear protofilament. 13 of such

protofilaments associate laterally to build a non-covalent cylindrical polymer of 24 nm diameter.

Since microtubules represent one of three filamentous structures indispensible for cellular cytoskeleton stability and function, small disturbances in their assembly can have tremendous consequences as observed for TBCE. A point mutation in this gene leads to an exchange of the amino acid tryptophan to glycine at the C-terminus of TBCE (Bommel et al. 2002; Martin et al. 2002). This mutation was first found in 1988 in the *pmn* (progressive motor neuronopathy) mouse mutant in a colony of NMRI mice at the Animal Department of the Panum Institute in Copenhagen (Schmalbruch et al. 1991).

In cultured primary motoneurons isolated from *pmn*-mutant mouse it was observed that the mutation does not affect the survival but disrupts axon elongation. *Pmn*-mutant motoneurons show a characteristic phenotype; they exhibit shorter axons and an increased number of axonal swellings (Bommel et al. 2002). Further investigations from Schaefer et al. (2007) show, that TBCE is a peripheral membrane-associated protein accumulating at the Golgi apparatus. In *pmn* mice, the chaperone is destabilized and lost from this organelle showing highly decreased protein levels in spinal cord compared to wild type. The ensuing reduction in tubulin levels and distal microtubule densities results from axonal microtubule loss progressing from distal to proximal leading to axonal degeneration in a "dying-back" mechanism. Furthermore, when TBCE protein levels were depleted in NSC34 cells, increased amounts of soluble α-tubulin and reduced amounts of precipitable α-tubulin were observed (Schaefer et al. 2007).

Recent results from Bellouze et al. (2014) suggest an ARF1/TBCE cross-talk organizing COPI vesicle formation as well as nucleation and polymerization of Golgi-derived microtubules (MTs). The authors observed that in the absence of TBCE these Golgi-derived MTs are lost, β-COP is degraded and membrane-recruitment of the tethers p115/GM130 is decreased. As a consequence of COP-vesicle subunit degradation, the function of the ER-Golgi intermediate compartment (ERGIC) representing the target of COPII-derived vesicles is disturbed and the Golgi starts to fragment. TBCE is recruited to the Golgi membrane by membrane-bound active ARF1 catalyzing COP1 coat assembly where it drives MT formation and

polymerization. These MTs are then hypothesized to stabilize the COPI coatomer by interacting with the β-subunit.

Other mutations in the gene coding for human *Tbce* cause several rare and severe disorders like the hypoparathyroidism-retardation-dysmorphism syndrome (HRD) and Kenny-Caffey syndrome, indicating the crucial role of the protein (Richardson and Kirk 1990; Parvari et al. 2002). The diseases are characterized by dysmorphic features, growth retardation, abnormalities of the extremities, hypothyroidism and mental retardation (Lee et al. 1983; Sabry et al. 1998; Parvari et al. 2007). Due to a 12 bp deletion in *Tbce* gene, the protein lacks four amino acids in the N-terminal CAP-Gly domain which is important for α-tubulin binding. This causes decreased microtubule density at the microtubule organizing center (MTOC), disturbed MT polarity and lower amounts of precipitable MTs while total tubulin levels remain unaltered (Parvari et al. 2002). Strikingly, a disruption of MTs was also observed upon overexpression of TBCE (Bhamidipati et al. 2000; Sellin et al. 2008; Tian et al. 2006) indicating that both – loss and overexpression of TBCE – negatively affects the MT network (Jin et al. 2009).

1.5 Vesicular trafficking and protein sorting

Mechanisms of cellular trafficking are crucial for all living cells in order to maintain homeostasis and to respond to extra- and intracellular signals. The intracellular traffic of vesicular packages is often accomplished by cytoskeletal-based molecular motors travelling along the intracellular cytoskeletal networks.

Via the dynamic secretory pathway, newly synthesized proteins are transported through the endoplasmic reticulum (ER) and the Golgi apparatus where they are processed (by enzymatic modification and proteolytic cleavage) and sorted to their final destination, the plasma membrane, extracellular space and endosomal/lysosomal subcellular compartments (Bonifacino and Glick 2004). Proteins destined for secretion, processing, or intracellular compartments leave the ER by membrane bound carriers budding from specialized ER exit sites (ERES; Figure 2), a process which is mainly controlled by vesicular coat proteins. The vesicles carry a coat protein complex II (COPII) operating the anterograde transport

(Farquhar and Hauri 1997; Barlowe et al. 1994; Barlowe 2003; Bannykh et al. 1996) to the ER-Golgi intermediate compartment (ERGIC) where the COPII coat is replaced by a second type of coat - the COPI coat (Scales et al. 1997; Stephens et al. 2000; Aridor et al. 1995). COPI vesicles then travel along microtubule tracks to the *cis*-Golgi cisternae with which they fuse (Scales et al. 1997; Presley et al. 1997; Blum et al. 1999).

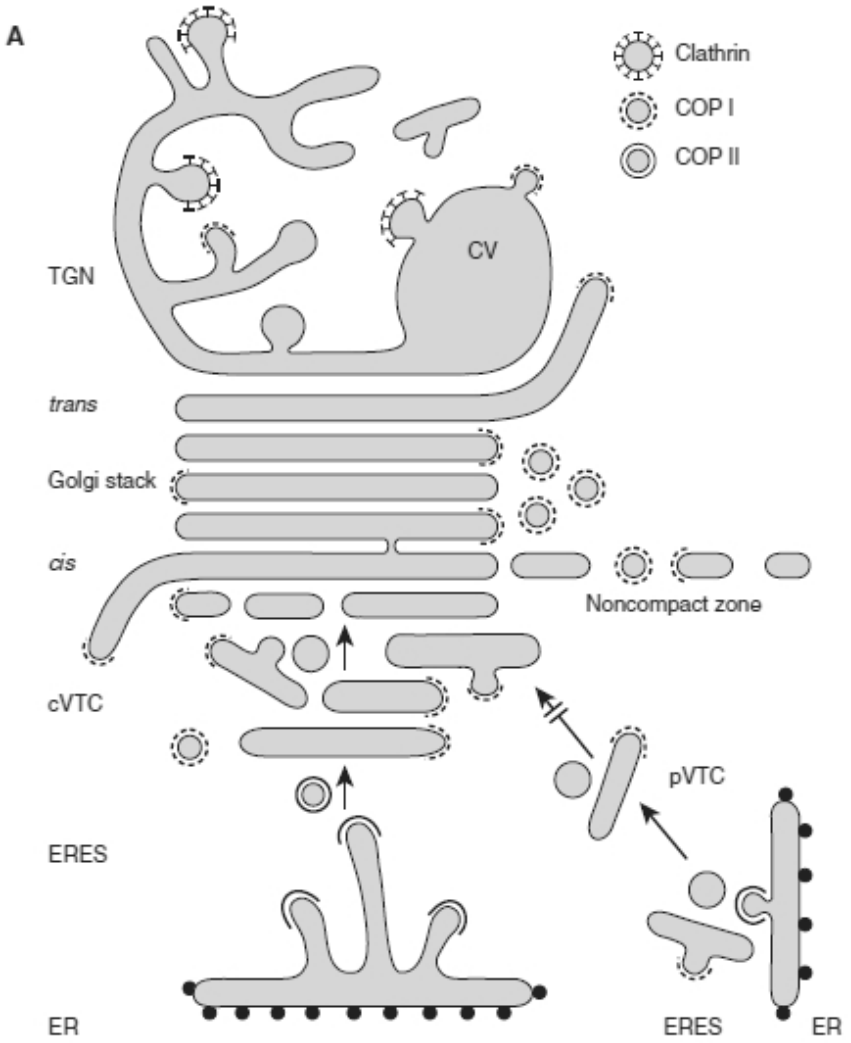

Figure 2: Scheme of transport from the ER to the Golgi apparatus and associated membranes
Schematic drawing of the intracellular trafficking from the ER to the *trans*-Golgi network and the different vesicles involved. Proteins leaving the ER via COPII vesicles which are replaced by COPI vesicles at the ERGIC (pVTC and cVTC). From there, proteins reaching the *cis*-Golgi apparatus are post-translationally modified as they are routing through this organelle until they arrive at the TGN where the proteins are sorted and send to their final destination. This step is mainly accomplished by clathrin vesicles. CV: condensing vacuole; cVTC: central vesicular and tubular shaped clusters; pVTC: peripheral vesicular and tubular shaped clusters (Klumperman 2011).

In general, the formation of COPI and COPII coats is supposed to be very similar in its mechanism involving the action of minimal components like the heteromeric coat complexes, ARF (ADP-ribosylation factor) and SAR1 (secretion-associated and RAS-related protein 1) GTPases, as well as regulatory GEFs (guanine exchange factors) and GTPase-activating proteins. Besides these proteins several other elements are needed to regulate COPI and COPII trafficking routes and thereby maintaining the structure and function of the organelle (Barlowe et al. 1994; Eugster et al. 2000; Bi et al. 2007; Yoshihisa et al. 1993). A disruption of the COPI trafficking by the toxin Brefeldin A inhibiting the ARF-GEFs results in the disassembly of the Golgi apparatus and the redistribution of its resident enzymes and proteins to the ER (Doms et al. 1989; Lippincott-Schwartz et al. 1989; Fujiwara et al. 1988; Donaldson et al. 1992). COPI and COPII vesicles differ in their origins. COPII coats solely assemble with budding profiles forming on the ER membrane, whereas COPI coats are not present at these ER-associated structures. Thus the presence of COPI budding vesicles can be used to differentiate between the ERGIC and the ERES (Martinez-Menarguez et al. 1999). High amounts of COPI coated buds can be observed pinching off from *cis*-Golgi cisternae with decreasing numbers towards the *trans*-side of the Golgi and the *trans*-Golgi network (TGN) (Oprins et al. 1993; Ladinsky et al. 1999). COPI vesicles also accomplish the retrograde transport from the Golgi to the ER (Martínez-Menárguez et al. 2001; Cosson et al. 2002; Letourneur et al. 1994; Emr et al. 2009). Before, it was mainly believed that COPI functions only as a retrograde carrier. Nevertheless, some publications also suggest an anterograde and retrograde COPI transport within the Golgi (Orci et al. 1997; Orci et al. 1986; Nickel et al. 1998; Aguilera Gomez and Rabouille 2015). Another well-established observation on spatial adaptations in the apparatus is the distribution of resident enzymes within this organelle. While early-acting enzymes are more concentrated in the *cis*-cisternae, enzymes for later processing steps are present in the *trans*-Golgi cisternae allowing a sequential processing of secretory cargo proteins while they move vectorially through the Golgi (Dunphy and Rothman 1985). After reaching the *trans*-Golgi network (Figure 2), the main site of protein and lipid sorting for post-Golgi destinations (reviewed by Griffiths and Simons 1986; Mellman and Simons 1992; Traub and Kornfeld 1997; and De Matteis and Luini 2008), the

cargos are sorted in a very complex manner mainly accomplished by clathrin coats (reviewed by De Matteis and Luini 2008). Besides the clathrin-mediated intracellular traffic involving Golgi, endosomes and lysosomes, clathrin coated vesicles represent transient products of clathrin-mediated endocytosis at plasma membranes (Pearse 1975, 1976; Pearse and Robinson 1990; Bonifacino and Rojas 2006). The formation of clathrin coated pits also involves different types of cargo adaptor proteins. The classical clathrin adaptors are so called adaptor protein complexes 1-4 (AP-1-4) which are composed of four subunits - two small, one medium and one large subunit - each having a specific function (Ahle and Ungewickell 1989; Shih et al. 1995). Studies showed that in addition to the anterograde transport from the TGN to endosomes, the AP-1 complex has also a role in the recycling from endosomes to the TGN (Ahle et al. 1988; Robinson 1990; Meyer et al. 2000; Meyer et al. 2001). While the AP-2 complex accomplishes the traffic of vesicles from the plasma membrane, AP-3 guides vesicles to lysosomes and AP-4 is found on vesicles in close proximity of the TGN (Robinson and Bonifacino 2001).

With their unique morphology - axons and dendrites far apart from the soma - neurons represent a very specialized and polarized cell type. Furthermore, their processes (axons and dendrites) are divided into distinct subdomains, such as distal and proximal dendrites, growth cones and synapses, axon initial segment and nodes of Ranvier. These specializations rely on even more precisely regulated trafficking as extensively reviewed by Horton and Ehlers (2003) and Lasiecka and Winckler (2011). Since intracellular trafficking plays a major role in neuronal function and survival, small dysregulations in this mechanism can have severe effects (Wang et al. 2014; Haase and Rabouille 2015). Defects in cytoskeletal proteins, structural Golgi proteins or molecular motors are observed to cause Golgi fragmentation in diseases like amyotrophic lateral sclerosis and other related neuron diseases (Haase and Rabouille 2015). The fragmentation of the Golgi apparatus is reported to be an early neuropathological hallmark of many neurodegenerative disorders preceding the loss of the axon and the cell body (Mourelatos et al. 1996; Vlug et al. 2005; Tong et al. 2012; van Dis et al. 2014).

1.6 The *Syap1* knockout mouse: Stem cell selection and mouse production

For a functional as well as molecular *in vivo* characterization of a new protein it is important to obtain a knockout mouse line. In the general context of the Sap47/Syap1 project the generation of a *Syap1* knockout mouse as a model for the study of mammalian Syap1 was therefore initiated. Mouse line production was performed at the Institute of Laboratory Animal Science in Vienna and funded by a grant from the INFRAFRONTIER-I3 mouse production Transnational Access program by the EU's Seventh Framework Programme for Research. In a mutational screen of the mouse X chromosome Cox et al. (2010) had already investigated 58 gene-trapped embryos derived from embryonic stem (ES) cells which are hemizygous null for X-chromosomal genes. No phenotypical abnormalities for male *Syap1* null embryos were observed at the E9.5 early embryonic stage. Due to their interest in genes affecting early embryonic development, they did not follow up their studies on a *Syap1* knockout mouse because the *Syap1* knockout did not have obvious effects in embryonic stages up to E9.5. Thus, it remained unclear whether depletion of Syap1 protein affects brain and other organs functions at later embryonic or postnatal stages. Therefore, in the INFRAFRONTIER-I3 approach a stem cell clone with conditional gene knockout potential was preferred which allows determining Syap1 function in specific tissues by crossing with the appropriate *Cre* recombinase mouse. The ES cell clone HEPD0680_2_C02 with targeted *Syap1* locus available from the Helmholtz Center in Munich was selected due the possibility of several manipulations of the *Syap1* gene (Figure 3). The 'knockout-first' lacZ-reporter-tagged *Syap1*^{tm1a} insertion allele with conditional potential was achieved by the insertion of the targeted mutation following the general strategy of EUCOMM.

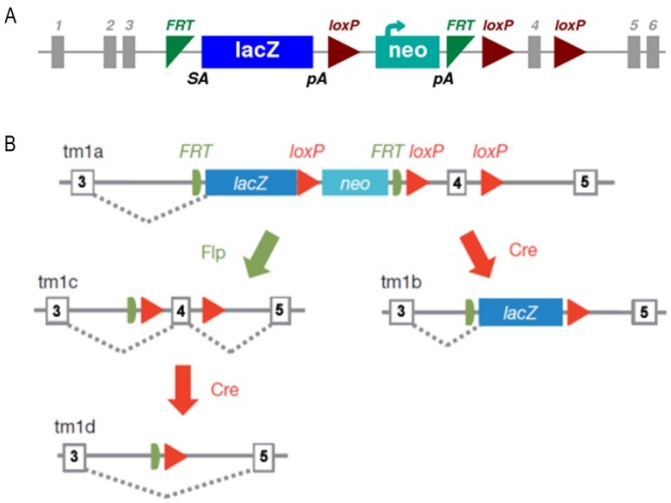

Figure 3: Scheme of the targeted-mutation-1a allele (*Syap1*$^{tm1a(EUCOMM)Hmgu}$) and conditional strategies
(A) The inserted cassette is constituted of a *FRT* site (flippase recognition target) followed by an *En2* splice acceptor site (*SA*) and *lacZ* sequence. This is followed by a *loxP*-flanked, promoter driven, neomycin-resistance selection cassette (*neo*). To simultaneously remove the *lacZ* and the *neo* cassettes, two *FRT* sites are placed upstream of the *lacZ* sequence and 5' of the second *loxP* site. A third *loxP* site is inserted downstream of the targeted exon-4. (B) Additional conditional crossings strategies.
Figure adapted from Skarnes et al. (2011).

The targeting cassette inserted in intron 3 (Figure 3A) includes a *FRT* site and a *lacZ* trapping element together with a mouse *engrailed-2* splice acceptor site (*SA*) and the SV40 polyadenylation sequences (*pA*) which was shown to be highly efficient in creating null alleles in mice (Skarnes et al. 1992; Mitchell et al. 2001) by disrupting the splicing of the targeted gene. Furthermore, the cassette includes a floxed, promoter driven neomycin-resistance selection cassette and a third *loxP* site downstream of the targeted exon-4. In case of residual exon-3 to exon-4 splicing, expression of intact Syap1 protein is observed, the *tm1a* mouse can be crossed e.g. with a global *Cre* deleter (*CMV*-Cre) which would result in the deletion of the neomycin-cassette and exon-4 leading to the generation of *tm1b*. Removal of exon-4 (74 bp) induces a frame shift and thereby no intact Syap1 protein can be expressed. The complete removal of the inserted cassette can be achieved by crossing the *tm1a* strain with transgenic *FRT* mice to obtain a mouse line with a floxed exon-4 but without the *lacZ* and *neo* element reverting *tm1a* to wild type. Further crossing with a *Cre* expressing line, exon-4 will be completely removed (*tm1d*). The protein fragment expressed from exon-1 to -3 - if not degraded - will most likely be not functional as it lacks the conserved BSD domain which was reported to be required for Syap1 function (Yao et al. 2013).

The selection of this clone with conditional potential allows studying the function of Syap1 in specific cells, tissues or at a certain developmental time point by crossing *tm1a* or *tm1c* mice with the necessary *Cre* mice (e.g. Nfl-*Cre*, nexin-*Cre*, GFAP-*Cre* or tau-*Cre*) (Skarnes et al. 2011; Skarnes 2015).

1.7 Aims of the thesis

Drosophila's Sap47 - the synapse-associated protein of 47 kDa - represents the founding member of the family of synapse-associated proteins whose members all contain a BSD domain. Since the Sap47/Syap1 protein family is conserved from *C. elegans,* fly and fish to mouse and human, the corresponding genes may be assumed to have a conserved function that is protected against random mutations by selection. The so far only sparsely studied protein family was termed "synapse-associated" as Sap47 was predominantly found in synaptic neuropil and in association with synaptic vesicles in glutamatergic boutons suggesting a synaptic function (Reichmuth et al. 1995; Saumweber et al. 2011; Hofbauer 1991; Hofbauer et al. 2009). This hypothesis is supported by the fact that after depletion of Sap47 in *Drosophila* larvae results in disturbance of synaptic plasticity as well as associative learning and memory (Saumweber et al. 2011). However, the fact that *Syap1* mRNA is found in most human tissues (Chang et al. 2001) and the observation that *Sap47* transcription is already detected in the early embryonic development (flybase (St Pierre et al. 2014)) and thus is not linked to synaptogenesis, indicates a rather general function of these "synapse-associated proteins".
Recently, Yao et al. (2013) observed that Syap1, the mammalian homologue of Sap47, is implicated in Akt phosphorylation upon growth factor stimulation in the context of adipocyte differentiation. Surprisingly, the distribution and role of Syap1 in the nervous system of vertebrates is so far completely unknown. This study was therefore implemented to characterize the localization and possible cellular function of Syap1 in the mouse nervous system using lentiviral knockdown techniques and the first generated *Syap1* knockout mouse as a model for Syap1 distribution and function in vertebrates.

2. Materials and Methods

2.1 Materials

2.1.1 Animals

The mice were maintained at the breeding facilities of the Institute for Clinical Neurobiology at the University Hospital of Wuerzburg. The animals were housed in a 12/12 h day-night-rhythm with free access to food and drinking water.

All procedures were performed strictly adherent to the German federal regulations on animal protection and the rules of the Association for Assessment and Accreditation of Laboratory Animal Care, with the explicit approval of the local veterinary authority.

2.1.1.1 CD1

In the present study, CD1 mice were used as a wild type mouse line. These mice were maintained as an outbred line obtained from the Charles River animal facility.

2.1.1.2 *Syap1* KO

Syap1 KO mice were generated at the Institute of Laboratory Animal Science in Vienna. Heterozygous, hemizygous and homozygous KO mice were further bred at our institute.

2.1.2 Cell lines:

2.1.2.1 HEK293T cells

Due to their high transfection efficacy Human Embryonic Kidney 293 cells (HEK293T) were used for lentiviral production and protein overexpression studies. These cells stably express the simian virus 40 (SV40) large T antigen which can bind to SV40 enhancers of expression vectors and thereby increase protein production. The cells were obtained from Invitrogen (R700-07).

2.1.2.2 NSC34 cells

The NSC34 cell line is a mouse-mouse neural hybrid cell line developed by fusing aminoptherin-sensitive neuroblastoma cells with motoneuron enriched embryonic spinal

cord cells. These immortalized and clonally uniform murine NSC34 cells are reported to exhibit motoneuron-like features. They are able to generate action potentials, express neurofilament triplet proteins, synthesize and store acetylcholine (Cashman et al. 1992). Additionally acetylcholine receptor clustering on co-cultured myotubes can be observed (Martinou et al. 1991). Due to these features NSC34 cells are preferentially used as a model to study selected aspects of motoneurons (Schaefer et al. 2007; Bellouze et al. 2014). The advantage of culturing this cell line compared to the expensive enrichment of embryonic motoneurons is the easy handling and fast reproduction. In this study these cells were mainly used for initial experiments and paradigms which were later tested on primary motoneurons. This cell line was obtained from Biozol (CED-CLU140).

2.1.3 Buffers and solutions

Cell culture	
Borate buffer	0.15 M Boric acid diluted in ddH_2O; pH 8.35; sterile filtered and autoclaved
Depolarization solution	30 mM KCl; 0.8% NaCl; 2 mM $CaCl_2$; diluted in ddH_2O; pH 9.5; sterile filtered and autoclaved
Laminin 111 solution	Laminin diluted in HBSS (final conc.: 2.5 µg/ml)
Motoneuron complete medium (full medium)	500 µM GlutaMax™; 2% heat inactivated horse serum; 2 % B27 supplement; diluted in Neurobasal® medium; sterile filtered
Medium for NSC34 and HEK293T cells	10% Fetal calf serum; 1% penicillin/streptomycin; diluted in DMEM with 500 µM GlutaMax™
PORN solution (1x)	PORN diluted in borate buffer; sterile filtered; (final conc.: 0.5 mg/ml)
Tris buffer	Tris diluted in ddH_2O; pH 9.5; sterile filtered; autoclaved; (final conc.: 10 mM)
SDS-Page and Western blot	
APS	10% APS dissolved in ddH_2O; aliquoted, freshly thawed
Blocking solution	5% Non-fat dry milk powder diluted in 1x TBST; heated up to 60°C while stirring; filtered
Blocking solution for detection with phospho-specific antibodies	5% Bovine serum albumin (BSA) diluted in 1x TBST; heated up to 37°C while stirring; filtered
Electrophoresis buffer (SDS-page)	250 mM Tris-base; 1.9 M Glycine; 1% SDS in ddH_2O; pH 8.9
Laemmli buffer (5x)	250 mM Tris HCl pH 6.8; 30% Glycerol; 10% SDS; 0.02% Bromophenol blue; 5% β-mercapto-ethanol in ddH_2O
TBS (10x)	0.1 M Tris-base; 1.5 M NaCl; in ddH_2O; pH 7.6

Transfer buffer	1x Electrophoresis buffer; 10% Methanol
Protein extraction	
Homogenizing buffer (synaptic vesicle isolation)	320 mM Sucrose; 4 mM HEPES-NaOH pH 7.3; 1x Protease inhibitors (cocktail tablet)
Lysisbuffer for (co-) immunoprecipitation (TBCE)	50 mM Tris pH 7.4; 1% Nonident P40; 150 mM NaCl; 2 mM EDTA; 1x Protease inhibitors (cocktail tablet)
Lysisbuffer for (co-) immunoprecipitation (Akt)	50 mM HEPES pH 7.5; 150 mM NaCl; 1 mM EGTA; 10% Glycerol; 1% Nonident P40; 1 mM DTT; 2 mM Sodium orthovanadate; 10 mM Glycerophosphate; 50 mM Sodium fluoride; 10 µg/ml Aprotinin; 10 µg/ml Leupeptin; 0.5 µg/ml Benzamidine; 0.25 mM PMSF; in ddH_2O
PHEM buffer (microtubule stabilization buffer)	60 mM PIPES; 25 mM HEPES; 10 mM EGTA; 2 mM $MgCl_2$; 1x Protease inhibitors (cocktail tablet); pH 6.9
Radioimmunoprecipitation assay buffer (RIPA buffer)	50 mM Tris pH 7.4; 150 mM NaCl; 1% Nonident P 40; 1% Sodium deoxycholiate; 0.1% SDS; 1 mM EDTA; 1x Protease inhibitors (cocktail tablet)
Genotyping	
1.6% Agarose gel	1.6 g Agarose powder dissolved in 1X TAE buffer; boiled until agarose powder completely dissolved
DNA extraction buffer	10 mM Tris HCl pH 7.5; 100 mM EDTA pH 8.0; 150 mM NaCl; 0.5% SDS; in ddH_2O
Loading dye (6X)	0.15% Bromophenol blue; 0.15% Xylene Cyanole FF; 5 mM EDTA (pH 8.0); 30% Glycerol; in ddH_2O
TAE buffer (50x)	2 M Tris-base; 5.7% Acedic acid; 50 mM EDTA; in ddH_2O

Immunostaining	
Blocking solution (immunocytochemistry)	10% Donkey serum; 0.1-0.3% Triton-X 100; in PBS; sterile filtered
Blocking solution (immunohistochemistry)	10% Donkey serum; 0.3% Triton-X 100; 0.1% Tween 20; in PBS; sterile filtered
Cryo-protection buffer	30% Ethyleneglycol; 25% Glycerol; 0.05 M Phosphate buffer in ddH_2O; pH 7.4
Fixative (4% Paraformaldehyde (PFA))	4%PFA dissolved in ddH_2O by heating up to 60°C under constant stirring; for clearing the solution a few drops of 1 M NaOH were added; filtered; solution was cooled down to room temperature; 0.2 M Na_2HPO_4; 0.2 M NaH_2PO_4; pH 7.4
Phosphate buffered solution (PBS, 10X)	1.37 M NaCl; 100 mM Na_2HPO_4; 18 mM KH_2HPO_4; 27 mM KCl; in ddH_2O; pH 7.4
Washing buffer (immunocytochemistry)	0.1% Triton-X 100; 0.2% Tween 20; in PBS
Washing buffer (immunohistochemistry)	0.1% Triton-X 100; 0.3% Tween 20; in PBS

Table 1: Buffers and solutions

2.1.4 Suppliers for media, solutions and supplements

Poly-D, L Ornithine (PORN)	Sigma-Aldrich; P8638
mouse Laminin 111 (EHS)	Invitrogen; 23017-015
Trypsin	Worthington; LS003707
Trypsin Inhibitor	Sigma; T6522
Neurobasal medium	Invitrogen-Gibco; 21103-049
B27 supplement (50X)	Invitrogen-Gibco; 17504-044
Horse serum	Linaris; SHD3250ZK
GlutaMax™	Invitrogen-Gibco; 35050-038
Hanks' BSS without Ca/Mg, with phenol red 1x	Invitrogen-Gibco; 14170-088

BDNF and CNTF	Institute for Clinical Neurobiology
Dulbecco's PBS without Ca/Mg 1x	Invitrogen-Gibco; 14190-094
DMEM high glucose, pyruvate, GlutaMax™	Invitrogen-Gibco; 31966-021
Non-essential amino acids (NEAA, 100X)	Invitrogen-Gibco; 11140-035
Penicillin/ Streptomycin	Invitrogen-Gibco; 15070-063
Fetal calf serum (FCS)	Invitrogen-Gibco; 10270-106
Donkey serum	Bio Rad; C06SBZ
FluorSave™	Millipore; 345789
EDTA-free Protease Inhibitor Cocktail	Roche, 04693159001

2.1.5 Kits

ECL™ Advance Western Blotting Detection Kit	GE Healthcare Life Sciences, RPN2135
ECL™ Prime Western Blotting Detection Kit	GE Healthcare Life Sciences, RPN2232
Bradford Protein Assay	Bio-Rad, 500-0006
QIAquick Gel extraction Kit	Quiagen; 28704
RevertAid First Strand cDNA Synthesis Kit	Thermo Fisher Scientific; K1621

2.1.6 Antibodies

2.1.6.1 Primary Antibodies

Antibody	Application	Supplier
Rabbit anti-Syap1	WB 1/3000, IF 1/200	Proteintech 16727-1-AP
Mouse anti-α-tubulin	WB 1/3000, IF 1/2000	Sigma T5168
Mouse anti-acetylated α-tubulin	WB 1/4000, IF 1/2000	Sigma clone T7451 Clone 6-1b-1
Rat anti-tyrosinated α-tubulin	WB 1/2000	Abcam ab6160 Clone YL1/2
Rabbit anti-Histone 3	WB 1/30 000	Abcam ab1791
Chicken anti-GFP	IF 1/2000	Abcam ab13970

Rabbit anti-GFP	WB 1/4000	Santa Cruz Sc8334
Rabbit anti-Akt	WB 1/4000	Cell Signaling #9272
Mouse anti-Akt	IF 1/50, IP 1/100	Cell Signaling #2966
Rabbit anti-phospho Akt^{Ser473}	WB 1/4000, IF 1/200	Cell Signaling #4060
Rabbit anti-phospho Akt^{Thr308}	WB 1/1000	Cell Signaling #9275
Rabbit anti-Calnexin	WB 1/4000	Enzo Life Science ADI-SPA-860
Goat anti-Calnexin	IF 1/500	SICGEN AB0037
Mouse anti-GAPDH	WB 1/4000	Calibiochem CB1001
Mouse anti-γ-adaptin	IF 1/1000	BD Transduction Laboratories A36120
Mouse anti-GM130	IF 1/500	BD Transduction Laboratories 610822
Mouse anti-COPI	IF 1/10	Gift from Robert Blum
Sheep anti-TGN38	IF 1/500	Novusbio NBP1-20263
Rabbit anti-Synaptophysin	WB 1/3000	Gift from R.Jahn
Mouse anti-Synaptobrevin	WB 1/10000	Synaptic Systems 104211
Mouse anti-Synapsin	WB1/4000	Gift from R.Jahn
Mouse anti-Cadherin	WB 1/500	Millipore MAB353
Ginea pig anti-vGlut	IF 1/2000	Synaptic Systems 1335304
Chicken anti-Tyrosin hydroxylase	IF 1/500	Abcam ab76442
Mouse anti-CalbindinD-28K	IF 1/1000	Sigma C9848
Guinea pig anti-Synaptophysin	WB 1/2000	Synaptic Systems 101004
Goat anti-Choline acetyltransferase	IH 1/1000	Millipore AB144p
Mouse anti-FLAG	WB 1/1000	Sigma F4042

Table 2: Primary antibodies

2.1.6.2 Secondary Antibodies

Antibody	Application	Supplier
Goat anti-rabbit HRP	WB 1/5000	Jackson Immuno 111-035-003
Goat anti-mouse HRP	WB 1/5000	Jackson Immuno 115-035-003
Goat anti-rat HRP	WB 1/5000	Rockland 612-103-120
Donkey anti-rabbit Cy3	IF 1/800	Jackson Immuno 711-165-152
Donkey anti-mouse Cy5	IF 1/800	Jackson Immuno 715-175-150
Donkey anti-chicken Alexa488	IF 1/800	Jackson Immuno 703-545-155
Donkey anti-sheep Alexa 488	IF 1/800	Jackson Immuno 115-165-003
Donkey anti-goat Alexa 488	IF 1/800	Jackson Immuno 705-545-147
Donkey anti-mouse Alexa 488	IF 1/800	Jackson Immuno 715-005-151

Table 3: Secondary antibodies

2.1.6.3 Others

4, 6-Diamidino-2-phenylindole dihydrochloride (DAPI)	Sigma-Aldrich; D-9542
Phalloidin Alexa 546 (1/50)	Molecular Probes; A22283
Bungarotoxin (BTX) Alexa 647 (1/500)	Invitrogen; B35451

2.1.7 Programs

GraphPad Prism 4

ImageJ

Photoshop 7.0 (Adobe)

Serial Cloner 2.6.1

2.2 Methods

2.2.1 *Syap1* knockout mouse genotyping

2.2.1.1 DNA isolation:

DNA from mouse biopsies were lysed in 500 µl of DNA extraction buffer and 20 µl proteinase K (20 mg/ml) and incubated overnight at 60°C on a thermo shaker until the tissue was completely dissolved. The following day 450 µl of 5% SDS and 150 µl of 3 M NaCl were added to the lysate and mixed by vortexing. The addition of 750 µl of chloroform was followed by another step of vortexing until the solution turned white. After centrifuging for 10 minutes with full speed (rcf = 16,000, Eppendorf 5417R) at 4°C the upper phase was transferred into a new Eppendorf tube. The DNA was precipitated with 700 µl isopropanol and again centrifuged with full speed at 4°C for 5 minutes. The supernatant was discarded and the pellet washed once by adding 500 µl of 70% ethanol and centrifuging again for 5 minutes. The supernatant was carefully decanted and pellet air dried. DNA was finally dissolved in 10 µl TE buffer at 65°C for 10 minutes.

2.2.1.2 Polymerase chain reaction (PCR)

Genotyping was performed using suitable primers (Table 8) for distinguishing *Syap1* knockout, heterozygous and wild type mice. The following reagents and polymerase chain reaction (PCR) conditions were used:

Reagent (stock)	Volume
DNA	2 µl
Taq buffer (10x)	2 µl
Betaine (5 M)	2 µl
dNTPs (2 mM)	2 µl
Syap1 fw primer (20 pmol)	0.5 µl
Syap1 rev wt primer (20 pmol)	0.5 µl
Syap1 rev ko primer (20 pmol)	0.5 µl
Taq polymerase	0.4 µl
Auqa ad iniectabilia	10.1 µl
Total volume	20 µl

PCR cycle	Duration	
94°C	5 min	
94°C	30 s	30 cycles
55°C	30 s	
72°C	60 s	
72°C	7 min	
25°C	hold	

Table 4: PCR protocol for *Syap1* knockout mouse line genotyping

The obtained PCR-products were separated in a 1.6% agarose-gel. 4 µl of 6x loading dye were added to each sample and 20 µl loaded onto the gel. A 100 bp marker was used due to the expected band sizes:

Wt: 589 bp KO: 274 bp Heterozygous: 589 bp and 274 bp

The bands were separated at 120 V.

2.2.2 DNA purification from agarose gel

In order to verify, if a correct amplification product was obtained, PCR was performed using a 5-fold reaction solution and the products were separated on an agarose gel. The band with the expected length was cut out from the gel and the amplification product was isolated and purified using the Qiagen gel extraction kit (protocol see manual) and sent for sequencing.

2.2.3 DNA sequencing

DNA sequencing was performed using 1 µg of isolated DNA and 20 pmol of primer in a total volume of 14 µl. Sequencing reaction was done by LGC genomics in a Ready2run reaction. The obtained sequence was then analyzed using Serial Cloner.

2.2.4 RNA isolation

RNA was isolated from the cerebral cortex of wild type and *Syap1* knockout mice. Therefore, a small piece of the cerebral cortex (ca. 1 g) was extracted, subsequently transferred to liquid nitrogen and stored at -80°C until use. For RNA isolation, the tissue was slowly thawed on ice and lysed in 1 ml trizol reagent and 3.5 µl β-mercaptoethanol with a syringe. After 10 minutes incubation at room temperature, 400 µl chloroform were added, mixed by inversion and incubated at room temperature for 5 minutes. The mixture was then centrifuged for 15 minutes at 4°C with 12,000 rcf and the upper phase transferred to a new reaction tube. 500 µl isopropanol were added to precipitate the RNA followed by another centrifugation step for 15 minutes at 4°C with maximum speed. The supernatant was carefully decanted and the pellet washed. Therefore, 1 ml of 70% ethanol was added, vortexed and centrifuged for 15 minutes at 4°C with maximum speed. The ethanol was then decanted and the pellet air dried for 10

minutes at room temperature. Finally, the RNA was dissolved in RNase-free water. The quantity and quality of RNA was analyzed by measurement at the Nanodrop spectrometer. The quality was assessed by the ratio of absorption at 260 nm and 280 nm. Ratio of 260/280 should be close to 2 for RNA.

2.2.5 cDNA synthesis

After RNA isolation, the RNA was treated with DNase to reduce contamination from genomic DNA. Subsequently this RNA was used to synthesize cDNA. Both steps were carried out following the manufacturer's instructions from Thermo Scientific "RevertAid First Strand cDNA Synthesis Kit".

2.2.6 RT-PCR

The obtained cDNA was then diluted 1:5 with EB-BSA (Tris-HCl pH 8.0 containing 10% BSA) and the protocol followed as previously described in Briese et al. (2016) using die the RT-primers listed in Table 8.

2.2.7 Production of *Syap1* knockdown and control lentiviruses

Knockdown of the *Syap1* gene in cells was achieved by RNAi approach. pLL3.7 lentiviruses were produced as previously described in Subramanian et al. (2012), expressing either shRNA against *Syap1* or a mismatch shRNA. Briefly, shRNA expressing pLL3.7 vectors were packaged with pRSV Rev, pMDLg/pRRE and pMD.G in HEK293T cells (Dull et al. 1998; Naldini et al. 1996). The cells were transfected with Lipofectamine™ 2000 (Invitrogen) in OptiMEM medium supplemented with 10% fetal calf serum (FCS) for 12-14 hours. Viral supernatants were harvested 72 hours after transfection and lentiviral particles concentrated from cleared supernatants by ultracentrifugation (Lentivirus production was performed by E. Spirk and H. Troll).

Both constructs co-expressed a GFP reporter gene as an internal infection control. Mismatch shRNA (Selvaraj et al. 2012) and *Syap1* knockdown vectors (generated by Funk N.) were obtained by cloning the appropriate mismatch short hairpin DNA sequence (5′-GAA AAA

AGG TTA GAA ACT TAA AGT GTT CTC TTG AAA CAC TTT AAG TTT CTA ACC A-3′) and the sequence for *Syap1* knockdown (5′-TGA GAC AAT TCA ACA GCA GAT TCA AGA GAT CTG CTG TTG AAT TGT CTC TTT TTTC-3′) into the pLL3.7 lentiviral backbone.

To assess the number of infectious particle, virus titering was performed using HeLa cells. Therefore, 300,000 cells in a total volume of 6 ml DMEM, 10% FCS and 1% penicillin/streptomycin were allocated to 12 x 1.5 ml Eppendorf tubes in such a way that the fist tube contained 550 µl, the last tube 450 µl and the other tubes 500 µl. For setting up a serial dilution ($1\text{-}10^{-12}$) 1 µl of virus was added to the first tube, gently mixed and 50 µl of the mixture transferred to the second tube. Again, the suspension was mixed and 50 µl transferred to the next tube. This procedure was repeated likewise for all other tubes and thereby creating a serial dilution. Each suspension was then transferred into one well of a 24-well plate and the HeLa cells cultivated (as described for HEK293T cells in 2.2.17.1) for 48 hours at 37%, 5% CO_2 and a relative air humidity of 95%. GFP fluorescence signals were investigated under the microscope. The number of infectious particles was determined from the last dilution in which a single infected cell was still detected.

2.2.8 Protein extraction from mouse tissue

For the analysis of Syap1 protein extraction, adult wild type mice were killed, tissues dissected and immediately transferred in a reaction tube to liquid nitrogen and stored at -80°C until use. For lysis, the tissues were thawed on ice and weighted. Five vol/weight (ml/g) of RIPA buffer were added and the tissue was incubated for at least 10 minutes on ice before sonication. After the tissue was lysed completely it was centrifuged at 20,000 rcf for 10 minutes at 4°C. The supernatant was transferred to a new reaction tube and the protein content was estimated with the Bradford Protein Assay (Bio-Rad) following the manufacturer's instructions. Equal amounts of protein (20 µg) were loaded onto the gel diluted in Laemmli buffer.

2.2.9 Protein isolation from mouse fat

After extraction of fat tissue RIPA buffer was applied and sonicated until the tissue was dissolved. Between each sonication step the suspension was kept on ice. Sonication was followed by a 20 minute centrifugation step at 12,000 rcf at 4°C. The fat formed a layer on top, cell debris formed a pellet. Therefore, the middle phase was removed using a 27-gauge needle and centrifuged again. The procedure was repeated two more times. Finally the middle phase containing proteins was subjected to Western blot analysis (20 µg; SDS-Page).

2.2.10 Crude subcellular fractionation of NSC34 cells

A crude subcellular fractionation of cells was performed following the protocol of Holden and Horton (2009) with minor changes. Instead of HEK293, HT1080 or HeLa cells, NSC34 cells were harvested until confluency and the required volume of buffer 1 (Digitonin-buffer) was calculated with the help of table 1 "Volumes of buffer required for a protocol scale up according to culture vessel surface area" (Holden and Horton 2009). The cells were pelleted down in a 5 minute centrifugation step using 400 rcf at 4°C. For unspecified centrifugation times in the protocol, a time of 10 minutes per centrifugation step was applied. After fractionation all of the obtained supernatants were subjected in identical volumes to 4-14% SDS gradient PAGE.

2.2.11 Synaptic vesicle isolation

Synaptic vesicles from adult brain lysates were enriched using differential centrifugation (Figure 4). Brains from four female adult mice (6-8 weeks) were dissected and washed three times with ice cold PBS. Then, the brains were cut into smaller pieces and homogenized completely in 20 ml homogenizing buffer (320 mM sucrose, 4 mM HEPES-NaOH pH 7.3, protease inhibitors, phosphatase inhibitors) with a Teflon-glas homogenizer. 500 µl were stored from the total lysate. Subsequently, the homogenate was centrifuged at 1,000 rcf for 10 minutes at 4°C to remove cell debris and nuclei. The pellet from this fraction (P1) was lysed with 10 ml of RIPA buffer. The supernatant S1 was centrifuged at 12,000 rcf for 15 minutes at 4°C and the supernatant S2 was stored. The resulting pellet P2 was dissolved in 10 ml of fresh

homogenizing buffer. After centrifuging for 15 minutes at 13,000 rcf at 4°C the fraction S2' was stored and the pellet P2' containing the synaptosomal fraction was dissolved in 3.6 ml of ice-cold water mixed with 400 µl of lysis buffer (hypotonic lysis). Furthermore, 33 µl of 1 M HEPES and protease inhibitors were added immediately and the solution homogenized in two more up-and-down strokes. Then, an ultracentrifugation step at 33,000 rcf at 4°C for 20 min followed. This fraction (LP1) was lysed in 2 ml of RIPA buffer and stored. The supernatant was centrifuged again at 260,000 rcf for 2 hours at 4°C. The supernatant was stored and the resulting pellet (LP2) was dissolved in 1 ml of RIPA buffer. For each fraction 500 µl of sample was stored for further immunoblot analysis with the exception of LS1 where 200 µl were stored.

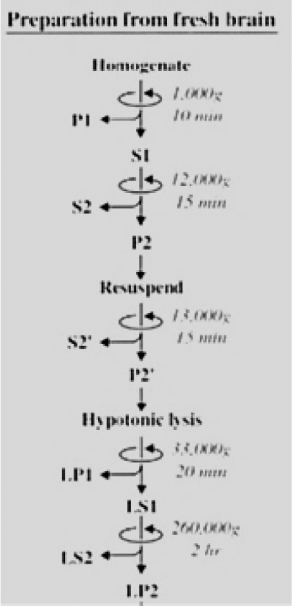

Figure 4: Centrifugation protocol for crude synaptic vesicle isolation
Centrifugation protocol was modified from Hell and Jahn (2006). Fresh mouse brain lysate was used for differential centrifugation in order to isolate synaptosomes. Centrifugation times were applied to each fraction as indicated in this scheme.

The following volumes of lysate, diluted in Laemmli buffer, were applied to Western blot analysis (vol/vol [%]): total 0.15; P1: 0.15; S1: 0.15; P2': 0.3; S2': 0.3; LP1: 0.15; LS1: 0.15; LP2: 1.00; LS2: 0.5.

2.2.12 Immunocytochemistry

Localization studies were performed by indirect immunolabeling of the proteins of interest. Therefore cells were grown on coverslips (10 mm, Hartenstein; DKR0) for the appropriate amount of days and then washed once with pre-warmed PBS before fixation with pre-warmed 4% paraformaldehyde (PFA) for 10 minutes at 37°C. Permeabilization of the cells and

blocking of unspecific epitopes was performed in the blocking buffer for 30 minutes at room temperature. Subsequently the primary antibodies were diluted in the blocking buffer and incubated in a humid chamber over night at 4°C. Next day, the coverslips were washed five times for five minutes each with washing buffer to remove unbound and excessive antibodies. Secondary antibodies (and/or fluorophore-coupled phalloidin) were also diluted in the blocking buffer and applied to the coverslips for one hour at room temperature. Then, they were washed again two times with the washing buffer followed by a 10 minute DAPI staining. After three additional washing steps, the coverslips were washed once with ddH_2O and mounted with FluorSave™ onto an objective slide. The stained slides were stored in a dark chamber at 4°C until they were analyzed by confocal microscopy.

2.2.13 Immunohistochemistry of vibratome sections

Adult wild type or *Syap1* knockout mice were euthanized by the application of CO_2 for approximately three minutes. After ensuring the death of the animal by assessing movement, stimulus perception and reflexes like the toe and cornea reflex, the animals were first perfused trans-cardially with PBS containing 0.4% heparin to remove the blood from arteries and veins. To fix the tissues, perfusion was then performed with 4% PFA for approximately 8 minutes. Brain and/or lumbar spinal cord were carefully dissected and post-fixed for at least two hours with 4% PFA at 4°C followed by three washing steps with PBS and storage at 4°C in PBS. The tissues were embedded in 6% agarose and 30 µm sections were produced by vibratome. The slices were stored in cryo-protection buffer at -20°C until use. Prior to immunolabeling, the sections were transferred to a 24-well dish and washed three times for 15 minutes each with 1 ml of PBS to remove cryo-protection buffer. Blocking and permeabilization were carried out in 1 ml blocking buffer for one hour at room temperature and one hour at 37°C. The antibodies were diluted in 300-500 µl blocking buffer and incubated for two days at 4°C on a shaker. Afterwards the sections were washed three times in washing buffer for 15 minutes and incubated with secondary antibodies diluted in blocking buffer for two hours at room temperature. Three additional washing steps (each for one hour) were performed prior to a 15 minute DAPI staining. Before mounting the sections on objective slides, they were washed

two times with PBS. The cover glasses were sealed with nail polish and stainings stored at 4°C before imaging.

2.2.14 Immunohistochemistry of neuromuscular junctions

To investigate the presence of Syap1 at neuromuscular endplates, the gastocnemius muscles from perfused adult wild type and *Syap1* knockout mice were dissected and post-fixed for two hours as described in 2.2.13. After fixation, single fibers were picked and transferred to a 96-well plate and washed for 30 minutes with PBS containing 0.1 M glycine. Subsequently the postsynapse was labeled with α-bungarotoxin for 20 minutes in PBS. The fibers were then washes with PBS for 20 minutes. Permeabilization and blocking was performed in blocking solution for one hour at room temperature. The primary antibodies were applied over night at 4°C diluted in blocking solution. Next day, the fibers were washed three times with 1x PBS for 10 minutes each and the secondary antibodies added. After one hour of incubation at room temperature, three washing steps à 10 minutes were performed and the fibers mounted on an objective slide.

2.2.15 SDS-polyacrylamide gel electrophoresis and Western blot analysis

To separate the proteins in an electrical field according to their molecular weight, the samples were subjected to SDS-polyacrylamide gel electrophoresis (PAGE). Therefore, a polyacrylamide gel was cast by using a mixture of mixing acrylamide and bisacrylamide which are able to form cross-links and thus providing a matrix. After the addition of the initiator ammonium persulphate (APS) and TEMED (N, N, N', N'-tetramethylethylenediamine) as a catalyzer, the two polymers start to form cross-links. The pore size of the gel is determined by the concentration of acrylamide and the ratio of acrylamide and bisacrylamide. To ensure, that the proteins are separated according to their molecular weight, sodium dodecyl sulfate (SDS) is added to destroy the interactions between hydrophobic amino acids and thereby giving a uniform negative charge to the proteins. Negatively charged proteins migrate from

cathode to anode, whereby lower molecular weight proteins run faster than those with a higher molecular weight.

The percentage of the resolving gel was chosen according to the expected molecular weight of the examined proteins:

Gel percentage	**10%**	**12%**
30% Polyacrylamide [ml]	5 ml	6 ml
1.5 M Tris-HCl (pH: 8.8) [ml]	3.75 ml	3.75 ml
10% APS [µl]	150 µl	150 µl
10% SDS [µl]	150 µl	150 µl
TEMED [µl]	6 µl	6 µl
ddH_2O [ml]	5.95 ml	4.95 ml
Total volume [ml]	15 ml	15 ml

Table 5: Composition of resolving gels

A stacking gel was cast on top of the fully solidified resolving gel and a comb with the required number of pockets was inserted:

Gel percentage	**4%**
30% Polyacrylamide [ml]	1.7 ml
1.5 M Tris-HCl (pH: 6.8) [ml]	1.25 ml
10% APS [µl]	100 µl
10% SDS [ml]	100 µl
TEMED [µl]	10 µl
ddH_2O [ml]	6.8 ml
Total volume [ml]	10 ml

Table 6: Composition of the stacking gel

The samples - unless otherwise stated - were diluted in Laemmli buffer (to a final concentration of 2x Laemmli buffer) and loaded into the pockets; unused pockets were filled up with Laemmli buffer to avoid irregular running patterns. For reference, a marker was loaded containing proteins of known masses and thereby, the molecular weight of proteins in the sample could be determined. The gel was run at 20 mA until the required separation of proteins was reached (~ 1.5-2 hours).

2.2.16 Western blotting

The gel was then "blotted" in order to transfer the proteins onto a nitrocellulose membrane. The Whatman paper and the nitrocellulose were incubated in SDS running buffer with 10% methanol prior to the blotting procedure. The stack of Whatman papers, nitrocellulose and gel was placed in the Biometra blotter and blotted for 2 hours at 120 mA. In order to check the efficacy of transfer, the membrane was stained with Ponceau-S, which labels proteins sticking to the nitrocellulose. After transfer, the membrane was blocked with 5% non-fat dry milk (or 5% BSA for phospho-proteins) in Tris-buffered saline-Tween-20 (TBST) for one hour at RT. Subsequently, the membrane was incubated with primary antibody diluted in blocking milk (or 5% BSA in TBST for phospho-proteins) overnight at 4°C. Before adding the secondary antibody coupled to horse radish peroxidase, the membrane was washed three times with TBST for 15 minutes. After incubation for one hour the membrane was washed again and the antigen-antibody complex was detected by enhanced chemiluminescence (ECL) on X-ray films. The protein levels were quantified by densitometric analysis using ImageJ (see http://lukemiller.org/index.php/2010/11/analyzing-gels-and-western-blotswith-ImageJ/).

2.2.17 Cell culture

2.2.17.1 Human embryonic kidney 293T (HEK293T) cell line

HEK293T cells are frequently used as an expression tool for recombinant proteins or overexpression of endogenous proteins. The cells are able to carry out posttranslational modifications which are required to generate functional and mature proteins. Fast and easy maintenance make this cell line to a widely used expression system.

HEK293T cells were initially cultured in an expansion medium containing 10% fetal calf serum (FCS) and 1% Geneticin in Dulbecco's modified Eagle's medium (DMEM) with GlutaMax™ (500 µM). Higher passages were than cultured in DMEM supplemented with GlutaMax™ (500 µM), 10% FCS, 1% penicillin/streptomycin and 1% non-essential amino acids (NEAA). Cells were split every third day and kept in an incubator at 37°C with a relative air humidity of 95% and 5% CO_2.

2.2.17.2 Transient transfection of human embryonic kidney (HEK) 293T cell line

Lipofectamine™ transfection was used to transfect host cells as described in the manufacturer's instructions. Lipofectamine™ 2000 is a cationic liposome formulation which is complexing with nucleic acid molecules and permeating the cell membrane. For transfection, the appropriate number of HEK293T cells were used for each condition, kept in DMEM with 10% FCS, 1% penicillin/streptomycin and 1% NEAA. First, DNA-Lipofectamine™ 2000 complexes were prepared and in another reaction tube the plasmid-DNA was diluted in Opti-MEM® I Reduced Serum Medium without serum. Before use, Lipofectamine™ 2000 was gently mixed with Opti-MEM® I-Medium. Both mixtures were incubated for 10 minutes at RT. Then the diluted DNA was combined with the diluted Lipofectamine™ 2000, gently mixed and incubated for 20 minutes at RT. These DNA-Lipofectamine™ complexes were added to the cells and incubated for another 10 minutes. HEK cells were plated in DMEM without penicillin/streptomycin. The medium was changed to DMEM with penicillin/streptomycin after 4-6 hours and were cultured for one day (for detailed protocol information see Invitrogen, Lipofectamine™ 2000) and used for further downstream biochemistry assays.

2.2.17.3 NSC34 cell line

The NSC34 cell line is a mouse-mouse neural hybrid cell line, which was developed by fusing aminoptherin-sensitive neuroblastoma cells with motoneuron enriched embryonic spinal cord cells (Cashman et al. 1992). The advantage of culturing these cell line compared to the expensive enrichment of embryonic motoneurons is the easy handling and fast reproduction.
The cells were cultured in Dulbecco's modified Eagle's medium (DMEM) supplemented with GlutaMax™ (500 µM), 10% FCS and 1% penicillin/streptomycin at 37°C under humidified air containing 5% CO_2. Splitting was done every third day.

2.2.17.4 Neural stem cell culture

Neuronal stem cell culture from embryonic mouse forebrains was performed following the protocol described in Gotz et al. (2005).

2.2.17.5 Primary motoneuron cell culture

Motoneurons were isolated from lumbar spinal cords of E13.5-14 old embryos as described in Wiese et al. (2010). The lumbar spinal cords were dissected and the ensheathing meninges were removed. 2-3 spinal cords were pooled and collected in 360 µl of HBSS on ice until all embryos were dissected. To form a uniform suspension of cells, the tissue was trypsinized for 15 minutes with 40 µl of 0.1% trypsin and trypsinization was stopped by adding 40 µl 0.1% trypsin inhibitor. In order to enrich the motoneurons, the cells were transferred to a $p75^{NTR}$ antibody coated plate and incubated for 45 minutes. During that time embryonic motoneurons, which express $p75^{NTR}$ receptor, attached to the $p75^{NTR}$-antibody. Unbound cells were removed by washing the panning plate gently three times with pre-warmed neurobasal medium (NB-medium). Calcium containing depolarization solution (1.5 µl/mm^2) was added which leads to calcium influx and thereby to re-organization of the actin cytoskeleton. Motoneurons detached from the antibody during membrane ruffling were collected by adding pre-warmed NB-medium supplemented with 2% horse serum and 2% B27 after 10-20 seconds, which inhibited membrane ruffling. Cells were centrifuged at 400 rcf for 5 minutes and the excessive media was removed. The cell pellet was carefully re-suspended in full medium (containing 500 µM GlutaMax™, 2% heat inactivated horse serum (HS) and 2% B27 supplement) and counted in a Neubauer counting chamber and the required number of cells was plated on poly-D, L-ornithin (PORN) and Schwann cell specific laminin 111 coated coverslips/cell culture dishes. PORN and laminin coating improve the attachment and neuronal differentiation of the cells. After one hour, when cells settled down, full medium was applied containing either BDNF [5 ng/ml] or CNTF [5 ng/ml]. Half of the medium was replaced after 24 h and then every second day (Wiese et al. 2010). Cells were kept in an incubator at 37°C with a relative air humidity of 95% and 5% CO_2 and cultured for up to seven days.

Lentiviral infection was performed prior to plating of the cells. To ensure a higher probability of infection, the virus was applied in a small volume to the cells and incubated for 10 minutes.

2.2.17.6 Motoneuron survival assay

For the motoneuron survival assay, 1,000 primary motoneurons were plated on 10 mm coverslips (Hartenstein, DKR0). On day one the number of cells which settled down in a marked area in the center of the coverslip containing about 20-100 cells was counted. The motoneurons were then cultured for seven days in the presence of BDNF [5 ng/ml], counted again and the survival rate was calculated. A control in which cells were cultivated without BDNF, was also included.

2.2.17.7 Axon length, dendrite and soma size measurements

Motoneurons were isolated (2.2.17.5) and cultured for five to seven days *in vitro* (DIV). After the cells were washed once with pre-warmed PBS, they were fixed and each condition stained against GFP and α-tubulin (for staining procedure see 2.2.12). Images were taken with the Keyence microscope and the axon length of at least 50 cells was measured with ImageJ. For dendrite length measurements, primary dendrites were traced, the soma size was determined by tracing the circumference of the soma and measured by ImageJ, respectively.

2.2.18 Microtubule fractionation

For microtubule fractionation, 400,000 - 500,000 motoneurons per condition (uninfected, sh-Syap1, mock and taxol control) were cultured for 5 DIV in presence of BDNF [5 ng/ml] in a 12-well Greiner dish. The cells were extracted with 100 µl microtubule stabilization buffer (PHEM buffer) containing 0.5% Triton X-100. In order to separate polymerized microtubules from soluble tubulins, the cells were centrifuged at 12,000 rcf for 10 minutes at 4°C. To prove a successful fractionation, one of the controls was treated with placitaxel (10 µM) for 2 hours to polymerize most of the microtubules prior to extraction. This control was extracted with PHEM buffer containing 10 µM placitaxel and 0.5% Triton X-100. After centrifugation, the supernatant was collected and 20 µl of 5x Laemmli buffer added. The remaining pellet was carefully washed with ice-cold PBS and dissolved in 120 µl 2x Laemmli buffer so that equal volumes for each fraction were achieved. Equal volumes of the fractions were then subjected to Western blot analysis.

2.2.19 Stimulation experiments

For stimulation experiments with primary motoneurons, the different conditions (unstimulated, sh-Syap1 and mock control) were cultured in full medium in presence of CNTF [5 ng/ml] for 5 DIV. To avoid BDNF-mediated Akt activation, motoneurons were cultured in the presence of CNTF as a neurotrophic factor, which also ensures cell survival (Sendtner et al. 1991). On day 5, full medium containing serum and B27 supplement was washed out twice with pre-warmed NB medium and starved overnight (12-14 hours) by incubation only in NB medium. The next day, 0.1% BSA coated BDNF [20 ng/ml] was diluted in NB medium and a 0.1% BSA vehicle was diluted with the same dilution factor in NB, as well. Vehicle stimulation was used to prove, that up-regulation of phospho-Akt was not due to contaminations of growth factors in the BSA fraction used. BDNF or the vehicle was applied for the indicated time periods, washed once with PBS and directly lysed in 2x Laemmli buffer. The samples were boiled for 10 minutes at 99°C prior to Western blot analysis.

For compartment-specific immunocytochemical analysis of Akt phosphorylation, the motoneurons were cultured in full medium in presence of CNTF [5 ng/ml] for 5 DIV on coverslips. On day 5 the cells were washed once with NB and starved for 6-7 hours in NB containing 2% B27 (without insulin). The cells were then stimulated for 5 minutes with BDNF [20 ng/ml] or vehicle and washed once with PBS and immediately fixed with 4% PFA. After fixation, the cells were stained against pan-Akt, $pAkt^{Ser473}$ and GFP (following the protocol of 2.2.12). Z-stacks of the soma, distal axon and growth cone were taken at the confocal microscope. The average intensity for each stack was used for quantification. Identical areas were measured for pan-Akt and $pAkt^{Ser473}$ and the background for each channel was subtracted from the mean intensities. Ratios of $pAkt^{Ser473}$/Akt were used for statistical analysis.

2.2.20 Brefeldin A treatment of cultured primary motoneurons

Motoneurons were cultured for 5 DIV and treated with 5 µg/ml BFA applied to NB medium for 30 minutes. BFA was then carefully washed out and the cells subsequently kept in full medium for two hours for Golgi reassembly. Then, the medium was washed out with

prewarmed PBS, fixed with 4% PFA for 10 minutes at 37°C and stained following the protocol in 2.2.12.

2.2.21 Co-immunoprecipitation

In order to study the interaction of two proteins, co-immunoprecipitations were performed. Co-immunoprecipitation is a widely used technique to study protein-protein interactions. It allows precipitating a certain protein from total cell/tissue lysate using a specific antibody whereby proteins which are interacting directly or indirectly are pulled down together in a complex. The obtained samples are then analyzed by Western blot analysis.

To identify potential interaction partners of Syap1, cells or tissue were lysed in the appropriate volume of lysis buffer, centrifuged at 20,000 rcf for 10 minutes at 4°C, and protein concentration of the supernatant was then estimated using Bradford Protein Assay (Bio-Rad). By this depending on the availability of cells or tissue, 150 µg – 1 mg of protein were obtained. The pellet was discarded. Subsequently, identical amounts of samples were pre-cleared for 45 minutes at 4°C on a spinning wheel in order to reduce non-specific binding of proteins to the agarose beads, resulting in an improved signal to noise ratio. Prior to pre-clearing 25-30 µl of protein A or G beads (depending on the species of the antibody; see datasheet of beads used) were washed three times with ddH_2O and once with lysis buffer to equilibrate the beads. After centrifugation at 100 rcf for two minutes at 4°C the supernatant was transferred to a new reaction tube and 10-50 µl (depending on protein concentration in the lysate) were stored for input control. The remaining supernatant was incubated for pulldown with the primary antibody or IgG control overnight on rotation at 4°C. The following day, 25-30 µl of fresh beads were washed again three times with ddH_2O and once with lysis buffer. Protein-antibody mixture was incubated with these beads for one hour at 4°C on rotation wheel and then centrifuged at 1,000 rcf for two minutes at 4°C. The obtained supernatant was stored for subsequent analysis. The beads were washed three times with lysis buffer, 2x Laemmli buffer was added and boiled at 99°C to elute the proteins from the beads. After centrifugation at 20,000 rcf for 10 minutes the eluate was transferred to a new reaction tube and stored at -20°C until use.

2.2.22 Protein cross-linking

The cross-linking of proteins prior to co-immunoprecipitation was performed following the protocol of Zlatic et al. (2010) with minor adaptations. Chemical cross-linking stabilizes a selective protein association and thereby an endogenous interaction of Syap1 and TBCE can be detected. Therefore, HEK293T cells were cultured until confluency in a culture flask. Buffer volumes indicated by Zlatic et al. (2010) were adjusted accordingly. Lysis buffer A was prepared as follows: 50 mM Tris pH 7.4, 150 ml NaCl, 2 mM EDTA and 1% NP40, thereby using the standard buffer as an interaction of Syap1 and TBCE was observed under these conditions after ectopic overexpression of the two proteins. Co-immunoprecipitation was then further carried out following the description under 2.2.21.

2.2.23 Microscopy

Images for determination of axon length were taken with the Keyence 0.43 microscope using a 20x objective. The length of axons was measured with ImageJ (Schneider et al. 2012). For localization analysis of Syap1, imaging was performed with the Olympus Fluo View^{TM} FV1000 confocal microscope. The Zeiss ELYRA S.1 microscope was used to take detailed images obtained by structured illumination microscopy (SIM). For immunocytochemical and immunohistochemical analysis of the antibody specificity and Akt phosphorylation identical settings and brightness and contrast adjustments were used. All final processing was performed with ImageJ and Photoshop 7.0 (Adobe).

2.2.24 Statistical analysis

For statistical analysis, at least three independent experiments were performed and quantified with the GraphPad Prism 4 software. Normally distributed values (≥ 3 independent experiments) were analyzed using the analysis of variance (ANOVA) with Bonferroni posthoc test; for nonparametric statistics the Kruskal-Wallis test with Dunn`s multiple comparison was applied. In case of only two conditions, the Student`s t-test was used.

3. Results

3.1 Syap1 antibody specificity test

3.1.1 Validation of antibody specificity for biochemical analysis

Initially, in order to study the localization and function of Syap1 protein, several commercially available antibodies (Abcam ab101498; Proteintech 16272-1-AP; Santa Cruz sc133412 and Sigma HPA00175) exclusively raised against the human Syap1 protein were tested for their specificity and cross-reactivity. By using the antibody provided by Abcam no proper signal (neither for human cell lysate (HEK293T) nor for mouse cell lysate (NSC34 and primary motoneurons) could be achieved in Western blots (data not shown), thus the antibody was not further investigated in its specificity. Santa Cruz and Sigma antibodies failed as well to detect a single band for mouse Syap1 protein but instead showed cross-reaction with other proteins of higher (60-70 kDa) or lower (43 kDa) molecular weight (data not shown) and therefore appeared not suitable for immunocytochemical analysis. By using the antibody obtained from Proteintech raised against the full-length human protein, one prominent band was obtained by Western blot analysis for HEK293T protein cell lysate (~ 55 kDa) as well as for NSC34 protein cell lysate (~56 kDa; Figure 5A). Between these two bands, a small difference in the electrophoretic mobility was observed, in agreement with a 13 amino acid longer mouse Syap1 protein (Ref.: NM_025932). The bands recognized by the antibody migrate significantly higher than the predicted molecular weight of approximately 40 kDa (human: 39.94 kDa; mouse: 41.36 kDa).

When FLAG-tagged mouse Syap1 protein (vector generated by Dr. Funk N. see 6.1) was overexpressed in HEK293T cells and lysates from untransfected and transfected cells investigated by Western blot analysis, two bands were detected with the Syap1 antibody when the protein was overexpressed (Figure 5B; right lane). The band for endogenous Syap1 was detected at 55 kDa and the band for the tagged protein was observed at approximately 60 kDa. This clearly shows that this antibody binds selectively to the human as well as to the mouse Syap1 protein.

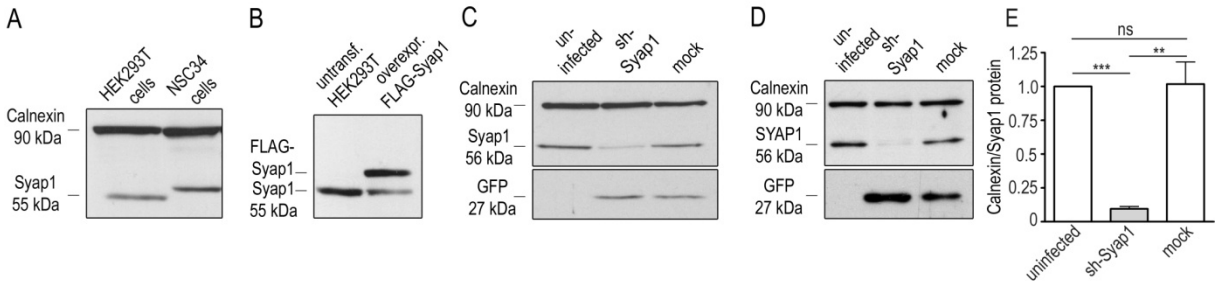

Figure 5: Validation of Syap1 antibody specificity in Western blot analysis

(A) Western blot analysis from HEK293T cell lysate revealed one band at 55 kDa; one band at around 56 kDa was observed in NSC34 cell lysate indicating that this Syap1 antibody cross-reacts with the 13 amino acid longer murine Syap1 protein. Calnexin served as a loading control. (B) When FLAG-tagged mouse Syap1 protein was overexpressed in HEK293T cells the endogenous as well as the overexpressed protein was recognized by the antibody. Lentiviral knockdown of Syap1 protein in NSC34 cells (C) and cultured primary motoneurons (D) led to a robust reduction of signals for Syap1 indicating that the antibody is also specifically recognizing the mouse Syap1 protein and does not cross-react with other proteins of the same molecular weight. Syap1 signal was not reduced in the uninfected and mock infected control. Calnexin again served as a loading control; GFP indicated a successful viral infection. (E) Densitometric analysis of Western blots with motoneuron lysates (5 DIV) revealed a significant reduction of Syap1 protein up to 90 ± 2% compared to both controls. Calnexin/Syap1 ratios were determined and normalized to the uninfected control (n = 8; one-way ANOVA with Kruskal Wallis test; ***: $P < 0.001$; **: $P < 0.01$; ns = not significant: $P > 0.05$). Bars represent means ± SEM.

In order to confirm, that the antibody is not cross-reacting with another protein at the same molecular weight and to further confirm its specificity, Syap1 protein levels were reduced in NSC34 cells (Figure 5C) and cultured primary motoneurons (Figure 5D) by lentiviral shRNA mediated *Syap1* knockdown. Therefore both cell types were infected with the knockdown virus and cultured for 5 DIV before the cells were lysed and analyzed by Western blot. The result shows that Syap1 protein levels are markedly reduced in NSC34 cells and primary motoneurons after *Syap1* knockdown whereas signals in both the controls (mock treated and uninfected) remained unaffected. Both lentiviruses (mock and *Syap1* knockdown) expressed GFP as an indicator for an efficient infection. The efficacy of *Syap1* knockdown in primary motoneurons cultured for 5 DIV was determined by densitometric measurements from Western blots (E). In comparison to uninfected and mock infected controls, Syap1 protein level was highly reduced. A reduction of up to 90 ± 2% can be achieved. The results verify the specificity of the Syap1 antibody and show that Syap1 protein levels can be highly reduced by *Syap1* knockdown allowing further functional studies.

3.1.2 Validation of antibody specificity for immunofluorescence analysis

In order to study the subcellular distribution of Syap1 protein, the specificity of the antibody for immunocytochemistry was investigated. Therefore, primary motoneurons were infected with the respective virus (mock and *Syap1* knockdown) and cultured for 5 DIV on coverslips. The cells were fixed and stained against GFP to distinguish infected neurons, against acetylated tubulin to visualize the entire cell, and against Syap1. Images were taken with a confocal microscope using identical settings and processed with equivalent brightness and contrast adjustments. In the overview of the motoneurons an overall reduction in Syap1 immunofluorescence was detected after lentiviral knockdown of Syap1 protein compared to both controls (Figure 6A). This reduction in Syap1 signal intensity provides further evidence for the specificity of the antibody also for immunocytochemistry and underlines the findings of the antibody specificity test in Western blots. Furthermore, the images demonstrate that Syap1 is present in the axon, dendrites and soma of cultured primary motoneurons. In the magnification of the soma (Figure 6B) the reduction in Syap1 immunofluorescence signal is even more obvious. The protein is distributed in a punctate pattern and strongly accumulates in perinuclear compartments.

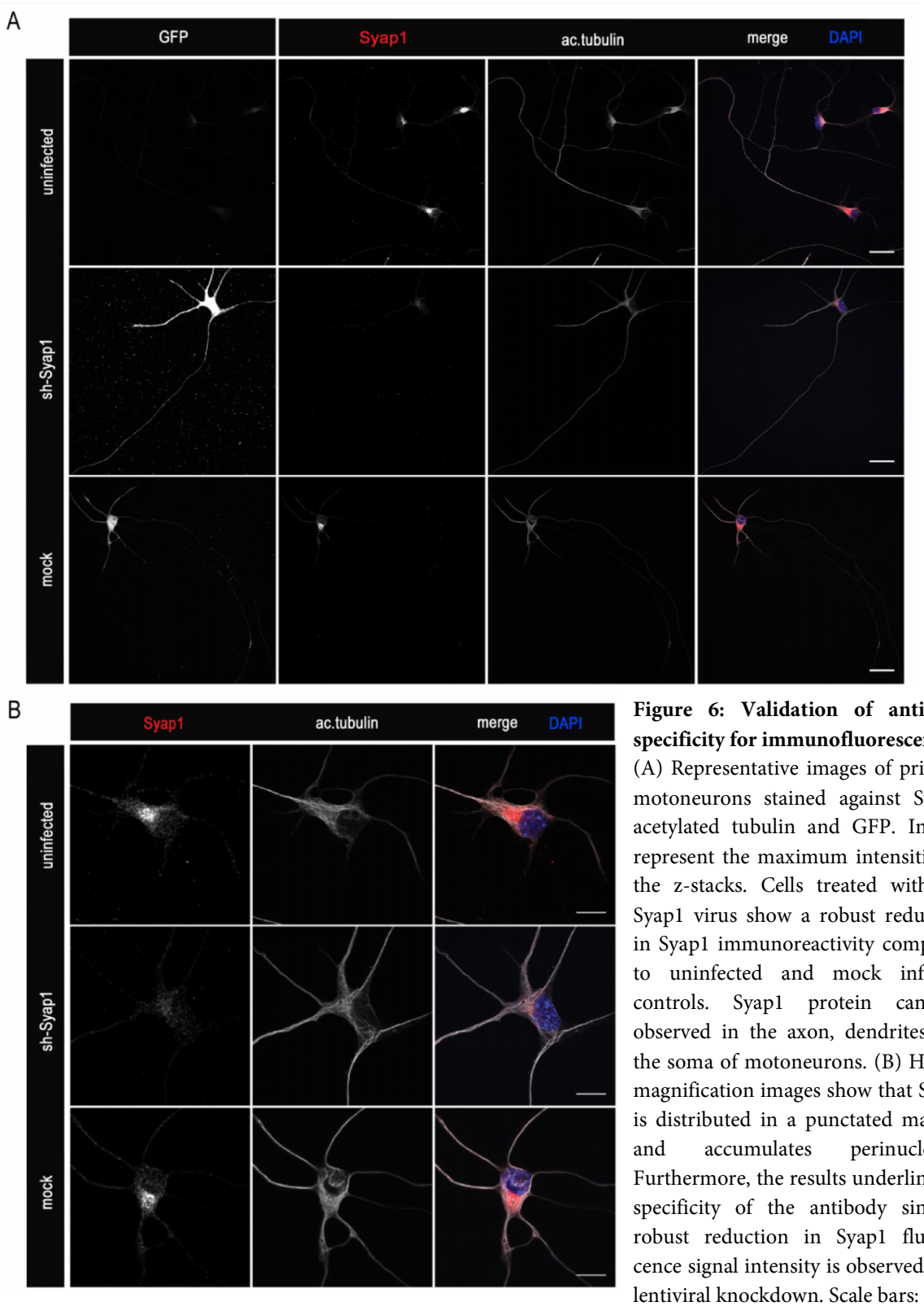

Figure 6: Validation of antibody specificity for immunofluorescence
(A) Representative images of primary motoneurons stained against Syap1, acetylated tubulin and GFP. Images represent the maximum intensities of the z-stacks. Cells treated with sh-Syap1 virus show a robust reduction in Syap1 immunoreactivity compared to uninfected and mock infected controls. Syap1 protein can be observed in the axon, dendrites and the soma of motoneurons. (B) Higher magnification images show that Syap1 is distributed in a punctated manner and accumulates perinuclearly. Furthermore, the results underline the specificity of the antibody since a robust reduction in Syap1 fluorescence signal intensity is observed after lentiviral knockdown. Scale bars: A: 25 µm; B: 10 µm

3.2 Subcellular localization of Syap1 protein

So far, nothing is known about the subcellular distribution of Syap1 protein. Its homologue Sap47 is present in the synaptic boutons of fly larval motoneurons and there it was found to localize in close proximity to synaptic vesicles by immuno-gold electron microscopy (Saumweber et al. 2011). Furthermore, analysis of density gradient centrifugation showed that Sap47 seems to be predominantly present in the cytoplasm of fly brain homogenates (Huber 2003; Reisch 2003). To gain first impressions on the subcellular distribution of Syap1 protein, the localization was investigated using immunocytochemical analyses since the specificity of the antibody was verified before (see Figure 6).

3.2.1 Syap1 accumulates in close proximity to organelles of the secretory pathway

During antibody specificity testing, a strong perinuclear Syap1 signal was observed which was reminiscent of that of the position of the Golgi apparatus in the cell. To test for a possible co-localization, several co-stainings were pursued using different Golgi markers in different cell types.

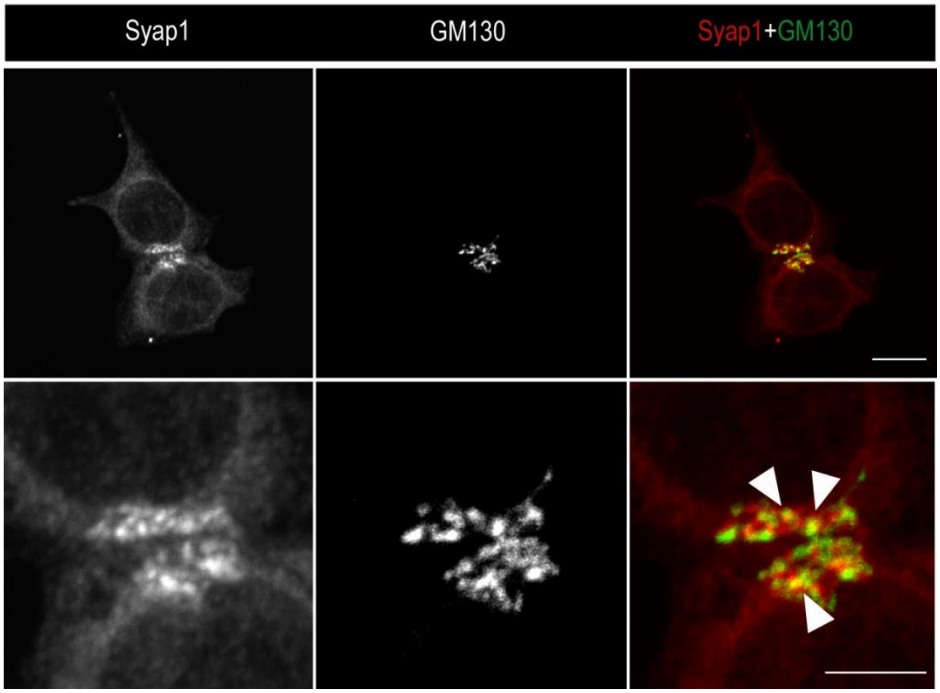

Figure 7: Co-stainings of Syap1 with GM130 in HEK293T cells

Representative images of the z-stacks are presented. Syap1 was distributed in a punctated manner and detected throughout the cytoplasm with a strong perinuclear accumulation close to the *cis*-Golgi compartment labeled by

anti-GM130 antibody. A few spots both of the obtained immunosignals were co-localizing, marked by the arrowheads in the magnification. Syap1 seems to accumulate in close proximity to the *cis*-Golgi but does not show an obvious co-localization. Some Syap1 immunofluorescence was also detected the nucleus. Scale bars: upper panel: 10 µm; lower panel: 5 µm.

In HEK293T cells, Syap1 is distributed in a similar manner as observed in primary motoneurons in the antibody specificity test. Syap1 is observed in the cytoplasm in a spotted manner and accumulates next to the nucleus (Figure 7, upper panel). Co-staining with the *cis*-Golgi marker GM130 (Golgi matrix protein of 130 kDa; (Nakamura et al. 1995)) revealed that Syap1 staining only occasionally overlaps with this part of the organelle but is found in close proximity to it. Only minor Syap1 immunofluorescence signals were detected in the nucleus.
Next, NSC34 cells were tested as well for their Syap1 distribution. Figure 8 clearly shows, that also in this mouse cell line, Syap1 distributes throughout the cytoplasm and accumulates near the *cis*-Golgi.

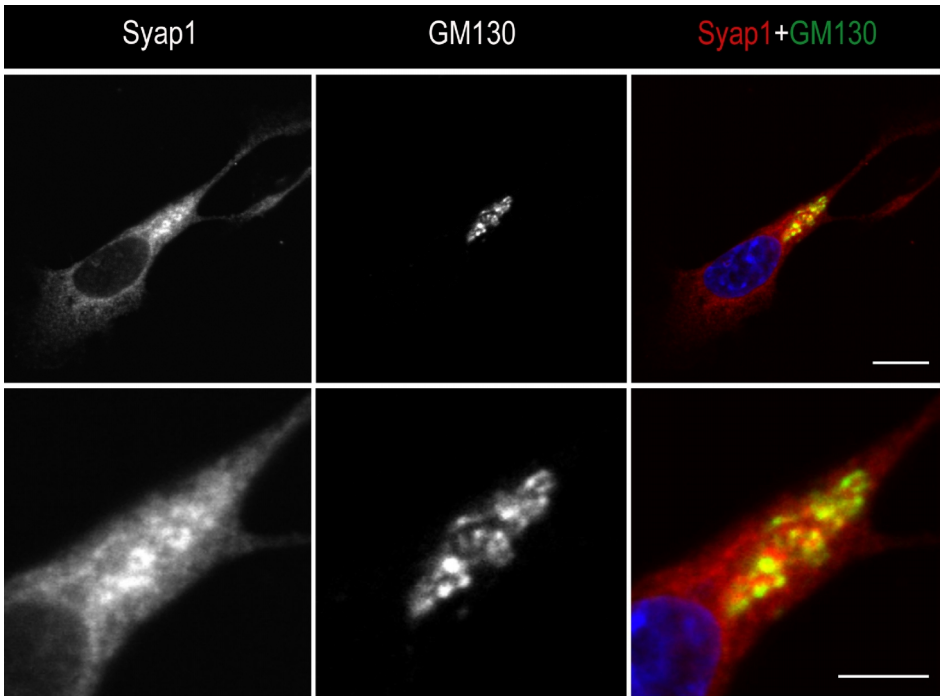

Figure 8: Co-stainings of Syap1 with GM130 in NSC34 cells
Representative images of the z-stacks are shown. Stainings revealed a cytoplasmic dotted pattern with an accumulation next to the nucleus. Only a few overlapping signals were obtained (arrowheads in magnification; lower panel). Scrutiny of individual sections indicates that Syap1 seems to be largely absent from the nucleus. Scale bars: upper panel: 10 µm; lower panel: 5 µm

As observed in HEK293T cells, only little overlapping signal with the *cis*-Golgi was obtained (Figure 8, lower panel) in NSC34 cells while only weak Syap1 immunoreactivity was observed in the nucleus.

To define the accumulation of Syap1 in the perinuclear region in primary motoneurons (Figure 6A and B), as well, super-resolution microscopy (Figure 9G-J) was performed after Syap1 and GM130/γ-adaptin co-staining (Figure 9A-F).

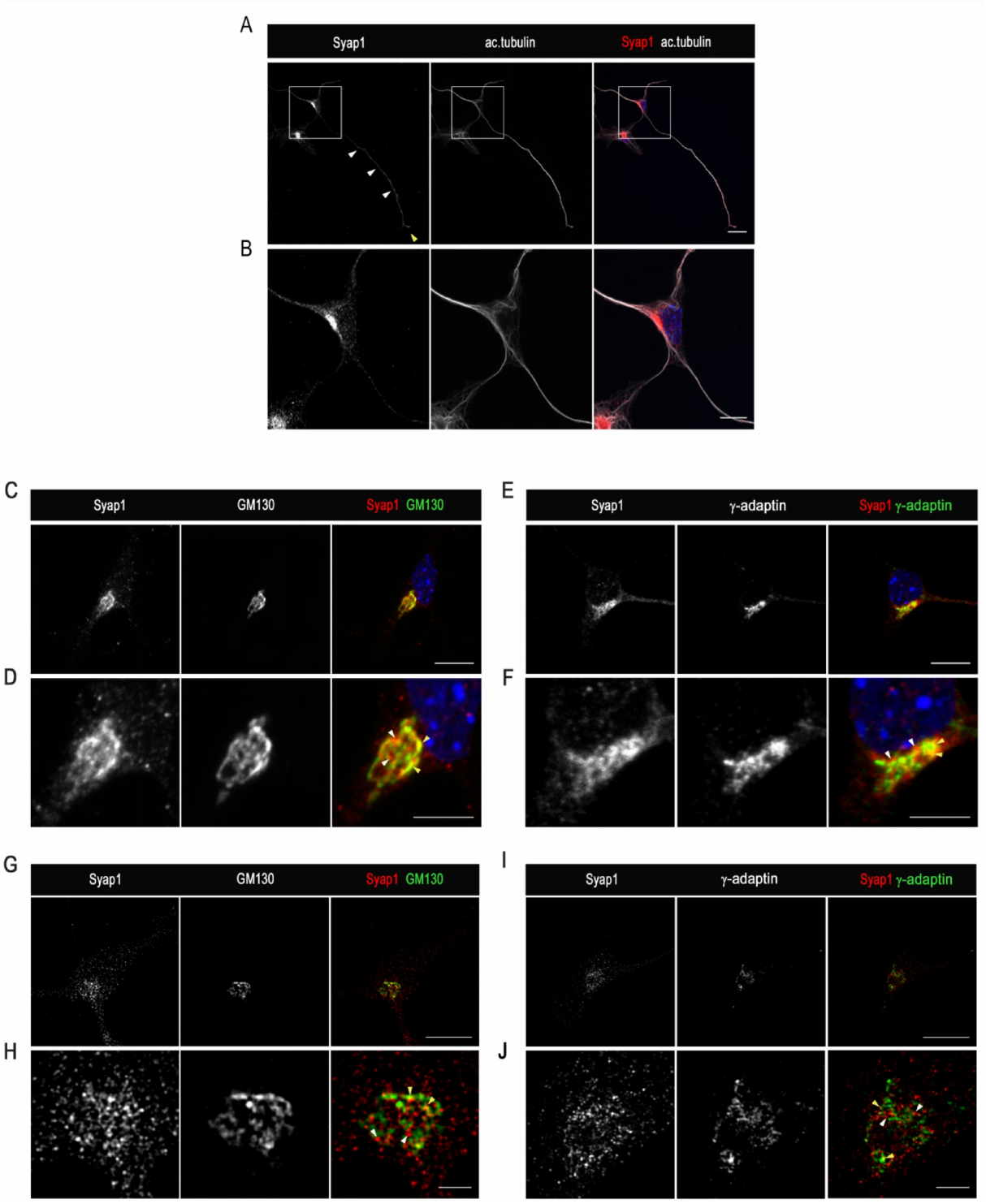

Figure 9: Co-stainings of Syap1 with acetylated tubulin/γ-adaptin and GM130 in motoneurons.
(A-F) Representative images of the z-stacks are depicted. (A) Immunofluorescence studies indicate that Syap1 is present in all compartments of a motoneuron. Positive Syap1 signals were observed in the soma, dendrites, axon (white arrow heads) and also in the distal part of the axon (yellow arrow head). A very prominent enrichment of Syap1 was detected next to the nucleus (B). Syap1 was detected in close proximity to the *cis*-Golgi marker GM130 (C and D) as well as to the *trans*-Golgi labeled by γ-adaptin (E and F). Co-stainings revealed a partial overlap of Syap1 with both labels (yellow arrow heads); in some regions only Syap1 positive immunoreactivity (white arrowheads) was observed. Single plane super-resolution imaging (G-J) of Syap1 with GM130 or γ-adaptin also revealed a perinuclear Syap1 accumulation with only rare co-occurrence of both labels (yellow arrow heads). Most of the Syap1 signal did not show an overlap with GM130 or γ-adaptin (white arrow heads). A few Syap1 signals were also detected in the nucleus. Scale bars: A: 25µm, B, C, E, G, I: 10µm; D, F: 5 µm; H, J: 2.5 µm

The highly reproducible and - as far as tested - obviously cell type independent perinuclear accumulation of Syap1 protein can also be observed in primary motoneurons (Figure 9A-J). As already shown in Figure 9A and B, Syap1 is present in dendrites, soma, axon and the distal part (yellow arrowhead in Figure 9A) of the axon. Co-labeling with *cis*- and *trans*-Golgi marker only revealed partial overlap with these structures indicated by yellow arrowheads (Figure 9Dand F). Super-resolution analyses of the distribution were consistent with the results obtained by confocal microscopy (Figure 9G-J). Spotted Syap1 signals are dispersed throughout the cytoplasm and show only rare co-occurrence with the *cis*-Golgi marker GM130 and the *trans*-Golgi labeled by γ-adaptin (yellow arrowheads in magnification of Figure 9H and J). Some Syap1 positive signals are also observed within the nucleus (Figure 9B, D, F, H and J).

Since only few overlapping signals of Syap1 and the Golgi markers GM130 and γ-adaptin were observed, another marker was used in order to define the perinuclear accumulation. The *cis*-Golgi represents only the entry site of the Golgi consisting of fused and concentrated transport intermediates coming from the ER-intermediate Golgi compartment (ERGIC) (Klumperman 2011). By using an antibody against GM130 and γ-adaptin, the *medial*-Golgi was not labeled by these markers. Therefore, co-stainings with COPI antibody were performed to distinguish all sides of the Golgi (see introduction).

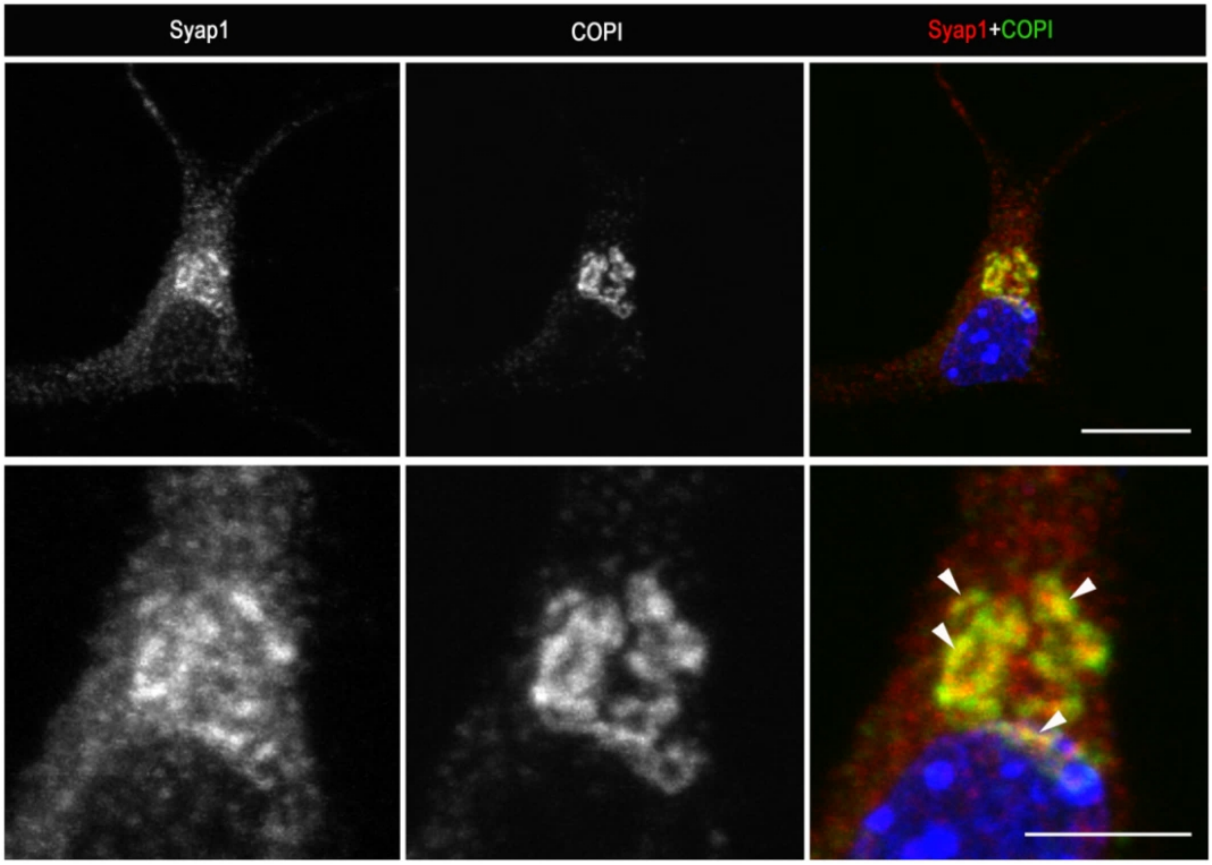

Figure 10: Co-stainings of Syap1 with COPI in motoneurons
Representative images of the z-stacks are shown. COPI staining revealed a prominent perinuclear signal which is overlapping with Syap1 in some points (arrowheads in magnification). Scale bars: upper panel: 10 µm; lower panel: 5 µm

By co-staining with a monoclonal COPI antibody, similar results were obtained compared to co-immunolabeling with GM130. Syap1 protein only partially overlaps with COPI signals but nevertheless this overlap it seems to be more extensive than with the GM130 marker (Figure 10). This would argue for a more *medial*- to *trans*-Golgi accumulation of Syap1.

Besides the strong perinuclear COPI signal in the ER and Golgi region, some single COPI positive spots in the soma, dendrites and along the axon can be observed which might also represent COPI coated vesicles since Golgi and ER compartments are not restricted to the soma but also found in the axon and dendrites (Ori-McKenney et al. 2012; Ramirez and Couve 2011). To examine if these COPI positive structures co-localize with Syap1 apart from the perinuclear accumulation, images were taken again with increased photomultiplier tube (PMT) voltage settings (Figure 11).

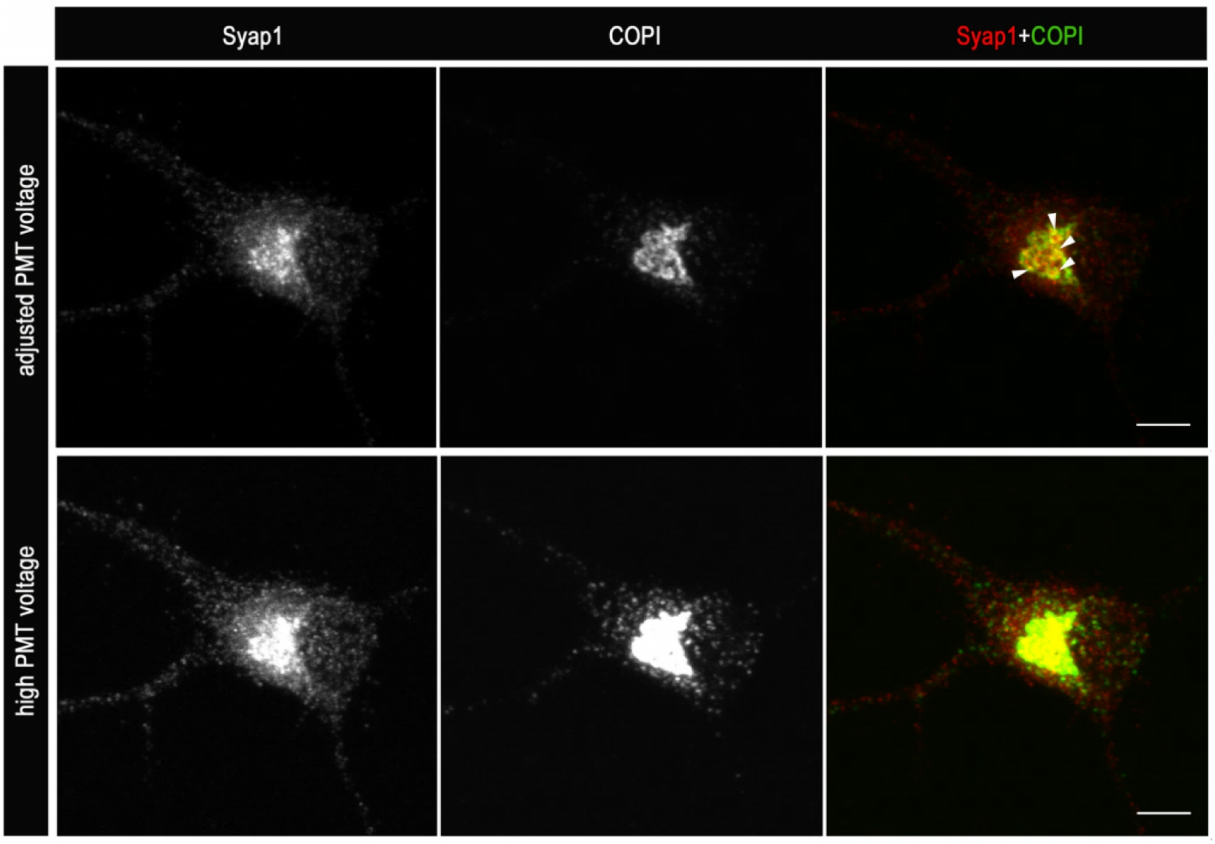

Figure 11: Co-staining of Syap1 with COPI in motoneurons with high PMT voltage
Representative images of the z-stacks are presented. Images were taken with adjusted PMT voltages (upper panel) and high PMT voltages (lower panel) to visualize also COPI positive structures besides the strong perinuclear signal. COPI staining revealed a prominent perinuclear signal which is overlapping with Syap1 in some points (arrowheads in upper panel). But Syap1, as well as COPI positive signals outside their perinuclear accumulation did not overlap (lower panel). Scale bars: 5 µm

Images obtained with adjusted PMT voltage settings revealed a reproducible partial overlap of Syap1 and COPI (Figure 11 upper panel) but the signals do not overlap apart from this perinuclear accumulation (Figure 11, lower panel). This suggests that Syap1 is not transported along with or in COPI coated vesicles.

After investigating a possible co-localization with structures of the ER-to-Golgi intermediate compartment (ERGIC; visualized by COPI staining), *cis*-Golgi (visualized by GM130 staining) and *intra*-Golgi (visualized by COPI staining) stainings against a *trans*-Golgi marker (TGN38) was included to define Syap1 localization. Triple-stainings with Syap1, GM130 and TGN38 were performed and the degree of overlap of Syap1 with the *trans*-Golgi was investigated.

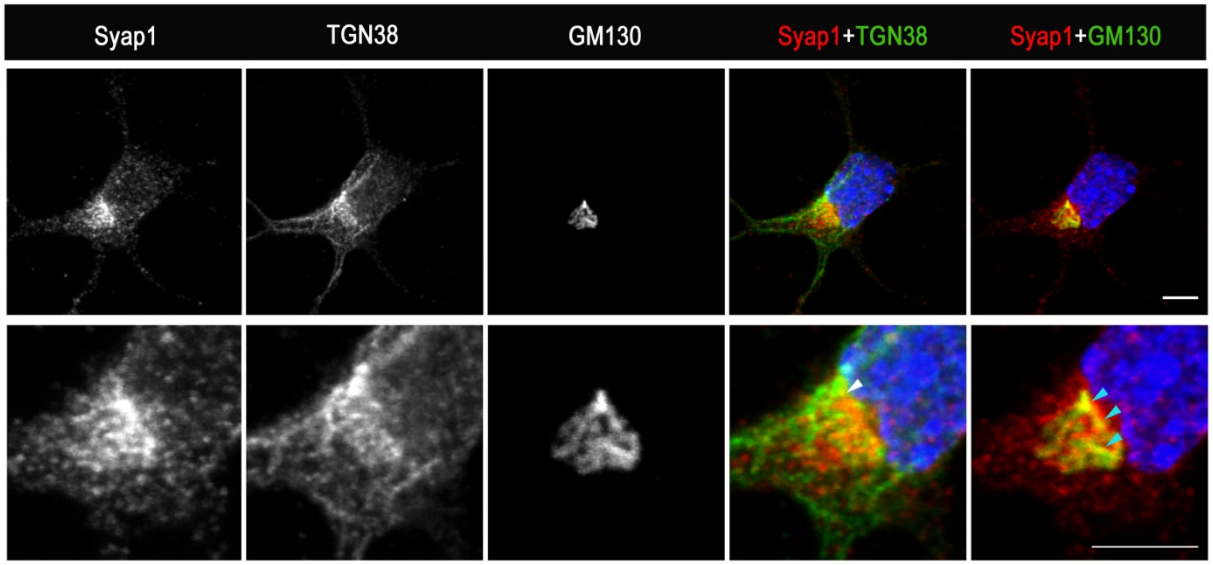

Figure 12: Co-stainings of Syap1 with GM130 and TGN38 in motoneurons
Representative images of the z-stacks are shown. A clear perinuclear Syap1 accumulation was observed which partially overlapped with the *cis*-Golgi (cyan arrowheads in the magnification) whereas almost no overlap was observed with the trans-Golgi marker TGN38 (white arrowhead in the magnification). Scale bars: 5 µm

Investigation of the triple-staining reveals a partial overlap for Syap1 and GM130 (Figure 12) signals as observed with structured illumination microscopy. Images from co-staining with TGN38 shows only minimal overlap with signals of Syap1 which seems to be largely excluded from the *trans*-Golgi network in the perinuclear region as well as in the axonal and dendritic compartment (Figure 12, lower panel).

Besides the Golgi network the endoplasmic reticulum is also known as a distinct perinuclear structure. Since overlapping signals of Syap1 with any of the Golgi markers was only observed partially, co-immunostainings were carried out with an ER marker (Calnexin) together with a marker against a component of the adaptor protein complex 1 (AP-1) which represents an adaptor for the clathrin coat (see 1.5).

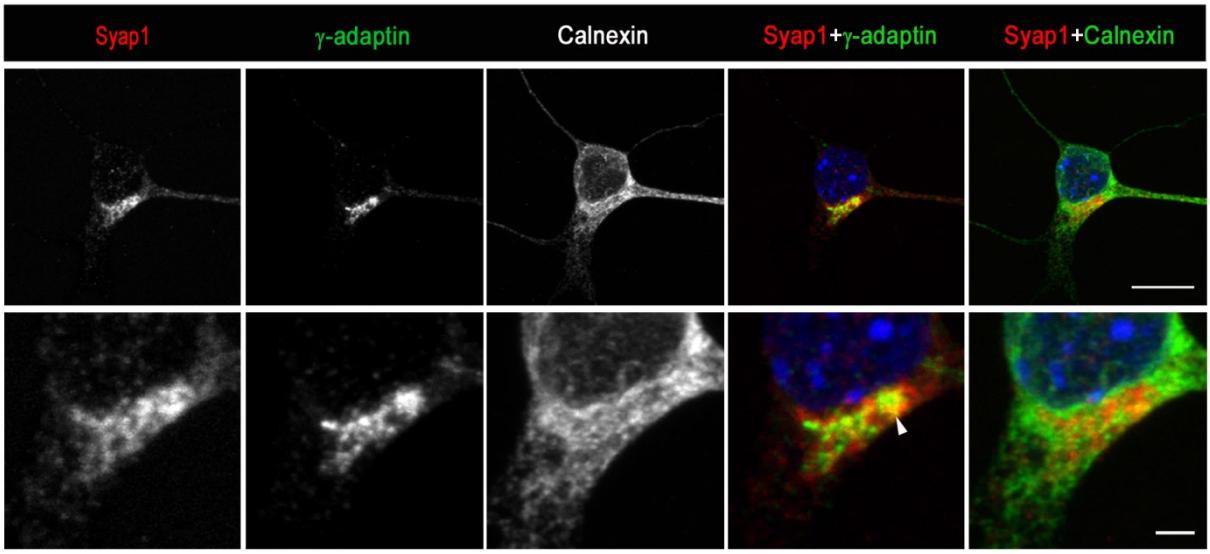

Figure 13: Co-stainings of Syap1 with Calnexin and γ-adaptin in motoneurons
Representative images of z-stacks of cultured primary motoneurons which were stained against Syap1, γ-adaptin and Calnexin. Syap1 signals did not show extensive overlap with Calnexin; also only minor overlapping signals were observed with γ-adaptin (arrowhead in lower panel). Scale bars: upper panel: 10 µm, lower panel: 5 µm

Immunocytochemical analyses revealed nearly no overlap in the signals from Syap1 and Calnexin in the perinuclear region. Only minor overlap was observed by co-staining against γ-adaptin at the region of Syap1 accumulation. There was also no indication of a co-localization of these two proteins in the periphery (Figure 13). This could indicate that Syap1 is not transported along with this subtype of clathrin coated vesicles which are accomplishing the anterograde transport from the *trans*-Golgi network to endosomes (Heilker et al. 1999) and are also believed to have a role in the recycling from endosomes to the TGN (Meyer et al. 2000).

3.2.2 Brefeldin A treatment disrupts Golgi association of Syap1

The close proximity of Syap1 to the Golgi compartment observed in several immunostainings suggested a strong association with the secretory pathway. In order to address whether a pharmacologically evoked Golgi fragmentation also causes disruption of the observed Syap1 accumulation - which would underscore its association with this cell organelle - cultured primary motoneurons were treated with Brefeldin A for 30 min. Brefeldin A reversibly inhibits ARFs (ADP-ribosylation factors) and thereby prevents the binding of COPI coats to Golgi membranes resulting in their complete vesiculation and fusion with the endoplasmic reticulum (Fujiwara et al. 1988; Doms et al. 1989; Lippincott-Schwartz et al. 1989; Donaldson

et al. 1992). Control cells were treated with DMSO for the same time. Another set of cells was treated in parallel with BFA for 30 minutes and the toxin was washed out enabling a reassembly of the Golgi apparatus. Subsequently, the motoneurons were PFA-fixed and stained against Syap1 and GM130 and imaged.

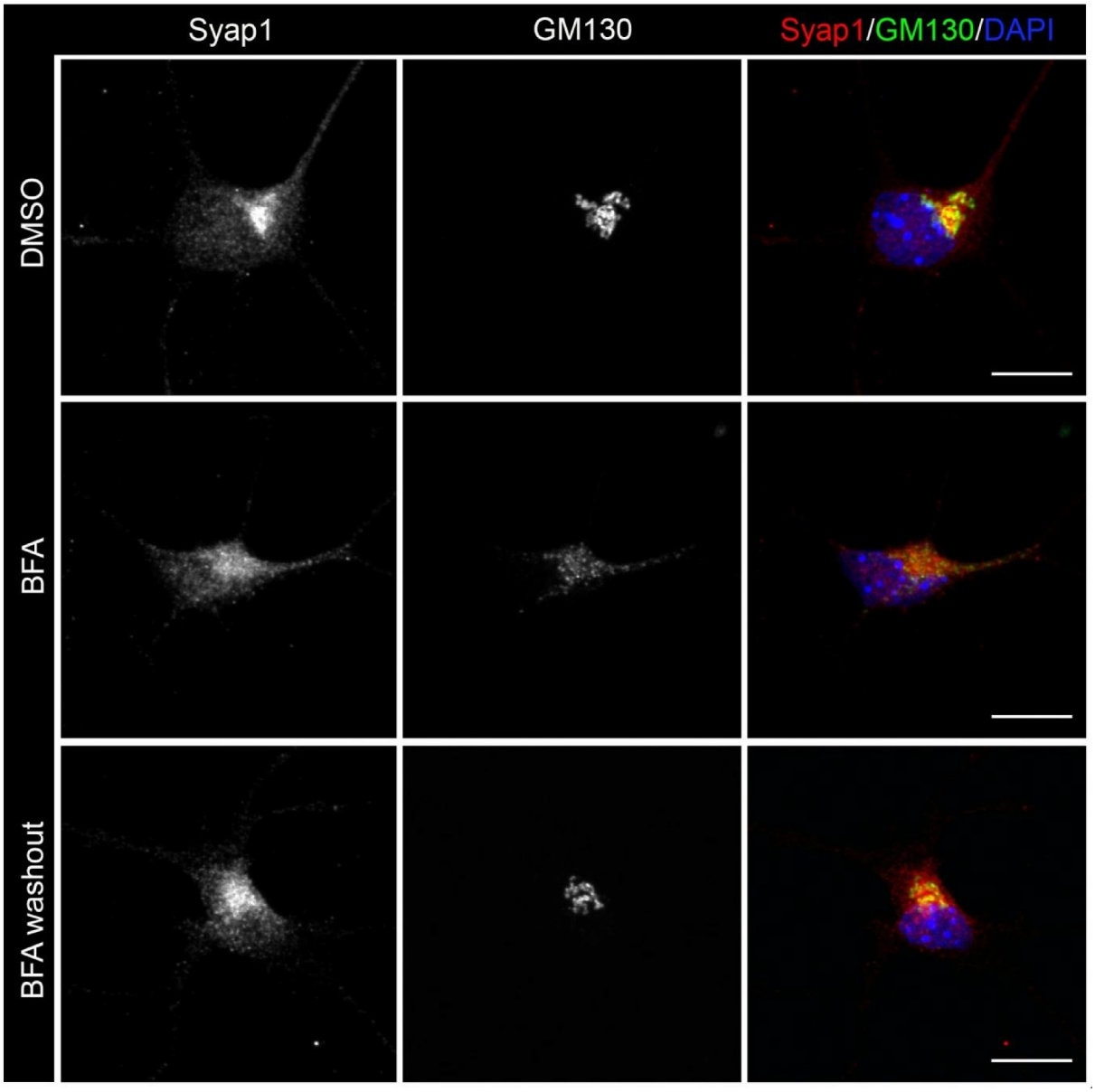

Figure 14: Localization of Syap1 protein after Golgi fragmentation

In motoneurons treated with a vehicle (DMSO) the typical Syap1 accumulation in close proximity to the Golgi apparatus can be observed (upper panel). After 30 min of BFA treatment the dissociation of the Golgi is clearly recognized by GM130 labeling (middle panel) showing dispersed Golgi elements throughout the cytoplasm. Similarly, Syap1 seems to lose its characteristically perinuclear accumulation, also distributing in a punctated manner in the cytoplasm. After washout and two hours of additional incubation in culture medium, the structure of the Golgi apparatus and perinuclear accumulation of Syap1 are recovered with a clearly distinguishable perinuclear localization (lower panel). Scale bars: 10 µm

In the control situation (DMSO) Syap1 was strongly enriched near the Golgi apparatus (Figure 14, upper panel) which was marked with a GM130-antibody. In BFA treated motoneurons this accumulation consistently disappeared resulting in a rather homogeneous distribution of Syap1 throughout the cytoplasm (Figure 14, middle panel) and thereby following the Golgi dissociation. This indicates that Syap1 accumulation at the Golgi might depend on intact vesicular transport mechanisms. When BFA was washed out and the cells further incubated for two hours in culture medium, the assembly of the Golgi as well as the accumulation of Syap1 close to this compartment was largely restored. Since the accumulation which was observed for DMSO treated neurons was slightly stronger than after the washout, the duration of reassembly might be prolonged in further experiments.

3.2.3 Syap1 is found in cytosolic and membranous fractions

Since the distribution pattern of Syap1 *in vivo* and *in vitro (*see 3.2.1 and 4.5) suggests a possible implication in trafficking and/or secretory pathways, a crude subcellular fractionation of cultured NSC34 cells was performed to test the localization by a biochemical approach. This method described by Holden and Horton (2009) allows a separation of cytosolic, membrane bound, nuclear and insoluble proteins using different buffers of increasing stringency for fractionation. Each fraction was then subjected to Western blot analysis and the efficacy of fractionation determined using suitable makers.

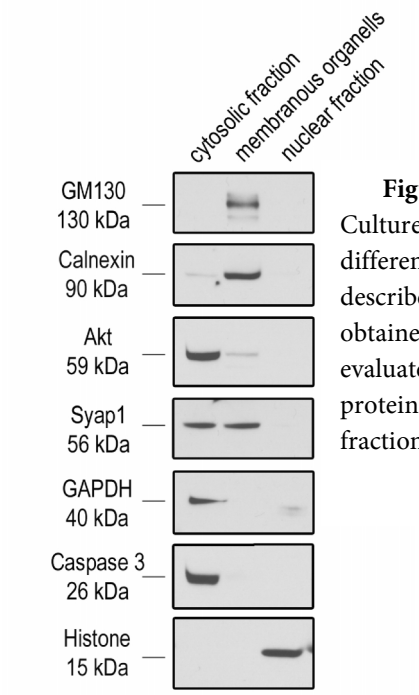

Figure 15: Crude subcellular fractionation of NSC34 cells
Cultured NSC34 cells were fractioned by using lysis buffers with differently stringency combined with several centrifugation steps as described in Holden and Horton (2009). Equal volumes of the obtained fractions were subjected to Western blot analysis and evaluated using appropriate markers for each fraction. Syap1 protein was detected in cytosolic as well as in membranous fraction.

The blot in Figure 15 shows that a proper fractionation was achieved since the proteins used as controls were found in the respective fractions. By this method GAPDH, pan-Akt and Caspase 3 were successfully enriched in the cytosolic fraction. The integral membrane proteins GM130 and Calnexin were only observed in the membrane fraction after extraction with NP40. Histone 3 was merely detected using a RIPA buffer for complete solubilization of nuclei and digestion of genomic DNA. In comparison with these marker proteins, Syap1 was enriched in the cytosolic fraction and the membranous fraction. This is compatible with the detection of Syap1 staining in NSC34 cells (and also other cell types) where the protein is detected in the cytosol and at the Golgi compartment (Figure 8). In the nuclear fraction, no signal for Syap1 was observed.

3.2.3 Syap1 is present in axonal growth cones and synaptic vesicles

In immunohistochemical preparations in *Drosophila* using the monoclonal antibody nc46, which recognizes the Syap1 homologue Sap47, selectively synaptic terminals were stained (Hofbauer et al. 2009; Reichmuth et al. 1995). Furthermore Sap47 was reported to localize in the boutons of larval neuromuscular junctions (Reichmuth et al. 1995) and was detected in close proximity to synaptic vesicles in motoneuron terminals of wild type larvae by immuno-electron microscopy (Saumweber et al. 2011). In order to investigate if Syap1 is also present in

growth cones of cultured primary motoneurons the cells were stained against Syap1 and phalloidin. This toxin binds specifically to F-actin which is highly abundant in the axon terminals (Forscher and Smith 1988) and thereby the entire structure of the growth cone was visualized (Figure 16).

Images in Figure 16 show that Syap1 protein can be detected in axon terminals of cultured primary motoneurons as the observed signal was reduced after *Syap1* knockdown. The protein localizes to the axonal shaft as well as to the tips of the finger-like filopodia.

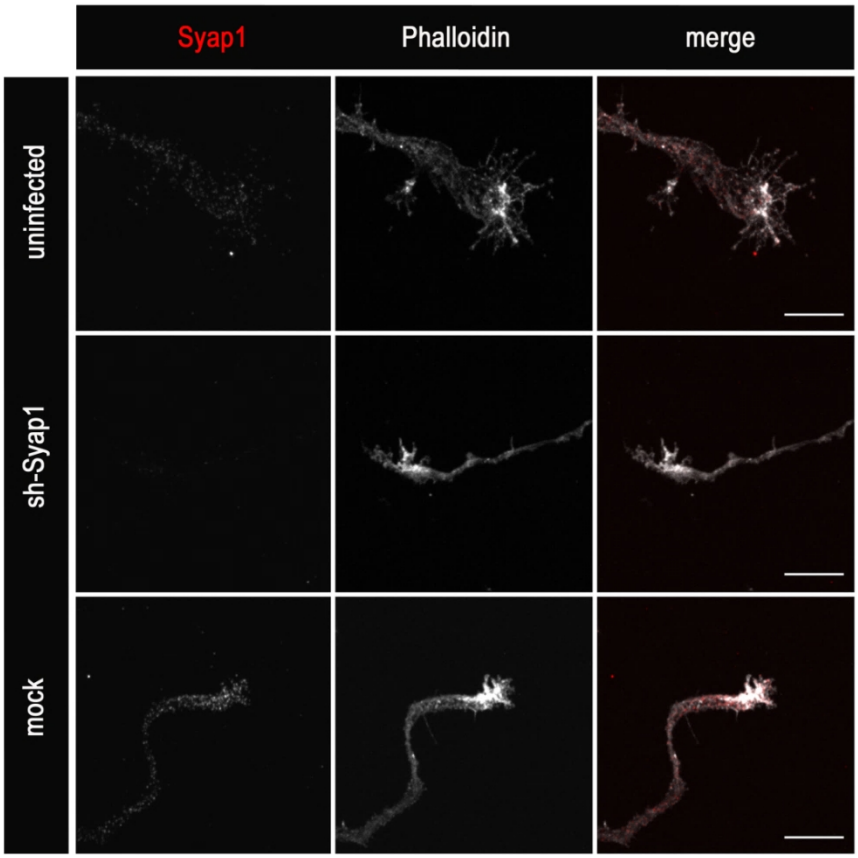

Figure 16: Syap1 is present in the axonal growth cone of motoneurons
Uninfected, sh-Syap1 and mock infected motoneurons were cultured for 5 DIV, fixed and stained against Syap1 and phalloidin. The images show that Syap1 signal was detected in both controls whereas a robust reduction of Syap1 immunofluorescence was observed after knockdown. Syap1 seems to be present in the axonal shaft as well as in the finger-like filopodia. Scale bars: 10µm

To further validate the immunocytochemical data with biochemical evidence that Syap1 is present in synapses, a crude synaptic vesicle isolation experiment was performed and the various fractions were analyzed by Western blot.

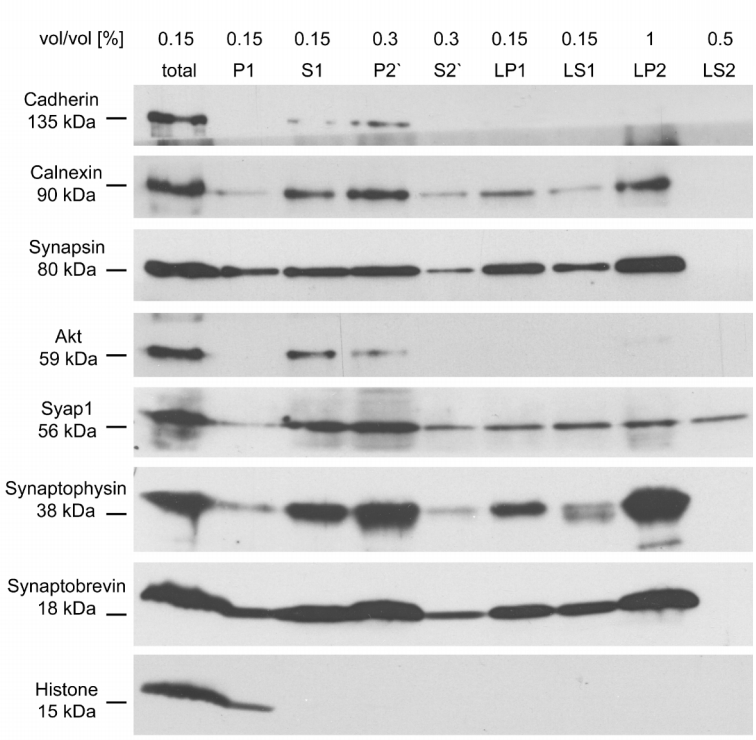

Figure 17: Crude synaptic vesicle fractionation from mouse brain Homogenized brains were fractioned by differential centrifugation. Samples were stored from each fraction and subjected to Western blot analysis to test for the presence of Syap1 in synaptosomes and synaptic vesicles. Appropriate markers for different fractions were used to control fractionation. In this experiment, Syap1 was present in each of the fractions with only minor portion in fraction P1 (unopened cells and cell debris). Markers for synaptic vesicles (Synaptobrevin, synaptophysin and synapsin) were highly enriched in the synaptic vesicle fraction LP2.

Figure 17 shows a representative Western blot of a crude synaptic vesicle fractionation from homogenized mouse brains illustrating the content of Syap1 and certain marker proteins in the different fractions. The purification protocol used was simplified from (Hell and Jahn 2006) (see2.2.11) and therefore results only in a very crude enrichment of synaptic vesicles, since a last centrifugation step on a sucrose gradient and chromatography on controlled pore glass beads (CPG) were not performed. It is important to note that in this context the investigated proteins can only qualitatively be compared between the resulting pellets and supernatants since different volumes per fraction after each centrifugation step were subjected to Western blot analysis (due to restricted loading capacity). A conclusion about the yield of enrichment when compared to the total lysate cannot be drawn. Protein markers from the same fractions can be compared, however.

From the total lysate (lane 1), pellet 1 (P1) and S1 were obtained in the first centrifugation step. P1 contains nuclei, unopened cells and large cell debris whereas the remaining cell organelles and cytoplasmic proteins are found in S1. Most of the proteins investigated in this experiment are found in S1 except Histone which represents a successful removal of all nuclei and unopened cells. S1 was then further divided in S2' and P2' by another centrifugation. P2' represents a crude fraction of isolated nerve terminals (synaptosomes). Such synaptosomes

are artificially produced synaptic structures which are formed during mild disruption of brain tissue, when the nerve terminals detach from their axons and connected postsynaptic and glial cells. Subsequently, synaptosomes are formed when the membranes of the pinched-off presynaptic boutons reseal and enclose the nerve terminal contents. These structures then contain the entire presynaptic terminal including cytoplasm, cytoskeleton, mitochondria, external membranes and synaptic vesicles and also parts of the attached postsynaptic side (e.g. membranes and postsynaptic density) (Schrimpf et al. 2005). In the crude synaptosomal fraction P2', most of the investigated proteins were enriched when compared to the supernatant S2'. Especially the marker for synaptic vesicles, Synaptobrevin (Baumert et al. 1989) and Synaptophysin (Wiedenmann and Franke 1985), were abundantly present which shows an effective fractionation. A strong band for Syap1 comparable to Synapsin – a marker for synapses (Thiel 1993) - was observed indicating that Syap1 could be indeed present in synaptosomes. This result was observed in all three independent experiments performed. The two transmembrane proteins Cadherin and Calnexin as well as Akt were also found in this crude synaptosomal fraction. Cadherins play an important role in cell adhesion being also responsible for linking pre- and postsynaptic sites (Arikkath and Reichardt 2008). Therefore they are to be expected in this fraction. Also Calnexin was recently reported to play a role at synaptic sites (Itakura et al. 2013). Akt is a cytosolic protein also found in synapses (Wang et al. 2003) and might for this reason be here detected in the P2' fraction. Nevertheless, contamination from one fraction to the other during the procedure could also be a possible reason. After the generation of a crude synaptosomal enrichment, the synaptic vesicles were released by an osmotic shock. Another high speed centrifugation step was performed to separate synaptic vesicles (LS1) from mitochondria, remaining Golgi apparatus and other membranous contaminations. Most of the investigated markers were still observed in fraction LP1. So, Calnexin which is an integral protein of the endoplasmic reticulum was pelleted down in this fraction. Syap1 was also found together with vesicle markers in the LP1 fraction. This could be due to contamination, improper opening of synaptosomes or due to the fact that Syap1 is attached to any of the components of these fractions. In the final centrifugation step the remaining synaptic vesicles in LS1 were pelleted down and are found in the crude

synaptic vesicle fraction LP2. It can be clearly observed that proteins integrated (Synaptobrevin, Synaptophysin) or attached (Synapsin) to the vesicle membrane are highly enriched in this fraction and absent from fraction LS2 indicating a low probability of contamination from LP2 to LS2. Syap1 was also observed but it was not enriched when compared to LS2 which only represented 0.5% of the total LS2 volume whereas 1% was loaded from LP2. This was consistent in all the three vesicle isolations which were performed.

The LS2 fraction represents proteins which are only weakly attached to synaptic vesicles or found in the lumen of the vesicles. Nevertheless, with this and even highly adopted purification protocols (Ahmed 2011) it is really difficult to exclude transport vesicles which are involved in the traffic between the endoplasmic reticulum and the Golgi apparatus. Those vesicles are also released during the initial homogenization. Therefore, a faint band of Syap1 in the "synaptic vesicle" fraction may also indicate an association of Syap1 with trafficking vesicles.

3.3 Syap1 protein is not restricted to synapses

The synapse-associated protein of 47 kDa in the fruit fly was initially discovered by screening a *Drosophila* cDNA expression library with the monoclonal antibody nc46 and was detected in most of the synaptic neuropil and in terminals of larval motoneurons (Reichmuth et al. 1995). Due to this synaptic localization and a molecular weight of 47 kDa in Western blot analysis, the protein was termed "synapse-associated protein of 47 kDa". However, Yao et. al. (2013) and Chang et al. (2001) already reported that *Syap1* mRNA is also present in several other tissues from human and mouse and not restricted to neurons since it was found for example in liver, heart, and fat tissue. To characterize Syap1 protein expression in the mouse and to obtain a first impression on the regional distribution in the nervous system equal amounts of protein lysates from adult mouse were subjected to Western blot analysis (Figure 18).

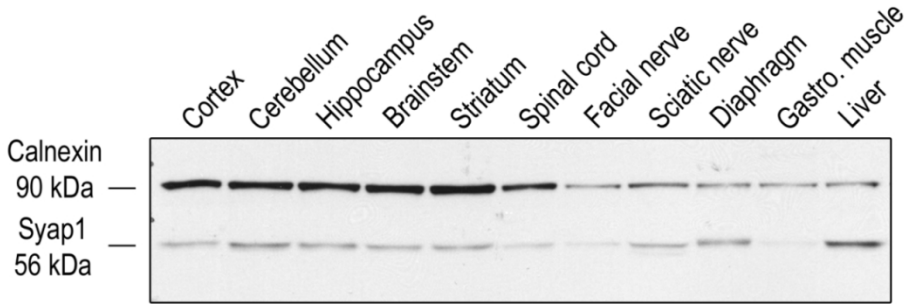

Figure 18: Syap1 protein expression several mouse tissues

Equal amounts of protein lysates from different mouse brain regions, two muscles and liver were subjected to Western blot analysis and the Syap1 expression pattern was investigated. The result reveals a consistent protein expression in all tested brain regions, in spinal cord, and in nerves. Furthermore, the protein was also detected in non-neuronal tissue such as muscle and liver.

The analysis of protein levels in different mouse tissues (Figure 18) revealed a clear and consistent abundance of Syap1 in all tested brain regions. The protein was also detected in the spinal cord, sciatic nerve and diaphragm at the expected molecular weight. Lower Syap1 levels were observed in the facial nerve and the gastrocnemius muscle. Consistent with previous mRNA data (Chang et al. 2001) and results from Yao et al. (2013), Syap1 was also found in non-neuronal tissues like muscles (gastrocnemius muscles and diaphragm) and liver indicating that it is not a nervous system-specific protein.

3.4 Functional analysis of Syap1 protein

It is well known that cultured primary motoneurons need neurotrophic factors for survival and growth of axons and dendrites. This allows studying the role of cell-independent factors and their impacts on several signaling pathways which are controlling axonal outgrowth and growth cone differentiation (Arakawa et al. 1990; Calof and Reichardt 1984; Sanes and Lichtman 1999; Sendtner et al. 2000). Therefore, the effect of *Syap1* knockdown on survival and axon elongation in primary motoneurons was first investigated. The graph in Figure 19A shows that *Syap1* knockdown did not affect the survival rate of primary motoneurons which were cultured for 7 DIV in the presence of BDNF. In comparison to the average survival of 63% for the uninfected control only a minor reduction to 60% (sh-Syap1) or 58% (mock) for the virus infected conditions was observed. A significant reduction to a survival of 23% was observed in the negative control when uninfected neurons were cultured without BDNF to prove that the survival in this assay is BDNF dependent.

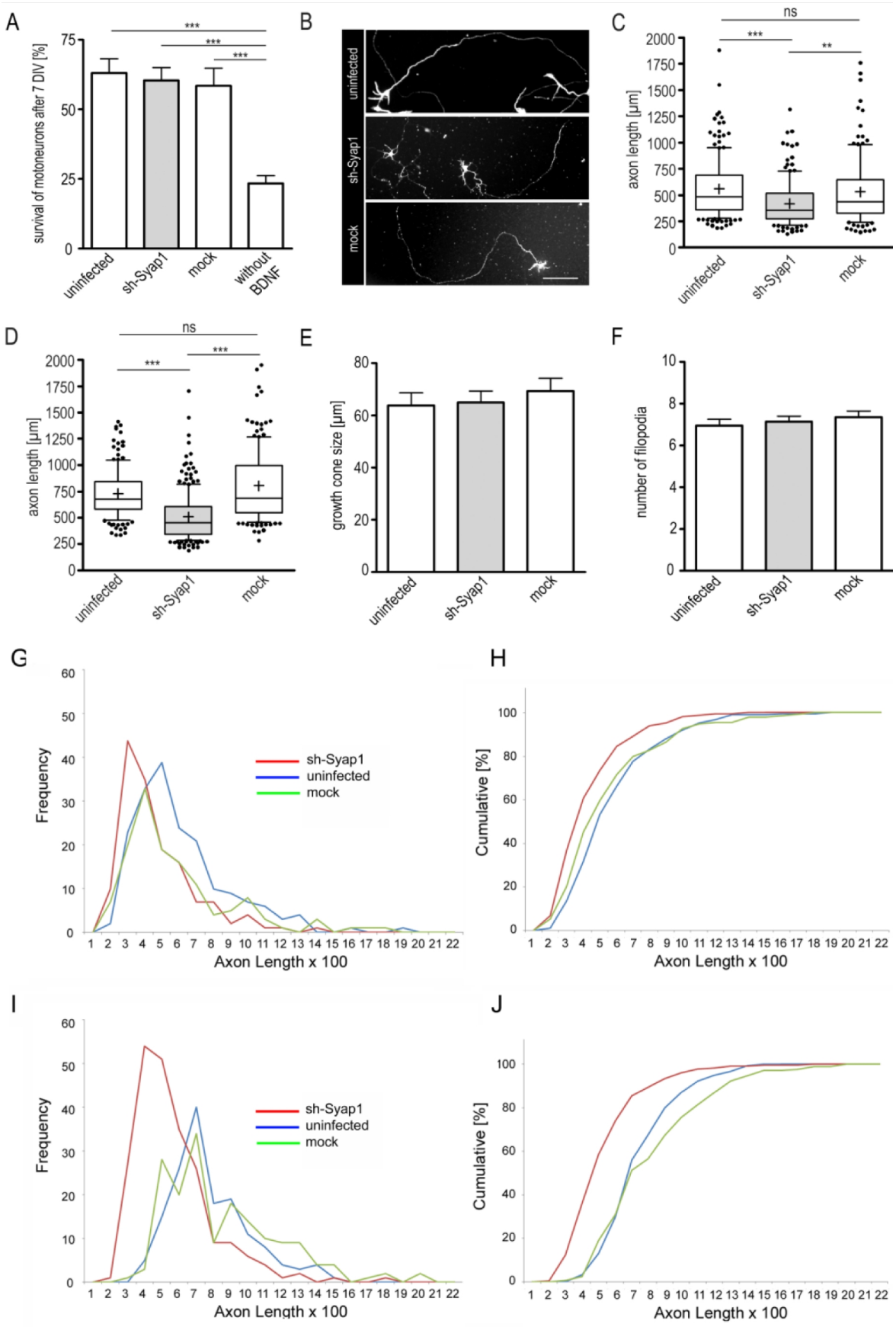

Figure 19: Functional effects of *Syap1* knockdown *in vitro*

(A) Analysis of motoneuron survival after *Syap1* knockdown. Primary motoneurons were cultured for 7 DIV in the presence of BDNF [5 ng/ml]. The cells were counted on day 1 and day 7 and the survival rate was calculated. No difference is observed upon *Syap1* knockdown compared to controls (uninfected and mock). To ensure that

the survival was BDNF dependent uninfected motoneurons were cultured in the absence of this neurotrophic factor. Under these conditions they show a significantly reduced survival rate (n = 7 independent cultures; one-way ANOVA with Bonferroni Post Hoc test; ***$P < 0.001$). (B) Representative images of seven days old motoneurons cultured in the presence of BDNF [5 ng/ml] which were fixed and stained against GFP and α-tubulin. Quantitative analysis of axon length after 5 DIV (C; n = 4 independent cultures; number of cells pooled per condition: uninfected: N = 183, sh-Syap1: N = 147, mock: N = 133; one-way ANOVA with Kruskal-Wallis test; ***: $P \leq 0.001$, **: $P > 0.01$; ns: $P < 0.05$) and 7 DIV (D; n = 3 independent cultures; number of cells pooled per condition: uninfected: N = 154, sh-Syap1: N = 227, mock: N = 168; one-way ANOVA with Kruskal-Wallis test; ***: $P \leq 0.001$, **: $P > 0.01$; ns: $P < 0.05$) revealed a significant reduction upon *Syap1* knockdown compared to controls. The following medians of axon length after 5 DIV were obtained: uninfected: 483.7 µm; sh-Syap1: 357.8 µm; mock: 434.9 µm (C). The medians after 7 DIV were: uninfected: 675.3 µm; sh-Syap1: 454.4 µm; mock: 687.1 µm (D). The growth cone size (E; one-way ANOVA with Kruskal Wallis test; n = 10 independent cultures, numbers of cells pooled per condition: uninfected: N = 75, sh-Syap1: N = 80, mock: N = 75; uninfected: 63.81 ± 4.87 μm^2; sh-Syap1: 64.90 ± 4.37 μm^2; mock: 69.26 ± 4.91 μm^2; ns > 0.05) as well as the number of filopodia (F; one- way ANOVA with Kruskal Wallis test; n = 9 independent cultures, number of pooled cells per condition: uninfected: N = 96, sh-Syap1: N = 95, mock: N = 94; uninfected: 6.95 ± 0.30, sh-Syap1: 7.14 ± 0.27, mock: 7.35 ± 0.30) was unaltered after *Syap1* knockdown in five days old motoneurons. (G – J) Frequency distributions and cumulative probabilities of axon lengths of uninfected, sh-Syap1 infected and mock infected motoneurons after 5 DIV (G, H) or 7 DIV (I, J) (class width 100 µm). Data in C and D represent medians with 1st and 3rd quartiles and 10th and 90th percentiles (boxes and whiskers, respectively). + = mean; • represent outliers. **: $P < 0.01$; ***: $P < 0.001$; ns: $P > 0.05$. Bars shown in A, E and F represent means ± SEM.

Primary motoneurons cultured for 5 or 7 DIV on laminin 111 in presence of BDNF [5 ng/ml] show a significant reduction in axon outgrowth upon *Syap1* knockdown by expression of the shRNA used here compared to the controls (Figure 19; 5 DIV; C, G, H and 7 DIV B, D, I and J). Although some *Syap1* knockdown motoneurons were able to reach the same maximum length after 5 DIV (~ 1,400 µm, Figure 19G and H) and after 7 DIV (~1,800 µm; Figure 19I and J) compared to controls, the majority of cells exhibit axons which were approximately 120 µm (after 5 DIV) and 200 µm (after 7 DIV) shorter than the controls. It is important to note already here that the shRNA used, which very effectively reduces Syap1 expression levels (see Figure 5), could also impair expression of other proteins due to off-target effects, such that the reduced axon length shown in Figure 19G-J may not be caused by reduced Syap1 levels (see 3.8.2).

There is evidence that disturbed growth cone formation can lead to a reduction in axon extension (Paglini et al. 1998; Rossoll et al. 2003). In order to determine if this is also true for the observed impaired axonal outgrowth after *Syap1* knockdown, primary motoneurons were cultured for 5 DIV fixed and stained with fluorescently labeled phalloidin. In addition, growth cone sizes of uninfected, mock infected and sh-Syap1 infected neurons were measured (Figure 19E) as well as the number of finger-like projections (filopodia; Figure 19F). There was neither

a difference in the size nor in the number of filopodia of the investigated growth cones. This suggests that Syap1 might not have an influence on the growth cone actin cytoskeleton since actin plays a major role in growth cone movement and neurite outgrowth (Jablonka et al. 2007; Rossoll et al. 2003; Yamada et al. 1970). Since growth cones tend to collapse after 7 DIV such that meaningful comparison of their sizes in no longer possible, growth cone size and number of filopodia were determined after 5 DIV (Bonanomi et al. 2008).

Besides the actin cytoskeleton, microtubules are key elements for neuronal stability and integrity. The properties of these highly conserved cytoskeleton components can be regulated by abundant and chemically diverse posttranslational modifications (PTMs). Tyrosination and acetylation were the first PTMs which were discovered (Arce et al. 1975; L'Hernault and Rosenbaum 1985) and are enriched in neurons (Song and Brady 2015). Tyrosinated tubulin is mainly found in highly dynamic compartments like the growth cones or dendrites as it represents the more instable pool of microtubules with a lifetime of a few minutes (Webster et al. 1987; Marcos et al. 2009; Baas and Black 1990) whereas acetylation is often found in long-lived MTs (lifetimes ~2-6 hours) (Bulinski et al. 1988) in the axons of mature neurons (Song and Brady 2015).

Recently, Yao et al. (2013) reported a crucial function of Syap1 in Akt activation. Furthermore, upon Akt deprivation a reduction in phosphorylation of the downstream targets S6K and GSK3β led to a decrease in axonal outgrowth *in vitro* due to their influence on MT stability (Diez et al. 2012; Scales et al. 2009; Onishi et al. 2007). Since a reduction in axon outgrowth was observed after *Syap1* knockdown, experiments addressing microtubule dynamics and stability were performed. Defects in proper MT assembly or stability can lead to shorter axons (Selvaraj et al. 2012; Schaefer et al. 2007; Rochlin et al. 1996). In order to pursue the hypothesis of altered MT dynamics or stability upon *Syap1* knockdown, total tubulin as well as acetylated and tyrosinated tubulin levels were investigated in cultured motoneurons. Hence, microtubule fractionations from control, mock infected and sh-Syap1 infected cells were performed separating the stable acetylated MTs from the highly dynamic tyrosinated tubulins (nascent MTs). In addition, a control which was treated with placitaxel for 2 hours – which stabilizes MTs by preventing depolymerization - was included to prove that effective

fractionation was achieved. Fractionation was performed with motoneurons cultured for 5 DIV which were lysed in microtubule stabilization buffer.

Figure 20 shows the immunoblot analysis of microtubule fractionation using specific antibodies against the posttranslational modification acetylation and tyrosination and an α-tubulin antibody detecting the tubulin irrespectively from its modification.

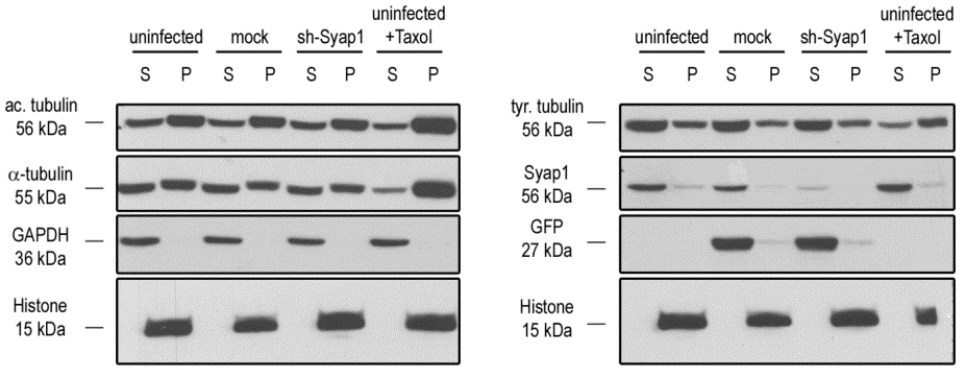

Figure 20: Microtubule fractionation with cultured primary motoneurons

Uninfected, mock infected and sh-Syap1 infected motoneurons were cultured for 5 DIV, lysed in microtubule fractionation buffer and fractionated by centrifugation (n = 3). Equal volumes of pellet and supernatant fraction were subjected to Western blot analysis and probed for pan-α-tubulin, acetylated tubulin and soluble tubulin. Acetylated tubulin (left blot) was predominantly found in the pellet fraction (P) whereas the tyrosinated tubulin (right blot) was mainly present in the supernatant (S). No differences in the precipitated (stable MTs) and soluble (nascent and dynamic MTs) tubulin levels were observed upon *Syap1* knockdown when compared to the uninfected and mock infected controls. To show the efficacy of fractionation, one control was treated with placitaxel prior to fractionation which stabilizes the microtubules. In line with expectations, most of the posttranslationally modified tubulin isoforms and accordingly the pan-tubulin were observed in the pellet and lower amounts in the soluble fraction. Histone and GAPDH served as loading and internal controls. The reduction of Syap1 protein upon lentiviral knockdown is demonstrated by Syap1 immunoblot signal (right blot).

Since acetylation at Lys40 only occurs on the existing MT polymer (Janke and Bulinski 2011) higher levels of these were pelleted down during centrifugation. Tyrosinated tubulin levels which represent the pool of αβ-heterodimers and nascent MTs were enriched in the supernatant. Alpha-tubulin was almost equally distributed among the fractions as expected. *Syap1* knockdown did not affect either fraction compared to the controls. This might indicate that neither the stability (indicated by acetylated tubulin levels) nor the dynamics represented by the incorporation of free αβ-heterodimers into the nascent MT is affected after Syap1 protein reduction. Therefore it is unlikely that the reduction in axon length is due to changes in MT stability or dynamics.

3.5 *Syap1* knockdown does not affect Akt phosphorylation in primary motoneurons

Recently, Yao et al. (2013) reported a crucial function of Syap1 in Akt phosphorylation in adipocytes upon growth factor stimulation. When Syap1 was depleted, the authors observed a significant reduction in Akt1 phosphorylation at Ser^{473}. In order to examine if the reduced axon length upon *Syap1* knockdown (Figure 19) is attributed to an incomplete phosphorylation of Akt, the experiments performed by Yao and colleagues were repeated in a similar way with cultured primary motoneurons.

In Panc28 cells maximal phosphorylation at Ser^{473} upon EGF stimulation occurred after 15 to 30 minutes and slightly decreased after 120 min (Yao et al. 2013). Since the kinetics of Akt phosphorylation at Ser^{473} and Thr^{308} in primary motoneurons could differ from the cell lines used by Yao and colleagues, the maximal phosphorylation levels were investigated. Serum and neurotrophic factor deprived motoneurons were stimulated with BDNF [20 ng/ml] for increasing durations ranging from 2 seconds to 30 minutes (Figure 21).

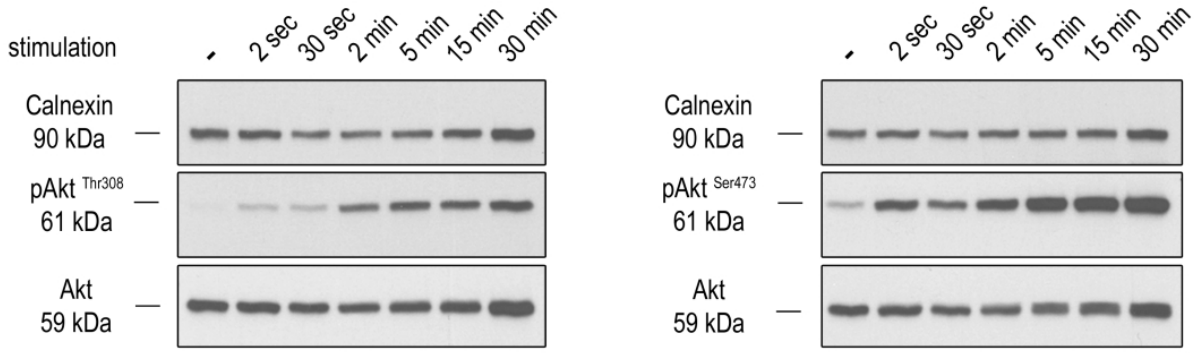

Figure 21: Akt phosphorylation kinetics in primary motoneurons

Motoneurons were cultured for 5 DIV, serum and neurotrophic factor starved overnight and subsequently stimulated with BDNF [20 ng/ml] for the indicated durations. Maximal phosphorylation at Ser^{473} and Thr^{308} was observed after 2-5 minutes. Calnexin and total Akt served as loading controls.

The results in Figure 21 show that cultured primary motoneurons already respond after 2 seconds of stimulation since a clear immunoblot signal was observed for both the investigated phosphorylation sites. Maximum Akt phosphorylation at Ser^{473} and Thr^{308} was observed after 2-5 minutes in cultured primary motoneurons. Similar phosphorylation levels still persisted up to 30 minutes of BDNF stimulation. These results indicate that the kinetics in response to a

neurotrophic factor in this cell type is faster than in Panc28 cells since the maximum phosphorylation at Ser^{473} was observed in after 5-15 minutes (see Yao et al., 2013; Figure 1B). This kinetics of Akt phosphorylation is consistent with findings performed with hippocampal neurons (Johnson-Farley et al. 2006; Johnson-Farley et al. 2007). For further studies of the impact of Syap1 protein on the Akt phosphorylation process at Ser^{473} in primary motoneurons, uninfected, mock and sh-Syap1 infected cells were stimulated for two or five minutes (Figure 22).

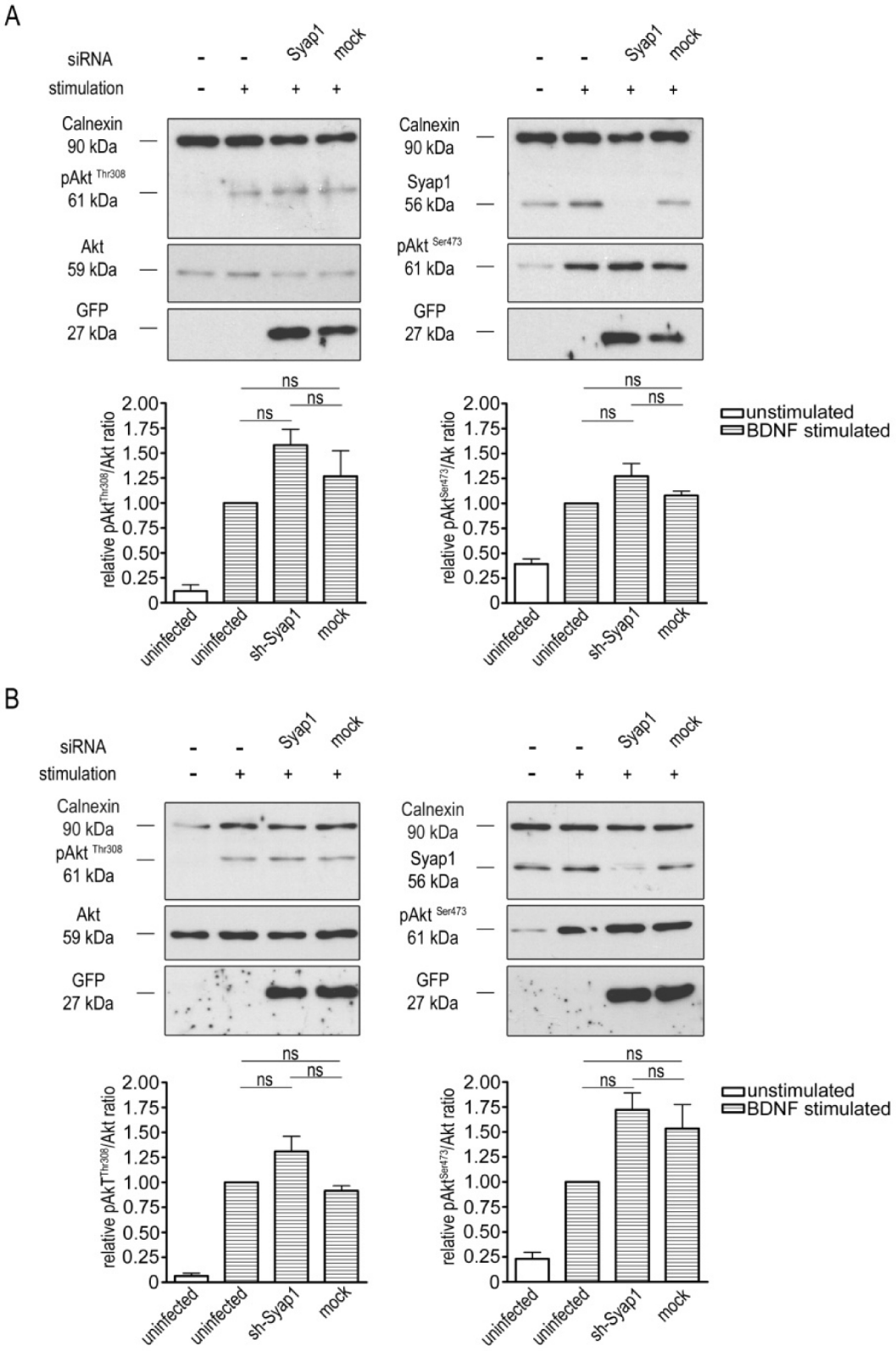

Figure 22: *Syap1* knockdown does not influence Akt phosphorylation at Ser^{473} and Thr^{308} in BDNF stimulated motoneurons

Primary motoneurons were cultured for 5 DIV, serum and neurotrophic factor starved overnight and stimulated for two (A) or five (B) minutes, respectively. Western blot analysis revealed no significant reduction in Ser^{473} or Thr^{308} phosphorylation levels after *Syap1* knockdown. Quantification for each phosphorylation site is depicted below the blot showing rather a tendency of an increase in phosphorylation at both sites than the expected reduction at Ser^{473} (n = 3; one-way ANOVA with Kruskal Wallis test; ns > 0.05). Bars shown represent means ± SEM.

Western blot analyses from uninfected, mock and sh-Syap1 infected cells being starved overnight and stimulated for two (Figure 22A) or five (Figure 22B) with BDNF [20 ng/ml] revealed no significant decrease in Akt phosphorylation levels at Ser^{473} or Thr^{308} upon *Syap1* knockdown compared to both controls. Statistical analyses from densitometric data (depicted below each blot) rather suggest a possible increase in phosphorylation at both sites for the two minute and five minute stimulation. There was no indication for a reduction in Ser^{473} phosphorylation as reported by Yao et al.

Next, since a reduction in axon length in *Syap1* knockdown motoneurons was observed when cells were grown in medium containing BDNF [5 ng/ml] without any further stimulation Akt phosphorylation levels in motoneurons were also investigated under these conditions (Figure 23).

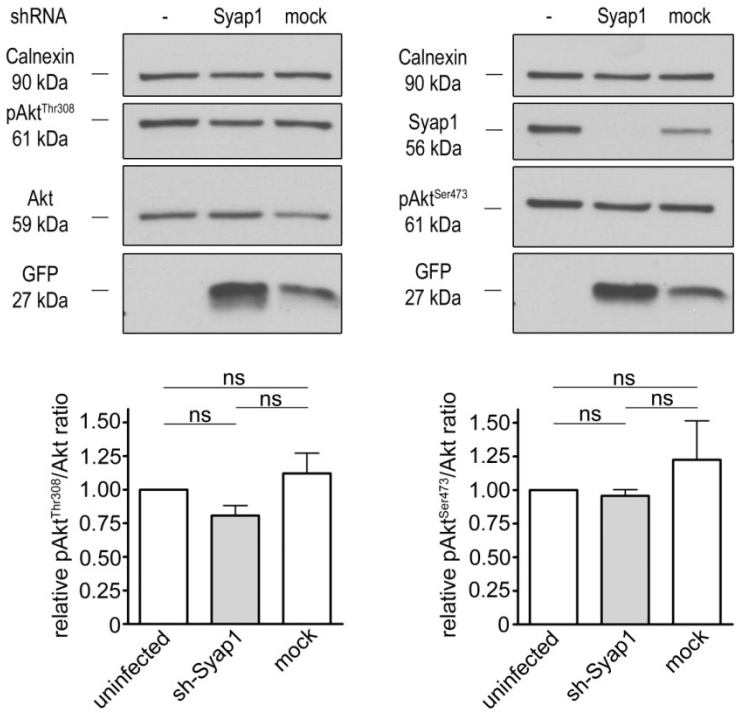

Figure 23: *Syap1* knockdown does not influence Akt phosphorylation at Ser^{473} and Thr^{308} in motoneurons
Motoneurons were cultured for 5 DIV in the presence of BDNF [5 ng/ml] without starvation and further stimulation and tested for effects of *Syap1* knockdown on Akt phosphorylation. Same volumes of cell lysates were subjected to Western blot analysis resulting in no significant reduction upon *Syap1* knockdown compared to the controls (depicted below in the quantitative analysis). Bars shown represent means ±SEM. Statistical analysis: one-way ANOVA with Kruskal Wallis test. Bars represent mean ± SEM.

Densitometric analysis from Western blots show that there is no significant reduction in Akt phosphorylation at Ser^{473} or Thr^{308} upon *Syap1* knockdown when primary motoneurons were cultured for 5 DIV in the presence of BDNF [5 ng/ml]. This indicates that the *Syap1* knockdown induced axonal outgrowth defect is not accompanied by reduced total Akt phosphorylation of the cells.

Nevertheless, the axon growth defect could also be caused by local changes in Akt phosphorylation in specific neuronal compartments upon *Syap1* knockdown. Such local changes could have been escaped detection in Western blot of total motoneuron lysates due to the high protein content of the soma. Therefore, phosphorylation levels in the soma, axon and growth cone of primary motoneurons were investigated separately by immunocytochemistry using Akt- and phospho- Akt^{Ser473}- specific antibodies. As described for Western blot analysis, the cells were also serum and neurotrophic factor deprived and stimulated for five minutes with BDNF [20 ng/ml]. The cells were immediately fixed and stained against GFP, Akt and pAkt^{Ser473} (Figure 24A). The immunocytochemical fluorescence signals were quantified for each compartment and each condition (unstimulated mock, stimulated mock, unstimulated sh-Syap1 and stimulated sh-Syap1) after 5 DIV (cultured in the presence of CNTF) and the mean intensity ratio of pAkt^{Ser473}/ Akt was then normalized to the unstimulated mock control. (Figure 24B). The graph clearly indicates that the pAkt^{Ser473} levels before and after stimulation did not differ between mock and sh-Syap1 infected cells in any of the investigated compartments of the motoneurons. These results are consistent with the data obtained from Western blots in Figure 22.

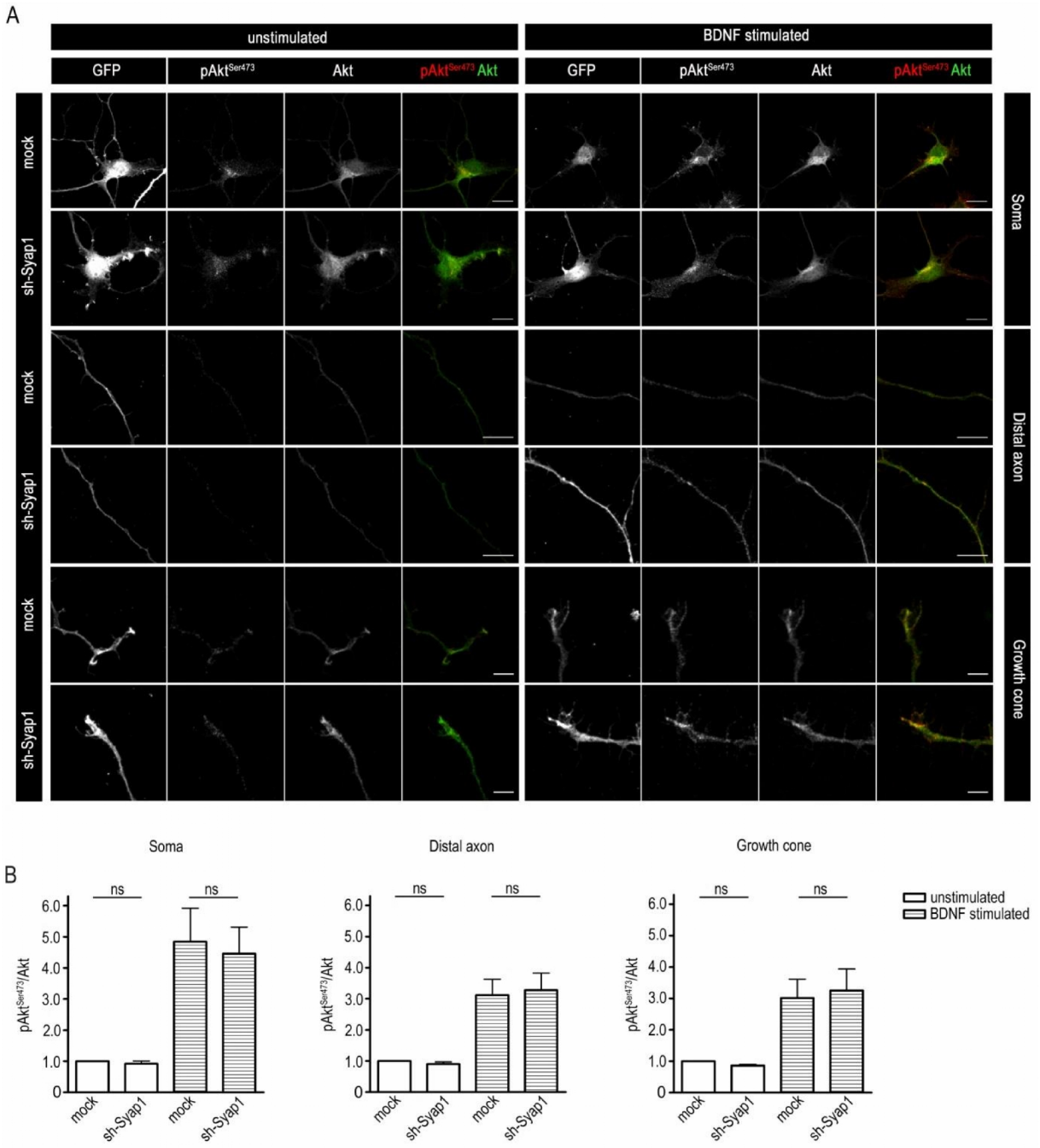

Figure 24: Compartment specific Akt phosphorylation in motoneurons after BDNF stimulation

Primary motoneurons were cultured for 5 DIV, serum and neurotrophic factor deprived and stimulated for 5 minutes with BDNF [20 ng/ml]. The cells were immediately fixed and stained against GFP, Akt and pAkt^{Ser473} to investigate a possible compartment specific difference in Akt phosphorylation levels after *Syap1* knockdown. Representative images of each compartment and condition before and after stimulation are shown in A (scale bars: soma and axon: 10 µm; growth cone: 5 µm). A strong increase of pAkt^{Ser473} fluorescence signal for mock infected and sh-Syap1 infected cells in each compartment were obtained after stimulation. (B) Quantification of pAkt^{Ser473}/Akt ratios revealed a strong increase of phosphorylation levels after BDNF stimulation in all compartments and conditions. No difference was observed in the relative pAkt^{Ser473} levels between mock infected and sh-Syap1 infected cells either before or after stimulation. The mean ratios measured per condition of an experiment were normalized to the corresponding mean of the unstimulated mock control (n = 5; one-way ANOVA with Kruskal Wallis test, total number of cells analyzed per condition: 78 – 93; soma: unstimulated sh-Syap1 infected: 0.92 ± 0.09; stimulated, mock infected: 4.85 ± 1.07; stimulated, sh-Syap1 infected: 4.46 ± 0.86; distal axon: unstimulated sh-Syap1 infected: 0.90 ± 0.07; stimulated, mock infected: 3.11 ± 0.51; stimulated sh-

Syap1 infected: 3.28 ± 0.55; growth cone: unstimulated, sh-Syap1 infected: 0.86 ± 0.04 ; stimulated, mock infected: 3.01 ± 0.60; stimulated, sh-Syap1 infected: 3.25 ± 0.70, $P > 0.05$). Data shown represent means ± SEM.

Similarly, Akt phosphorylation levels were examined under unstimulated conditions in DIV 5 motoneurons cultured in the presence of BDNF in order to test if a local change already occurs in an initial state when there is a sustained and basal Akt stimulation.

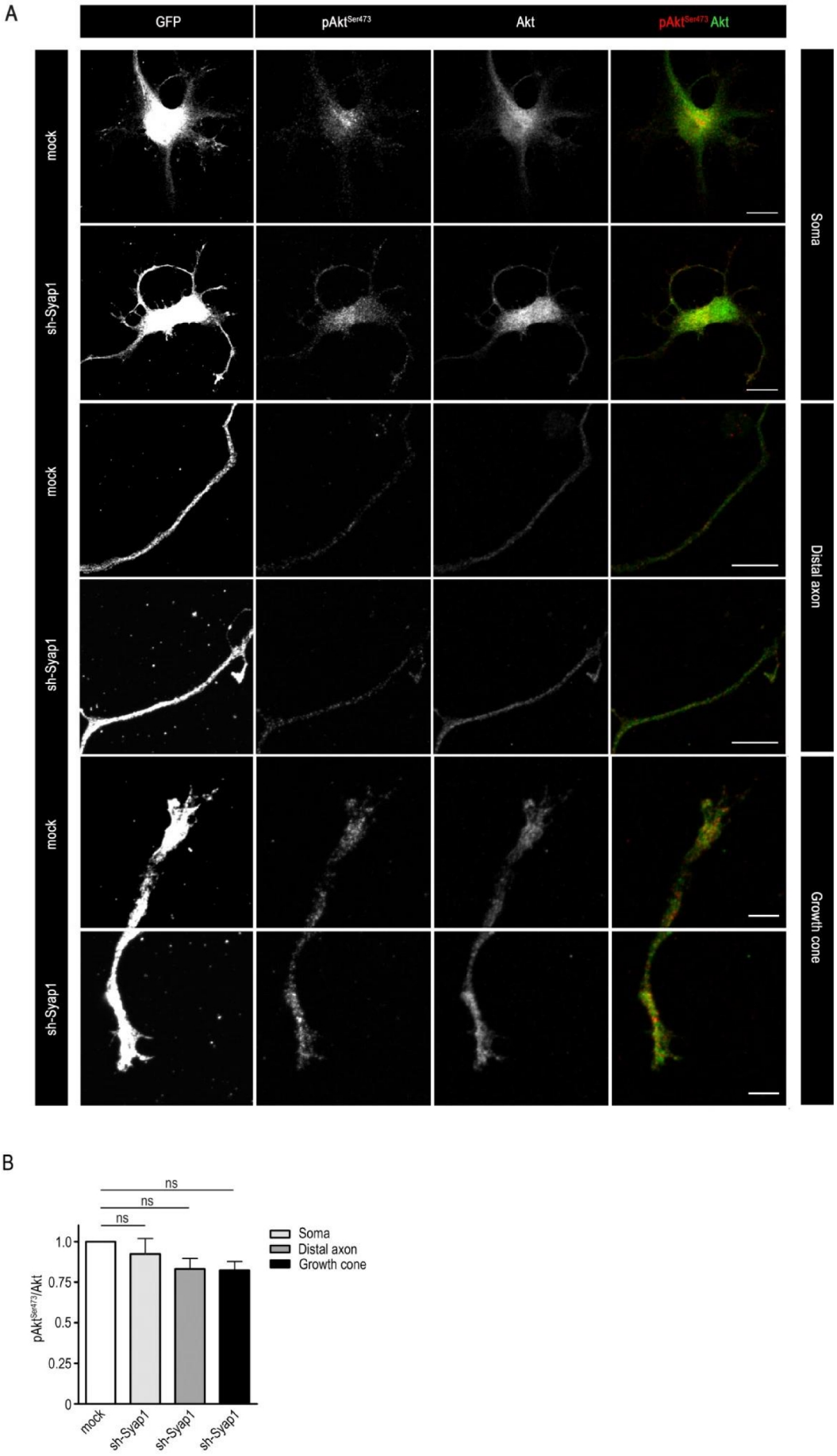

Figure 25: Compartment specific Akt phosphorylation in motoneurons without stimulation

Primary motoneurons were cultured for 5 DIV in the presence of BDNF [5 ng/ml] without starvation or stimulation, fixed and stained against GFP, Akt and $pAkt^{Ser473}$ to investigate a possible compartment specific difference in Akt phosphorylation levels after *Syap1* knockdown. Representative images of each compartment and condition are shown in A (scale bars: soma and axon: 10 µm; growth cone: 5 µm). No obvious difference was observed in confocal images between the two conditions (A). (B) Quantification revealed no significant difference between the mock infected and sh-Syap1 infected condition when the mean ratios measured per condition of an experiment were normalized to the corresponding mean of the unstimulated mock control (n = 4; one-way ANOVA with Kruskal Wallis test, total number of cells analyzed per condition: 68-80; sh-Syap1 infected: cell body: 0.92 ± 0.09; distal axon: 0.83 ± 0.06; growth cone: 0.82 ± 0.05; $P > 0.05$). Data shown represent means ± SEM.

The results shown in Figure 25 did not reveal any change after *Syap1* knockdown in compartment specific Akt phosphorylation at Ser^{473} investigated under the described conditions.

In summary, from all the experiments performed, no differences in Akt phosphorylation were observed upon *Syap1* knockdown under the mentioned conditions.

3.6 Possible interaction partners of Syap1

3.6.1 Possible interaction of Syap1 and TBCE protein

Another part of the characterization of Syap1 protein implicated to find endogenous interaction partners of this protein based on preliminary data or publications.

Preliminary work from N. Funk, B. Thangaraj and D. Schmitt had provided evidence of a possible interaction between Syap1 and TBCE protein. These studies were initially pursued, because by performing a yeast-two-hybrid screen, TBCE-like was detected as an interaction partner candidate of Sap47 (N. Funk, unpublished data). TBCE-like is a regulator of microtubule stability being able to destabilize MTs (Bartolini et al. 2005). Thus, although the two proteins show a related domain structure, TBCE-like counteracts TBCE, which promotes α-tubulin folding. Based on these facts and in view of the requirement of intact TBCE to prevent motoneuron degeneration, investigations of a possible interaction were performed using overexpression constructs of Syap1 and TBCE. Co-immunoprecipitation (Co-IP) studies of ectopically expressed HA-TBCE and FLAG-Syap1 in PC-12 and HEK293T cells indicate an interaction between these two proteins. Interestingly, the interaction was reduced by the $TBCE^{pmn}$-mutation (N. Funk, B. Thangaraj and D Schmitt., unpublished).

Due to these preliminary results, co-immunoprecipitations with endogenous proteins were performed. These data would then clarify if the two proteins also interact under physiological condition within a cell.

Co-immunoprecipitations were first performed with HEK293T cells under similar conditions (buffers and procedure) as used in the experiments in which the interaction was observed for overexpressed Syap1 and TBCE (Figure 26A). The eluates were then analyzed by Western blot. Since both investigated proteins have similar molecular weights (Syap1: 55 kDa (human); 56 kDa (mouse), TBCE: 59 kDa) blots were in general first probed for the co-immunoprecipitated protein and in a second step for the efficacy of the immunoprecipitation (IP) to exclude misinterpretation of bands remaining from incomplete stripping. For each experiment an IgG control was included in order to verify that a potential band in the eluate for the co-immunoprecipitate does not result from unspecific protein binding to the beads or the constant region of the immunoglobulin.

After the analysis of the co-immunoprecipitation (Figure 26A) no band with immunoreactivity for TBCE was observed in the eluate after pulldown with Syap1 antibody.

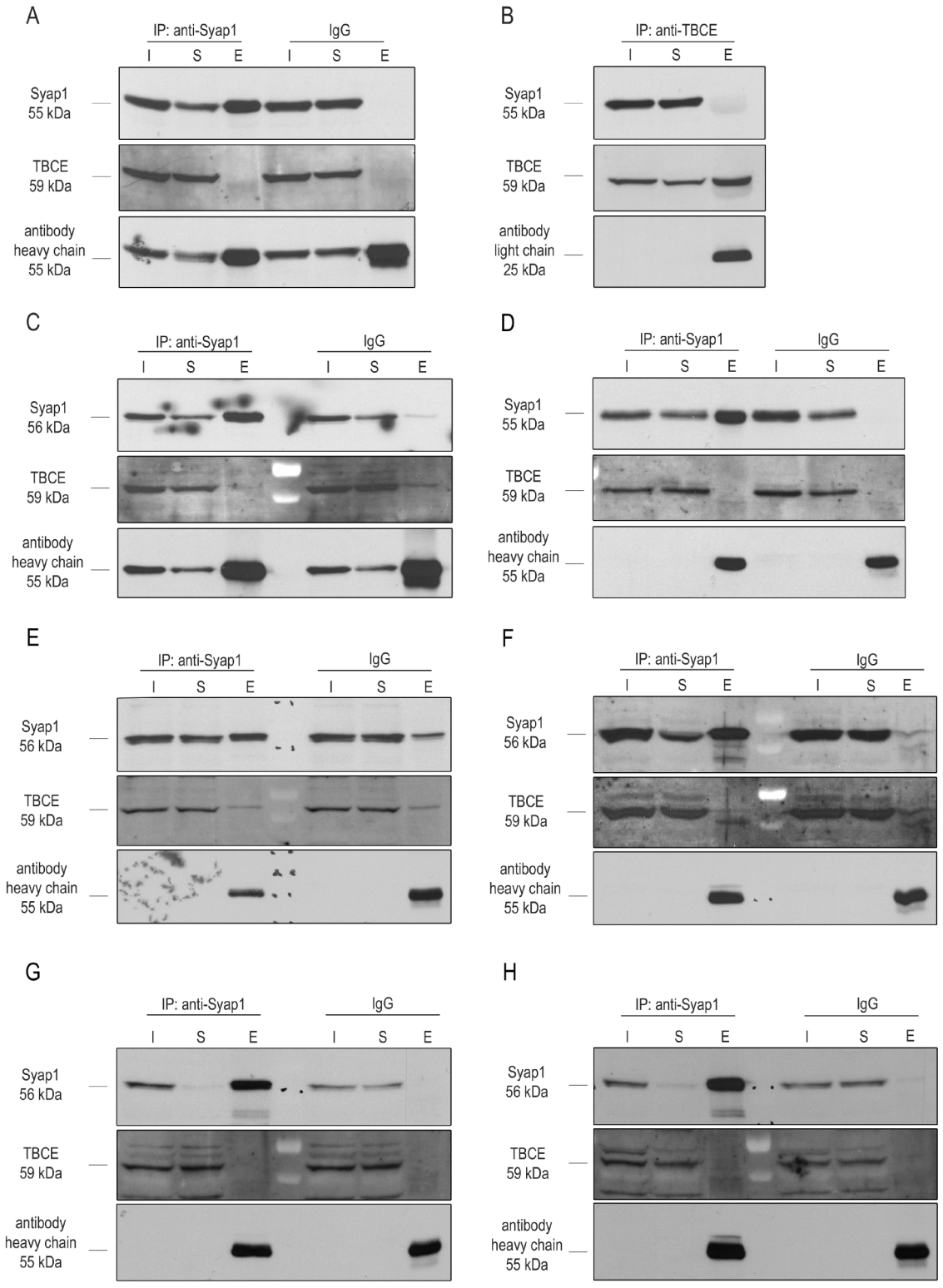

Figure 26: Co-immunoprecipitations testing for an interaction of Syap1 and TBCE

(A) Co-immunoprecipiation performed with HEK293T cells under conditions, under which an interaction was observed for ectopically expressed Syap1 and TBCE. (B) Co-immunoprecipiation performed with HEK293T cells using rabbit anti-TBCE antiserum for pulldown. (C) Co-immunoprecipiation performed with HEK293T cells using lysis buffer without detergent. (D) Co-immunoprecipiation performed with HEK293T cells using a cross-linker. (E) Co-immunoprecipiation performed with NSC34 cells under conditions, under which an interaction was observed for ectopically expressed Syap1 and TBCE. (F) Co-immunoprecipiation performed with embryonic mouse spinal cords. (G) Co-immunoprecipiation performed with adult mouse spinal cord. (H) Co-immunoprecipiation performed with adult mouse cortex. I: input; S: supernatant; E: eluate.

Syap1 protein was enriched from total HEK293T cell lysate (input lane) indicated by the strong band in the eluate lane. Similar use of antibody amounts for pulldown in Syap1 and IgG condition is shown by almost equal immunoreactivity for the heavy chains. Bands in input and supernatant lanes were observed due to incomplete stripping of the blot after probing for immunoprecipitation. Nevertheless, although immunoprecipitation of Syap1 was successful, no indication for an interaction with TBCE was obtained under these conditions. In the same set of experiments, it was tried to pull down TBCE using the rabbit-anti TBCE antiserum and test for a co-immunoprecipitation of Syap1 (Figure 26B). TBCE was slightly enriched but Syap1 seemed not to be co-precipitated with this protein as no band was obtained in the eluate.

It is known that different amounts of detergent can influence the efficacy of immunoprecipitation and thereby the yield of co-immunoprecipitation. Since antibody-antigen interactions are usually more stable than the interaction between co-immunoprecipitated proteins, protein-protein interactions are sometimes difficult to preserve under high detergent concentration (Yang et al. 2009). Therefore, co-immunoprecipitation was repeated using a lysis buffer without any detergent (150 mM NaCl, 50 mM Tris pH 7.4, 2 mM EDTA, 2 mM EGTA, 1x protease- and phosphatase inhibitors). HEK293T cells were mechanically opened using a glas-glas homogenizer and the initial IP protocol was followed. The result can be seen in Figure 26C. Syap1 was immunoprecipitated but no band was obtained for TBCE in the eluate lane. A slight band was present in the IgG control eluate indicating that some proteins were unspecifically binding to the beads which could be due to inefficient washing.

Protein-protein interactions can be highly diverse concerning their binding properties. Interactions can be permanent due to a strong and/or irreversible binding, very weak or transient (Perkins et al., 2010). Since a strong and direct interaction between Syap1 and TBCE probably would have been detected in one of the tested co-immunoprecipitations shown in Figure 26A-C, a cross-linking procedure prior to IP protocol was applied. The cross-linker used for the experiment in D is a homobifunctional and cleavable cross-linker which is cell membrane permeable and therefore able to cross-link intracellular proteins. Hence, in case Syap1 and TBCE interaction is only very weak or transient and thereby failed to be detected in the above

immunoprecipitations, the interaction could perhaps be stabilized by the cross-linker and the complex pulled down. The Western blot in D shows that also after stabilizing protein-protein interactions, no TBCE was co-immunoprecipitated.

Although Syap1 and TBCE protein are expressed in HEK293T cells, NSC34 cells (a mouse cell line) was used in order to test for a possible cell type specific interaction of these proteins. Previous co-IPs were indeed also performed in HEK293T cells but the interaction only tested for overexpressed murine proteins. However, also in a different cell line, there was no indication of an endogenous interaction of Syap1 and TBCE under the tested conditions (E). Furthermore, co-immunoprecipitations were accomplished using mouse embryonic spinal cord tissue (F), adult spinal cord (G) and cortex (H) to investigate a possible interaction. As shown for Syap1 before (Figure 18) and indicated by input bands, both proteins are expressed in these tissues and Syap1 was successfully enriched. Nevertheless, no interaction was observed under the applied conditions in any of the tested tissues in this biochemical approach.

3.6.2 Possible interaction of Syap1 and Akt protein

In 2013, Yao et al. already reported an interaction of Syap1 and Akt in murine and human cell lines for ectopically expressed as well as endogenous proteins upon EGF stimulation. This interaction appeared accomplished by the BSD domain and was prevented when mutations were inserted in the FW motif of this domain. In order to test, if this observed interaction can also be reproduced with the available cell lines, co-immunoprecipitations were performed using similar conditions following the protocol published by Yao et al. (2013).

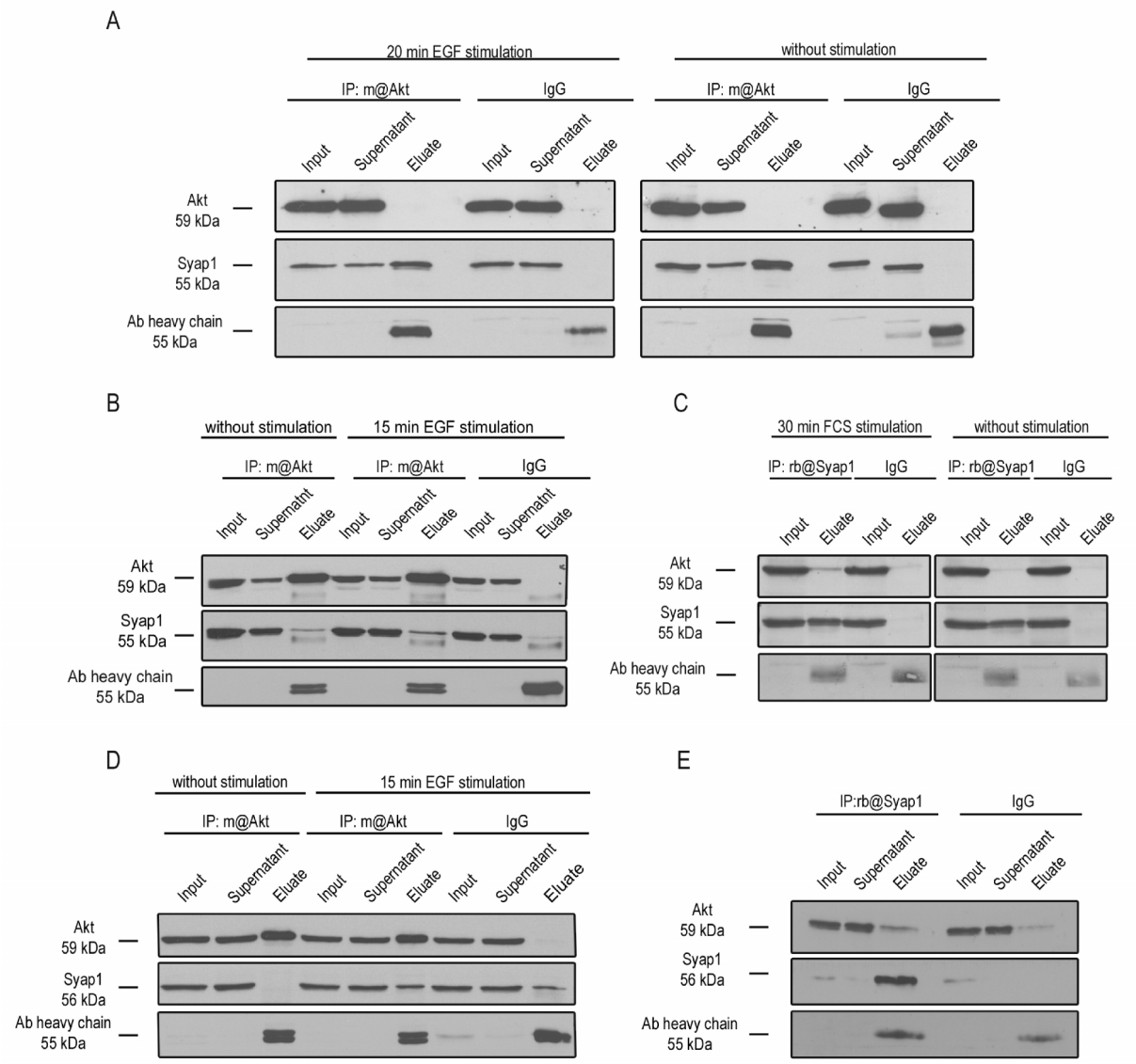

Figure 27: Co-immunoprecipitations for analysis of a possible Syap1-Akt interaction

(A) Primary mouse embryonic fibroblasts were starved over night and stimulated with EGF (50 ng/ml) for 20 minutes. Subsequently, immunoprecipitation was performed using the rabbit anti-Syap1 antibody and the interaction with Akt was tested in cell lysates from stimulated and unstimulated cells. Neither in the stimulated nor in the unstimulated condition an interaction was observed after probing the blot with a rabbit anti-Akt antibody detected with an HRP conjugated light chain specific rabbit anti-rabbit serum. (B) HEK293T cells were also starved for 12 hours prior to EGF (50 ng/ml) stimulation and co-immunoprecipitation. When Akt was efficiently pulled down only a very faint band was observed when probed for the co-immunoprecipitated Syap1 in lysates from unstimulated HEK293T cells. After stimulation a slightly stronger band was observed for Syap1 when compared to unstimulated cells and the IgG control. (C) Syap1 protein was immunoprecipitated with the polyclonal rabbit anti-Syap1 antibody from cell lysates from FCS stimulated and unstimulated NSC34 cells. Here, only low amounts of Akt were co-immunoprecipitated in the FCS-stimulated condition whereas almost no protein was co-immunoprecipitated in the non-stimulated condition. (D) In neuronal stem cells isolated from embryonic forebrains no interaction could be detected in lystates from unstimulated cells whereas a clear band was visible after a 15 minute EGF stimulation. However, a comparably strong band was observed in the IgG control indicating a cross-reaction with the beads. (E) Also in brain lysate from adult mouse no clear interaction was observed although an efficient pulldown of Syap1 was achieved. Only a faint band in the eluate of co-immunoprecipitated Akt1 was detected. An IgG control was included for each experiment in order to verify that a potential band in the eluate for the co-immunoprecipitate does not result from unspecific protein binding to the beads.

The results shown in Figure 27 indicate no clear interaction of Syap1 and Akt under the applied conditions and for cell types used. Only in a few experiments Syap1/Akt1 was co-immunoprecipitated (Figure 27B, C and others (not shown)) but the stoichiometry of Syap1-Akt co-immunoprecipitation was markedly lower than what was reported by Yao et al. (2013). However, co-immunoprecipitations are very critical to reproduce concerning the experimental settings. Even minor deviations in buffer contents or incubation times can be crucial for the results. Furthermore, although different cell types and tissue were used trying to reproduce the published interaction of Syap1 and Akt the authors of the paper used immortalized mouse embryonic fibroblasts for immunoprecipitation. This could be another explanation for the different results in the co-immunoprecipitation experiments.

3.7 Initial characterization of the first *Syap1* knockout mouse

3.7.1 Changing the genetic background

Heterozygous female X-chromosomal *Syap1*-knockout mice (*Syap1*$^{+/1tma}$) on C57BL/6N background were obtained from the Institute of Laboratory Animal Science in Vienna and crossed repeatedly to C57BL/6J mice in the Institute for Clinical Neurobiology in Wuerzburg to produce male and female knockout animals of C57BL/6J background because C57BL/6N mice are known to show a specific neurological phenotype and are therefore unsuitable as background when the influence of a specific gene knockout on nervous system function is to be characterized. Heterozygous F2-females and hemizygous F2-males were then further crossed to also obtain homozygous *Syap1*$^{tm1a/tm1a}$ (*Syap1*$^{-/-}$) female mice.

3.7.2 Establishment of a genotyping protocol

Initially, prior to the expansion of the *Syap1* knockout line, a genotyping protocol had to be established. Specific primer pairs were selected which allow the distinction of homozygous, hemizygous, heterozygous and wild type animals. The forward primer (**fw**) was designed to bind in the intronic sequence positioned directly in front of the insertion site of the cassette guaranteeing a binding in the knockout and wild type situation. To distinguish the wild type allele the reverse primer (**wt rev**) was selected to target the large intronic region between the

second *loxP* site and exon-4. A PCR (polymerase chain reaction) product using wt rev primer and fw primer will only be obtained for alleles which do not carry the insertion cassette. The reverse primer for the knockout allele (**ko rev**; list of primer sequences see Table 8) was designed to bind in the artificially inserted *En2* splice acceptor site in front of the *lacZ* element of the cassette (Figure 28). Therefore no PCR product will be generated in wild type condition. The expected PCR product size was electronically determined using Serial Cloner. The following products were expected in a successful genotyping reaction: wt: 274 bp; ko: 589 bp; heterozygous: 274 bp and 589 bp.

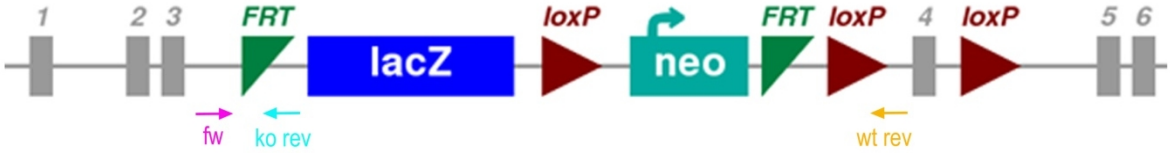

Figure 28: Localization of *Syap1* genotyping primers

Next, the conditions (buffers, amount of DNA, reaction temperatures, PCR cycles) for an efficient PCR result were determined starting with a standard PCR protocol. An annealing temperature of 58°C was initially used for testing. Since the annealing temperature of the ko rev primer was the most critical parameter, a gradient PCR using DNA from a heterozygous animal was used for protocol optimization (Figure 29). Temperatures ranging from 55°C to 61.8°C were used to examine the optimal ko rev primer annealing temperature. At 55°C the highest amount of PCR product was obtained.

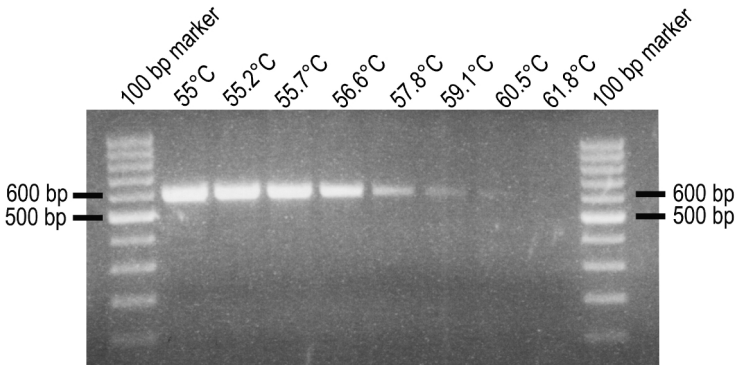

Figure 29: Gradient PCR
In order to optimize hybridization temperature for ko rev primer, gradient PCR was performed using temperatures ranging from 55 °C-61.8 °C. The highest amount of PCR product was obtained at 55 °C.

Besides optimizing the annealing temperature, the number of PCR cycles was reduced from initially 35 to 29 cycles to avoid amplification of unspecific products. Additionally, 0.5 M of the isostabilizing agent betaine was added to the reaction which is known to increase the yield

and specificity of PCR products (Sarkar et al. 1990; Varadaraj and Skinner 1994; Baskaran et al. 1996). It facilitates strand separation and equalizes the contribution of GC- and AT-base pairing to the stability of the DNA duplex (Melchior and Von Hippel 1973; Rees et al. 1993). The final adapted protocol allows a fast and reliable genotyping of animals of the *Syap1* knockout mouse line. Figure 30 shows an example of the DNA amplification products and their sizes in an agarose gel.

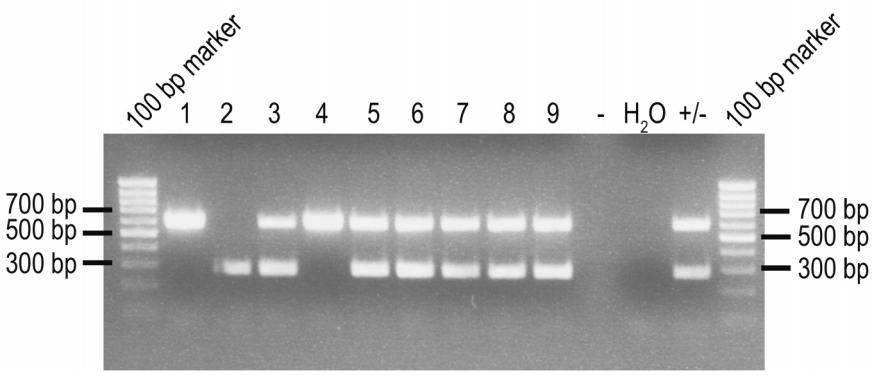

Figure 30: Example of a genotyping result

After PCR the DNA samples from different animals (1-9) were subjected to agarose gel electrophoresis and separated. H_2O served as a control to guarantee no contamination of any buffer or primer; +/- was used as a positive control from an already genotyped heterozygous mouse. The following genotypes were determined: 1 and 4: ko; 2: wt; 3, 5, 6, 7, 8 and 9: heterozygous.

The specificity of the PCR products was verified by sequencing. Therefore a PCR with 10 times of the standard volume was performed and the DNA extracted from the agarose gel. After purification, the samples were sent for sequencing and the results analyzed. For wild type and *Syap1* knockout the respective sequences were obtained indicating a high specificity of the selected primers and the protocol.

3.7.3 Phenotypic characterization of the *Syap1* knockout mouse

The analysis of the hitherto obtained offspring genotypes are shown in Table 7. The data are compatible with an assumption of reduced viability (Chi-square test $P < 0.01$) of female mice homozygous for the *Syap1*^{tm1a} allele. However, further generations of *Syap1*^{tm1a} mutant mice need to be investigated for a profound statistical analysis.

P	**X/Y x X/X$^-$**				**X$^-$/Y x X/X$^-$**			
F1	X/Y	X$^-$/Y	X/X	X/ X$^-$	X/Y	X$^-$/Y	X/ X$^-$	X$^-$/ X$^-$
Nb	16	23	28	19	9	3	15	4

Table 7: Frequencies of offspring genotypes

The table shows the distribution of genotype offsprings (F1) of the parental crosses (P) after three generations of *Syap1*^{tm1a} mutant mice. The numbers (nb) indicate that progeny of wild type males and heterozygous females are consistent with Mendelian inheritance (P = 0.30) while progeny of mutant males and heterozygous females could indicate a deleterious effect of the *Syap1*^{tm1a} allele (Chi-square test P < 0.01).

Nevertheless, neither homozygous nor hemizygous or heterozygous mutants showed apparent differences in morphology or size even when compared to wild type littermates (Figure 31).

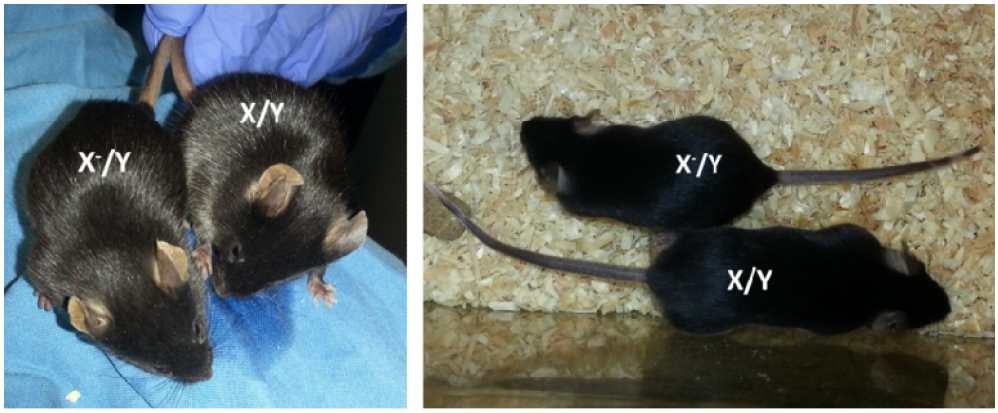

Figure 31: Pictures of *Syap1* wild type and *Syap1* knockout littermates

The pictures show two male littermates – a *Syap1* wild type (X/Y) and *Syap1* knockout (X$^-$/Y). No obvious differences in their morphology are detectable.

Since Yao et al. report a suppression of adipocyte differentiation after *Syap1* knockout cells *in vitro* a reduction in body weight of knockout mice was expected. Therefore the body weight of littermates from male adult *Syap1* knockout and wild type mice was determined. No significant difference was noted between the two genotypes (weight ratio mutant/wild type 0.996 ± 0.025, 4 age groups, 12 knockout and 12 wild type animals, P = 0.56).

Considering that the *tma1* mutation in the *Syap1* gene does not delete *Syap1* coding sequences it was tested if any residual intact transcript or protein was generated due to exon-3 to exon-4 splicing when the En-2 splice acceptor site was ignored. Therefore, qRT-PCR with cDNA isolated from wild type and knockout cortices was applied to assess the amount of exon-3-exon-4. To exclude alternative splicing, exon skipping or an alternative transcription start due

to the insertion of the gene trap cassette, another qRT-PCR was performed for exon-8-exon-9 which are downstream of the insertion site (see 4.1). After isolation and reverse transcription of RNA from wild type and knockout littermates, intron spanning exon-3 to exon-4 as well as exon-8 to exon-9 primers (Table 8) were used for analysis. Figure 32 shows that exon-3 to exon-4 mutant transcripts were highly reduced to 5.68 ± 0.54% of wild type levels (n=6). Exon-8 to exon-9 containing transcripts were reduced in *Syap1*$^{-/-}$ to 14.8 ± 2.9% (n=3). Each qRT-PCR was performed in two technical replicates for at least three times. GAPDH was used for normalization of cDNA levels between samples in each experiment.

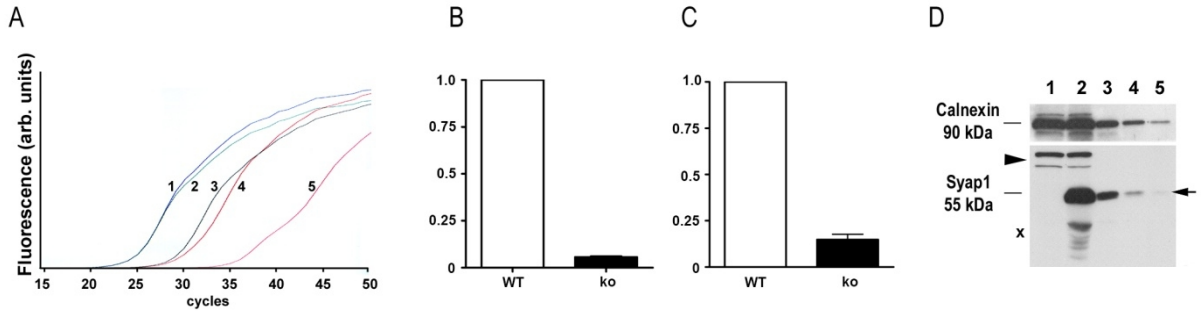

Figure 32: Verification of *Syap1* knockout by qRT-PCR and Western blot analysis.
(A) Amplification plot of *Syap1* transcripts using mRNA from cerebral coritces. Primers spanning exon-3 and exon-4 show that the levels are reduced in *Syap1* mutant (curve 3 and 4) by a factor of 30 compared to wild type (curve 1 and 2). Curve 5 represents the detected background when no reverse transcriptase was added during cDNA synthesis. (B) Quantification of generated *Syap1-En2* transcripts in wild type and *Syap1* knockout mice. Knockout transcript levels were reduced to 5.68 ± 0.54% (n=6) of wild type levels. (C) Quantification of exon 8-exon 9 containing transcripts in wild type and *Syap1* knockout mice. 14.8 ± 2.9% (n=3) exon 8-exon 9 containing transcripts were detectable in Syap1 mutant mice compared to wildtypic animals. (D) No signal of Syap1 protein is detected by Western blot in hippocampal lysates from knockout animals after intensive protein loading (60 µg, undiluted) and high exposure (lane 1). The two weak upper bands detected above 56 kDa (arrowhead) are unspecific (lane 1 and 2); the lower bands recognized by the Syap1 antibody (x) presumably represent degradation products. Lanes 3-5 show different dilutions of wild type lysate where a discernible signal was still generated at a dilution factor of 1:100 (arrow) indicating that Syap1 protein levels are reduced to less than 1% in *Syap1* knockout mice. Calnexin served as a loading control. Lanes: 1, *Syap1* knockout (60 µg); 2, wild type (60 µg); 3, wild type diluted 1:10; 4, wild type diluted 1:30; 5, wild type diluted 1:100

Using the Syap1 antibody (characterized in 3.1) no trace of Syap1 signal was observed in hippocampal lysates from *Syap1*$^{-/-}$ mutant mice after increased protein loading (60 µg) and extended exposure (Figure 32D) whereas in corresponding wild type lysates a strong signal at 56 kDa as well as background (arrowhead) and degradation products (x) were detected. Even at a dilution of 1:100 a slight signal can still be detected in the wild type condition (arrow) indicating that Syap1 protein levels are reduced to less than 1% in the *Syap1* knockout. Based on the observations that the Syap1-EN2 fusion protein lacks more than 80% of the primary

Syap1 structure (Figure 3A) (including the functionally relevant BSD domain) (Doerks et al. 2002; Yao et al. 2013) and that intact Syap1 protein is absent in *Syap1* knockout mice (<1%, Figure 32C), the *Syap1*^{tm1a} was regarded to be a null allele.

3.7.4 Syap1 protein distribution *in vivo*

The expression of Syap1 and the Syap1 antibody specificity were already shown in 3.1 and 3.3. In order to confirm these results and to exclude cross-reactivity of the antibody with proteins of similar molecular weight, tissues from wild type and *Syap1* knockout mice were analyzed by Western blot (Figure 33).

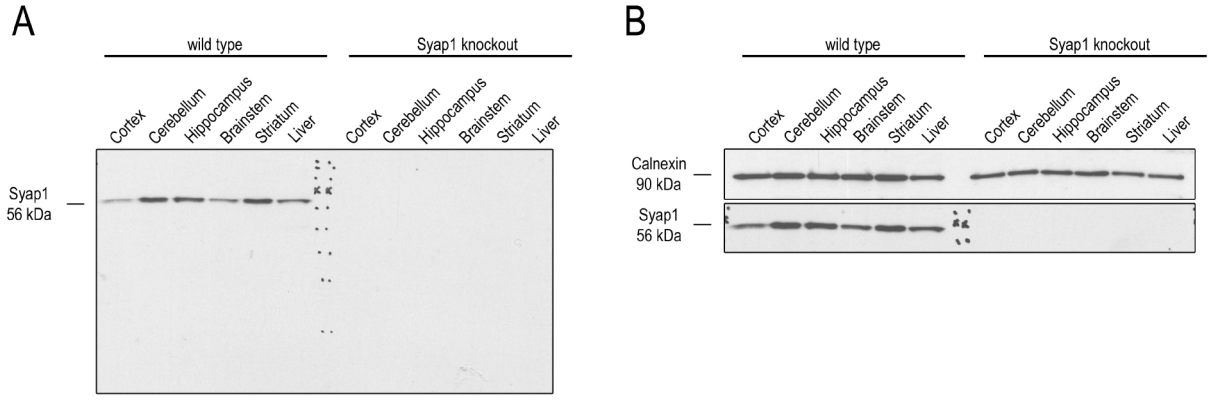

Figure 33: Antibody specificity and *Syap1* knockout confirmation

Tissue lysates from different brain areas and liver were analyzed by Western blot. Equal amounts of lysates were subjected to analysis. (A) Complete Western blot probed for Syap1 shows clear and comparable levels of Syap1 immunoreactivity at 56 kDa in the wild type whereas no band was observed in tissues from knockout animals. (B) The blot shown in (A) was probed for Calnexin which served as loading control.

Syap1 signal at 56 kDa was detected in all investigated brain areas as well as in the liver from wild type animals (Figure 33) - consistent with the results obtained in Figure 18. These bands were absent in the tissues obtained from a *Syap1* knockout mouse. The right blot shows the upper part of A including a control (Calnexin) to prove adequate protein loading. The availability of a knockout mouse now allowed the investigation of Syap1 protein distribution in wild type tissues sections, since the antibody specificity can be examined by comparison with corresponding knockout sections. So far specificity had only been verified by lentiviral knockdown *in vitro* which cannot exclude cross-reactivity in immunohistochemical slices. Since there is no report on distribution or function of Syap1 in the mammalian nervous system so far, several distinctive regions in the mouse brain were analyzed with respect to the

tissue distribution of Syap1 immunoreactivity. Therefore, 30-40 µm vibratome slices from mouse brain of wild type and *Syap1* knockout animals were generated and stained against Syap1 protein and indicated co-markers.

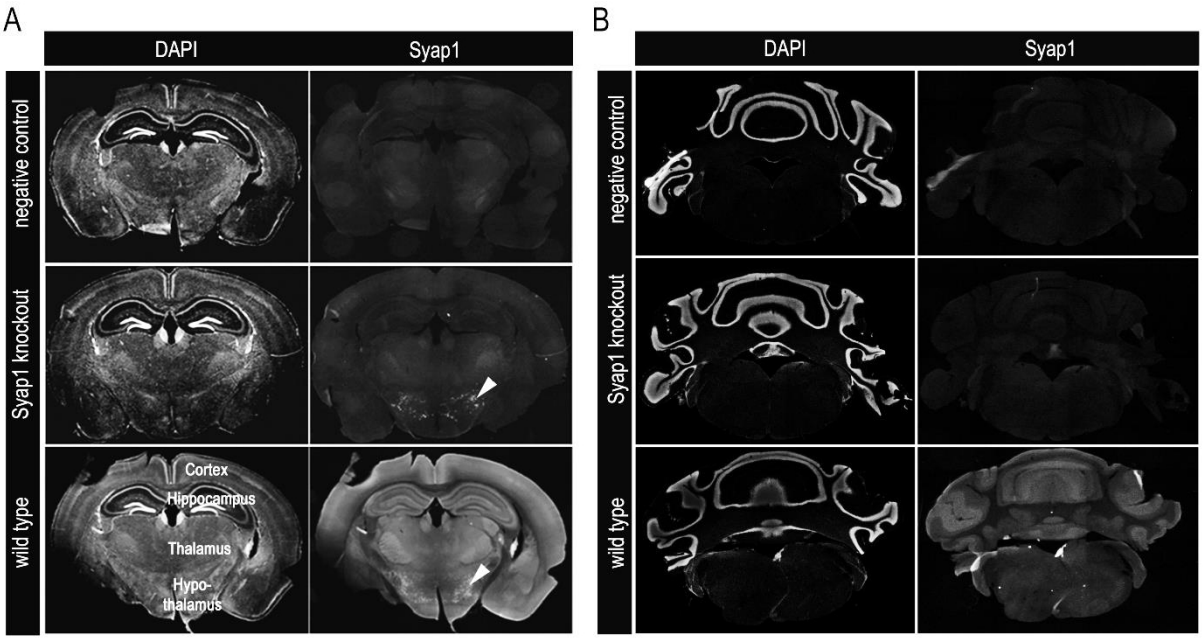

Figure 34: Overview of Syap1 protein distribution in the mouse cerebrum and cerebellum
Coronal sections of wild type and *Syap1* knockout mouse brains were stained against Syap1 and DAPI. A negative control (no primary antibody) was also included to rule out unspecific binding of the secondary antibody. In coronal sections of the cerebrum, a diffuse Syap1-specific immunolabeling was detected throughout the neuropil, preferentially found in the gray matter neuropil. A certain pool of cells in the hypothalamic region (arrowhead) was unspecifically stained by the Syap1 antibody as they were also detected in the knockout sections but not in controls without primary antibody. In the cerebellum (B), a strong Syap1 immunofluorescence signals were observed particularly in the molecular layer of the cerebellar cortex

The comparison of coronal sections of wild type and *Syap1* knockout mouse cerebra reveled strong Syap1 immunoreactive signals throughout the entire neuropil with regions of distinct distribution patterns. However, unspecific fluorescence signals were also observed in individual cells in the hypothalamus (Figure 34 arrowhead) or in the cortex (Figure 35) which were absent in negative controls (not incubated with Syap1 antibody) indicating distinct cross-reactivity of the Syap1 antibody with an unknown antigen. Thus a comparison of wild type and knockout stainings which were processed under identical conditions was necessary for a specific characterization of Syap1 distribution.

Low magnification images of brain slices revealed a diffuse Syap1 labeling in most of the regions (Figure 34A, lower panel) with a particular localization pattern in the grey matter

neuropil when compared to neuronal localization patterns visualized by DAPI counterstaining (Figure 34B, lower panel). Strong and diffuse Syap1 signals were especially observed in the hippocampus, thalamus and cortical regions as well as in the molecular layer of the cerebellum which were easily distinguishable from the weak staining of cerebellar medulla.

In order to gain more information about Syap1 protein distribution in defined regions of the mouse brain (e.g. cortex, thalamus, hippocampus and cerebellum), high magnification images were taken and different co-markers used helping to identify certain cell types.

In the entire medial cerebral cortex a strong and mainly homogenous Syap1 signal was observed in comparison to knockout sections where only slight unspecific cross-reactions of the antibody were detected partially resulting from the secondary antibody (Figure 35). Although very intense and rather homogenous pattern of Syap1 protein was discernible in all the layers (layer I-VI) of the cortex. For a more detailed conclusion of Syap1 distribution in the cortex and its expression in different cell types, further co-stainings with e.g. layer-specific antibodies (Hadjivassiliou et al. 2010).

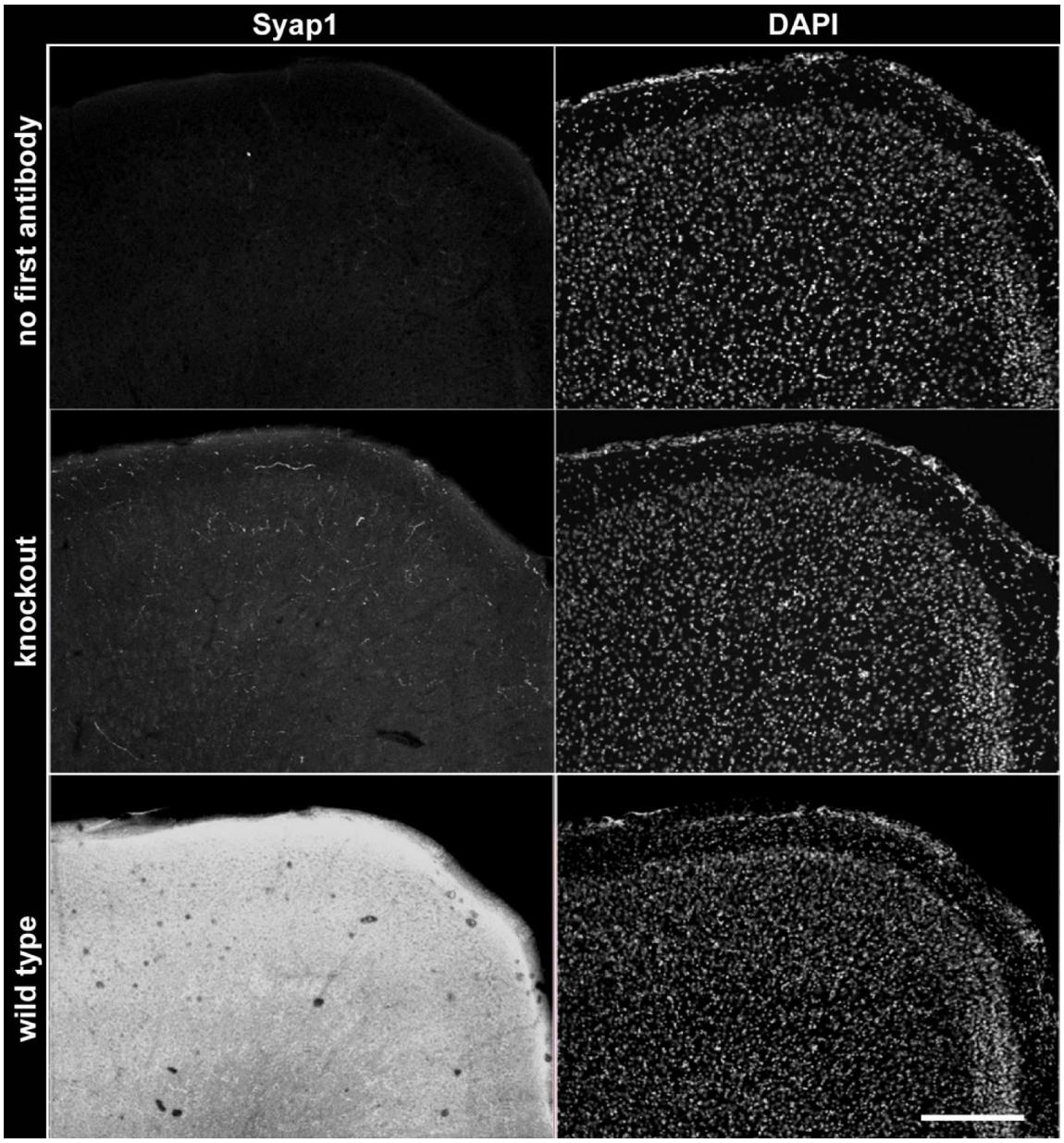

Figure 35: Syap1 antibody specificity exemplified in cortical brain sections

Syap1-antibody cross-reactivity was tested in cortical brain sections in order to compare the obtained immunofluorescent signals from wild type and knockout slices and to examine unspecific binding of the secondary antibody (top left). Stainings without a primary antibody (top left) revealed some minor unspecific cross-reactivity of Syap1 antibody as seen in *Syap1* knockout sections (middle left). Nevertheless, the unspecific cross-reactivity in these structures is outshone by the strong specific signals in wild type section (bottom left). Scale bar: 250 µm

In the olfactory bulb – the first site of processing olfactory information incoming from receptor cells in the nasal epithelium – intense Syap1 labeling was detected in distinct structures of this relay station. There, high expression of Syap1 protein was especially observed in the olfactory nerve layer and the olfactory glomeruli (Figure 36). These spherical structures are sites where glutamatergic terminals of the olfactory nerve, apical dendrites of

mitral cells, dopaminergic periglomerular cells and tufted cells form synapses (reviewed by Figueres-Onate et al. 2014). Some light Syap1 signals were also perceived in somata of mitral cells located in an orderly row in the olfactory bulb (Figure 36). No prominent staining was noticed in the perikarya of the tyrosine hydroxylase (TH) immunoreactive dopaminergic periglomerular cells.

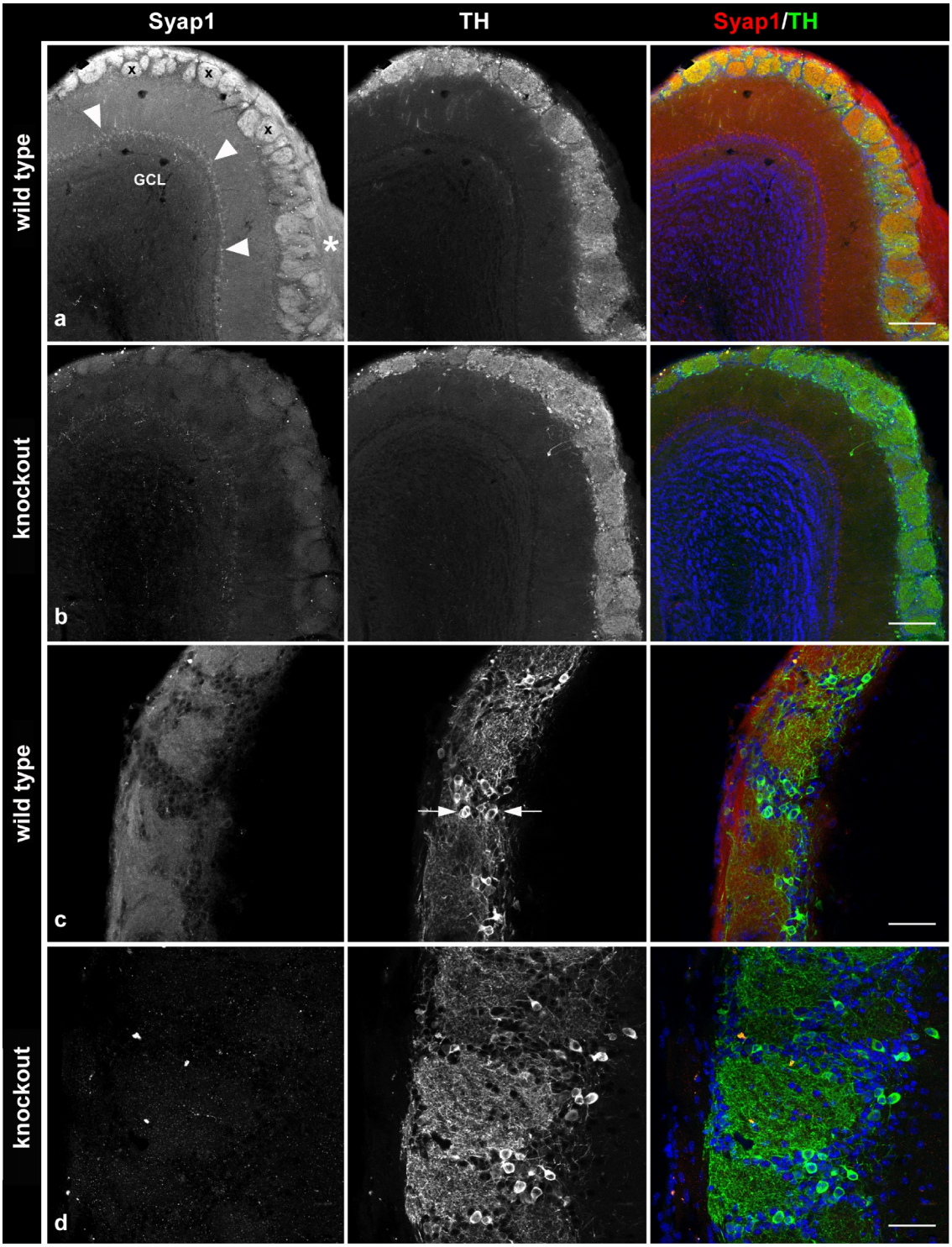

Figure 36: Syap1 distribution in the olfactory bulb

In the olfactory bulb of wild type mice, strong Syap1 signals are observed in the olfactory nerve layer (white asterisk) and olfactory glomeruli (x) (a, c). Weaker Syap1-specific immunoreactivity is found in the somata of mitral cells (white arrowheads in a) but almost no signal was detected in the granule cell layer. The co-staining with anti-TH-antibody (middle column) demonstrates the distribution of Syap1 in the glomerular neuropil (c, white arrows) but the protein seems to be present only in low levels or absent from the dopaminergic periglomerular cells. The antibody showed some slight cross-reaction in knockout sections (b and d) with unknown antigens which was clearly distinguishable from specific signals. GCL: Granule cell layer, scale bars: a, b: 200 µm; c, d: 50 µm.

Another brain region of apparently strong Syap1 immunolabeling is the thalamus (Figure 34 and Figure 37). There, Syap1 especially accumulates perinuclearly in close association with the *cis/medial*-Golgi marker GM130 (Nakamura et al. 1995) in numerous neurons (identified by their typical nuclei in DAPI-staining), which can be clearly observed in high magnification images (Figure 37a', c').

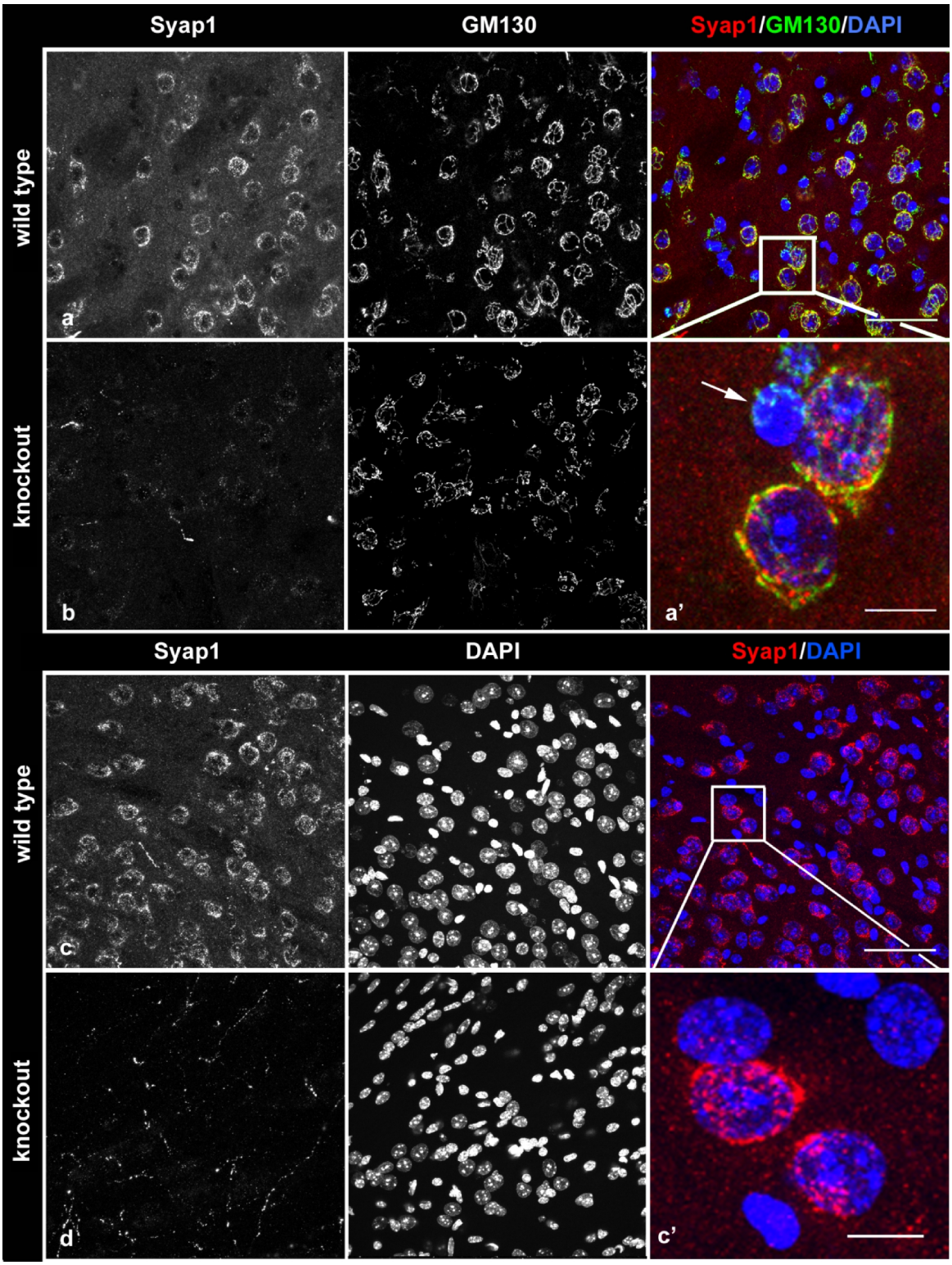

Figure 37: Syap1 distribution in the thalamus

Strong and specific Syap1 staining (a and c, left panel) in the thalamus was observed in brain sections of wild type mice. By double staining with the Golgi marker GM130 (a, middle panel), Syap1 protein was identified as perinuclear accumulation close to the Golgi apparatus (a and a', right panel). An overlap of both signals is indicated by yellow color seen in a'. The arrow in a' points to a Syap1-negative and GM130 positive cell presumably representing a non-neuronal cell (as indicated by a small and intensely DAPI stained nucleus). This perinuclear Syap1 accumulation seems also to be restricted to a certain subpopulation of neurons since some of the neurons (identified by their nuclei) are devoid of Syap1-specific immunolabeling (c right panel and enlargement c'). Images of knockout controls (b and d) only show fine fiber-like structures labeled by the Syap1-antibody indicating an unspecific cross-reaction. Scale bars: 25 µm (a, c); 5 µm (a', c')

Nevertheless, not all cells displayed an accumulation of Syap1 near the Golgi apparatus (Figure 37a, c right panel, a', c'). Those cells presumably represent a non-neuronal cell type as they show a comparatively small and heterochromatin-rich nucleus.

This hypothesis was supported by a co-staining with GFAP-labeling to identify some types of astrocytes (Eng et al. 1971) and NeuN, a neuronal marker (Mullen et al. 1992). NeuN-positive cells displaying a large euchromatin-rich nucleus show the typical perinuclear Syap1 accumulation (Figure 38 b, left image), while GFAP-positive astrocytes and probably other non-neuronal cells with relatively small and heterochromatin-rich nuclei (indicated by DAPI staining) do not display this typical perinuclear Syap1 staining (Figure 38a).

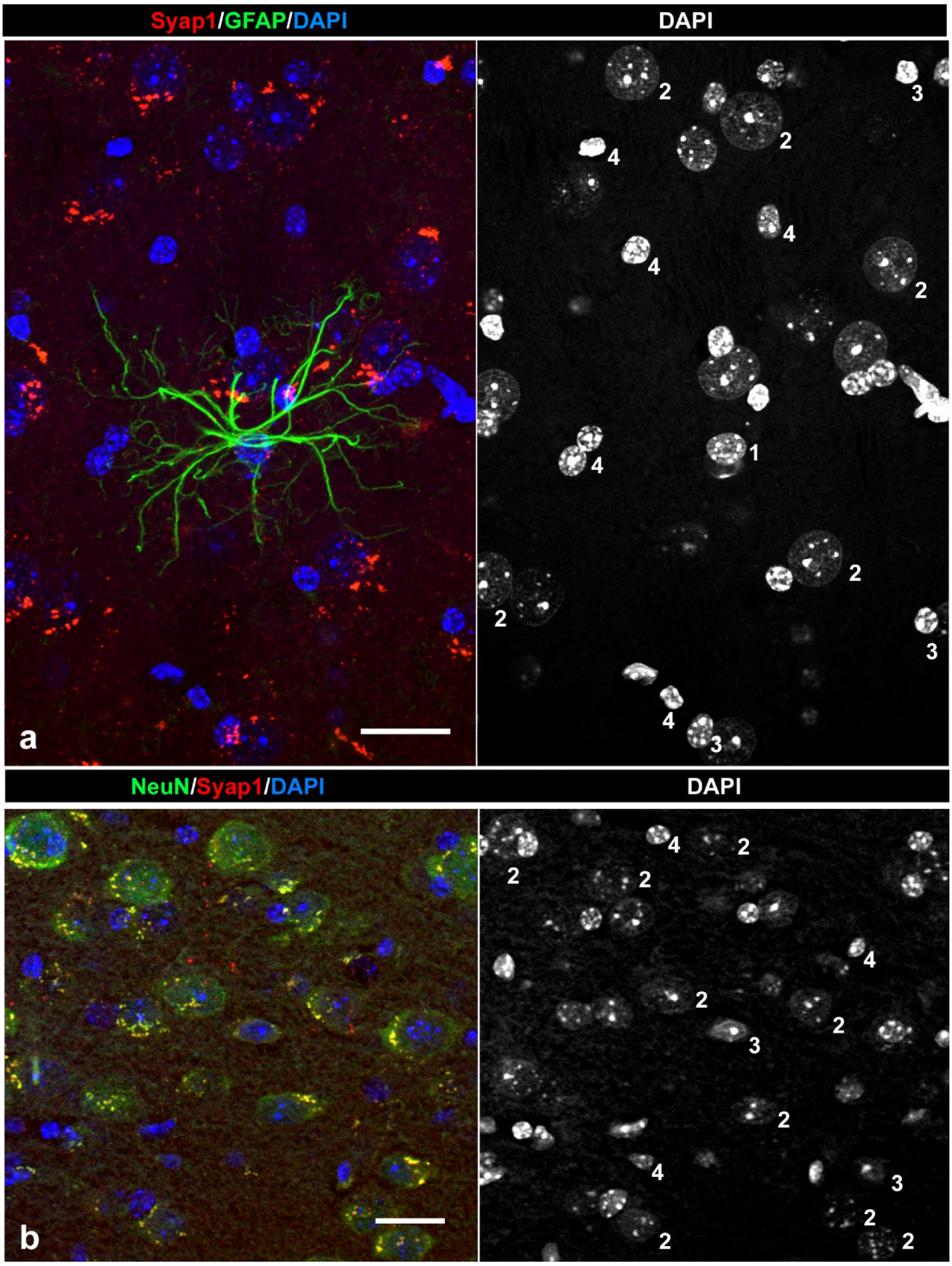

Figure 38: Syap1 seems to be rarely expressed in astrocytes and other non-neuronal cells of the thalamus
(a) Image of a GFAP-labeled astrocyte in the thalamus (corresponding nucleus labeled by "1" on the right). Almost no Syap1 immunofluorescence can be detected when compared to NeuN-positive cells showing a large euchromatin-rich nucleus and perinuclear accumulation of Syap1 ("2"). No Syap1 signal was detected in NeuN-negative cells. In few cases Syap1 signals were also observed near small nuclei ("3") but might rather be associated with the nuclei of a neuronal cell in their close proximity. Most of the small nuclei seem to lack a detectable Syap1 signal ("4"). (b) Double staining with Syap1 and NeuN of the thalamus indicates that Syap1 is present in most of the neurons (numbering of nuclei as in a). Scale bars: 20 µm

This hypothesis is invigorated by a characteristically and highly reproducible Syap1 staining in the hippocampus - a very crucial structure of the limbic system primarily associated with

learning and memory (Leuner et al. 2006; Gould et al. 1999; Belnoue et al. 2011). Here, only low concentrations of Syap1 are observed in the CA1 and CA3 region (small arrowheads in Figure 39a) whereas in the CA2 pyramidal layer (big arrowheads in Figure 39a and at higher magnification in c) it is highly abundant in almost all perikarya. In these neurons, strong perinuclear signals in close regional proximity to the Golgi apparatus can be identified, too (Figure 39c, inset). In the stratum moleculare and stratum lacunosum-moleculare medium intense and dispersed Syap1 immunostaining is detected. Comparatively low and medium high Syap1 levels are observed in the stratum oriens and stratum radiale in the CA1 region, respectively. Unlike the sparse perinuclear Syap1 staining in cells of the dentate gyrus, strong labeling of the hilus can be detected (Figure 39a, e).

In summary the data suggest that Syap1 expression is under cell-(sub) type specific control.

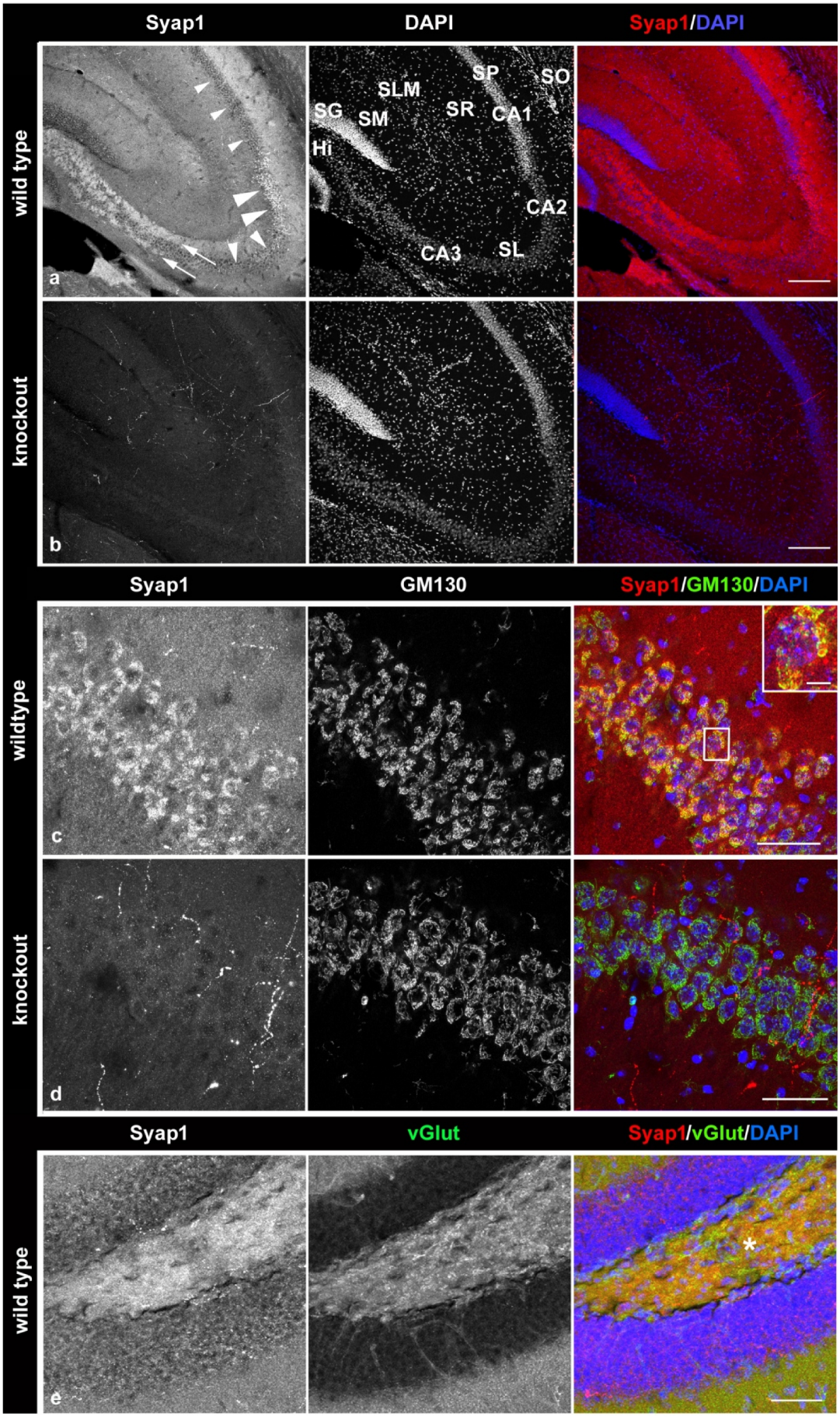

Figure 39: Syap1 distribution in the hippocampus

Syap1 stainings of wild type sections revealed a general distribution in the hippocampal neuropil with especially high occurrence in CA2 perikarya (a, large arrowheads) where a strong regional proximity to the Golgi can be observed (c and enlargement) when co-stained with GM130. In CA1 and CA3 perikarya Syap1-specific immunofluorescence was detected to a lesser extent (small arrowheads). Knockout images (b, c) ensure the specificity of the stainings observed and interpreted in the wild type situation. The Syap1 protein is further found in the stratum lucidum and can be also discovered in the infra- and suprapyramidal mossy fiber pathway arising from the dentate gyrus granule cells (arrows). Comparison of Syap1 and vGlut1 double labeling in the hilus (asterisk in e) revealed partial co-localization of both proteins indicating the presence of Syap1 at glutamatergic mossy fiber boutons. Nevertheless, the protein can also be seen in vGlut1-negative structures. Hi, hilus; SG, stratum granulosum; SL, stratum lucidum; SLM, stratum lacunosum-moleculare; SM, stratum moleculare; SO, stratum oriens; SP, stratum pyramidale; SR, stratum radiatum. Scale bars: 200 µm (a, b), 50 µm (c, d, e), 10 µm (enlargement in c)

This labeling extends in two bands of high Syap1 levels from the hilus into the CA3 region, following the adjacent CA3 somata (arrows in Figure 39a) which represent the supra- and infrapyramidal mossy fiber fields originating from the dentate gyrus. The observed Syap1 staining is also observed in the stratum lucidum of CA3 into the CA2 region (Figure 39a). Using the vesicular glutamate transporter vGlut1 for a presynaptic localization (Takamori et al. 2000), Syap1 was found to partially co-localize with this protein in the mossy fiber pathway (Figure 39e), presuming the presence in these giant glutamatergic mossy fiber terminals but also in vGlut1-negative elements.

Investigation in the occurrence and distribution of Syap1 in the cerebellum again revealed a marked perinuclear staining in the perikarya of Purkinje cells (Figure 40a, c, e, asterisk). In these cells, near their emerging dendritic branches Syap1 is associated with the Golgi apparatus identified by a GM130 co-staining (Figure 40c').

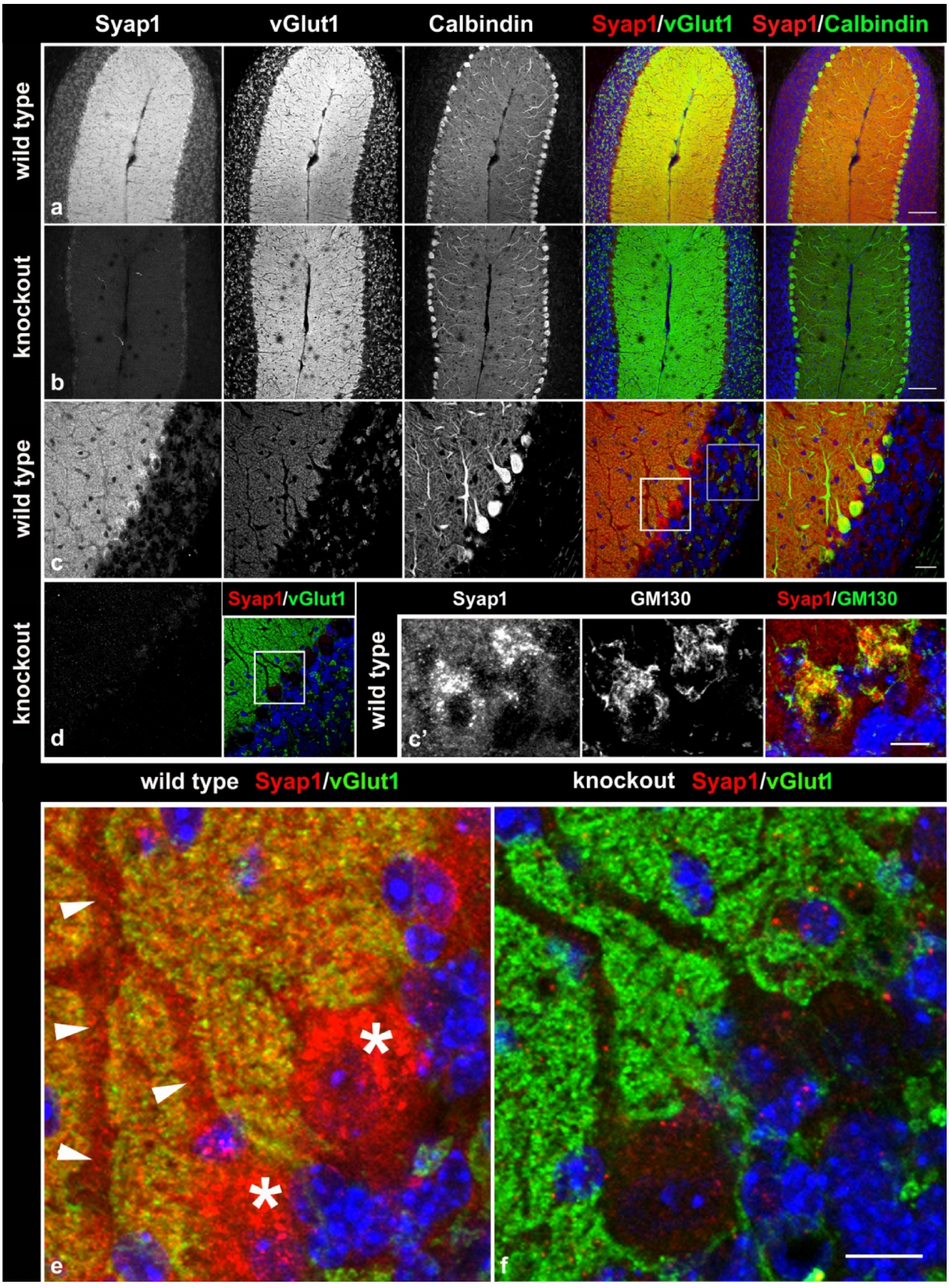

Figure 40: Syap1 distribution in the cerebellum

Sagittal sections of wild type cerebella show a distinct perinuclear accumulation of Syap1 in the cytoplasm of Purkinje cells identified by double-staining with Calbindin (a, c, e asterisk). There, co-labeling with the Golgi marker GM130 reveals again a partial overlap of Syap1 with the Golgi apparatus (enlargement c') but it is also detected in the characteristic dendrites of these cells (e, arrowheads). Furthermore, in the molecular layer, the protein shows a strong regional proximity in the glutamatergic neuropil labeled by anti-vGlut1 marking the

vesicular glutamate transporter of glutamatergic synapses (a, c, e; compare with knockout sections in b, d and f). Blue: DAPI. Scale bars: 100 µm (a, b), 25 µm (c, d), 10 µm (c', e, f)

Moreover, Syap1 is present in the extensive dendrites of the Purkinje cells (Figure 40e, arrowheads, enlargement of c white square) and can be observed in the molecular layer neuropil where climbing and parallel fibers make synapses with the dendritic tree of the Purkinje cells. As already detected in the hippocampus, Syap1 immunofluorescence also partially overlaps with vesicular glutamate transporter vGlut1 (Figure 40a, c, e; compare with knockout images in b, d, f). This partial overlap is also observed in the granular layer where medium levels of Syap1 immunofluorescent signals are identified at the big mossy fiber terminals of cerebellar glomeruli. However, not all Syap1 signals overlap with the detected vGlut1 puncta (Figure 40c, gray square magnified in Figure 41).

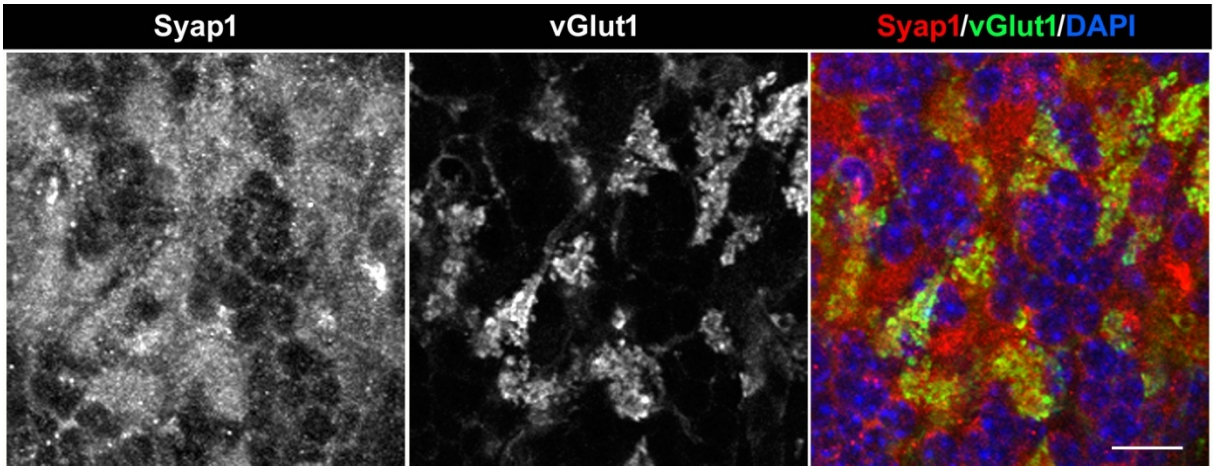

Figure 41: Syap1 and vGlut1 overlap in the cerebellum
In Syap1 and vGlut1 dual-immunolabelings partial overlap at glutamatergic mossy fiber terminals in the granule layer is observed, suggesting again a presynaptic localization of Syap1 at glutamatergic synapses. However, not all vGlut1 positive structures are also positive for Syap1. Scale bar: 10 µm

After addressing the question of Syap1 distribution in the brain, studies were performed to define its localization in the spinal cord and at neuromuscular junctions. In the spinal cord, choline-acetyl-transferase (ChAT) positive motoneurons also show a prominent Syap1 staining (Figure 42a, c, d) underlining the finding that Syap1 protein is expressed in motoneurons (Figure 6). Nonetheless, cells positive for Syap1 but negative for ChAT were observed indicating that the protein is expressed in other cells than motoneurons in the spinal cord, too (Figure 42a, magenta arrows). The relatively high signal of the Syap1 antibody in the

cholinergic cell bodies of the knockout sections (Figure 42b, d) could indicate that the antibody coss-reacts with an unknown antigen preferentially located in these cells. However, the much stronger signal in wild type sections with the typical perinuclear localization is interpreted to represent the Syap1 protein, associated with GM130 immunoreactivity in the cell body (Figure 42d, white arrows). The presence of Syap1 in ChAT-positive synaptic boutons attached to the motoneurons (Figure 42c, white arrowheads) needs to be investigate more precisely e.g. using high resolution microscopy, since an obvious accumulation of Syap1 was not detected in those structures.

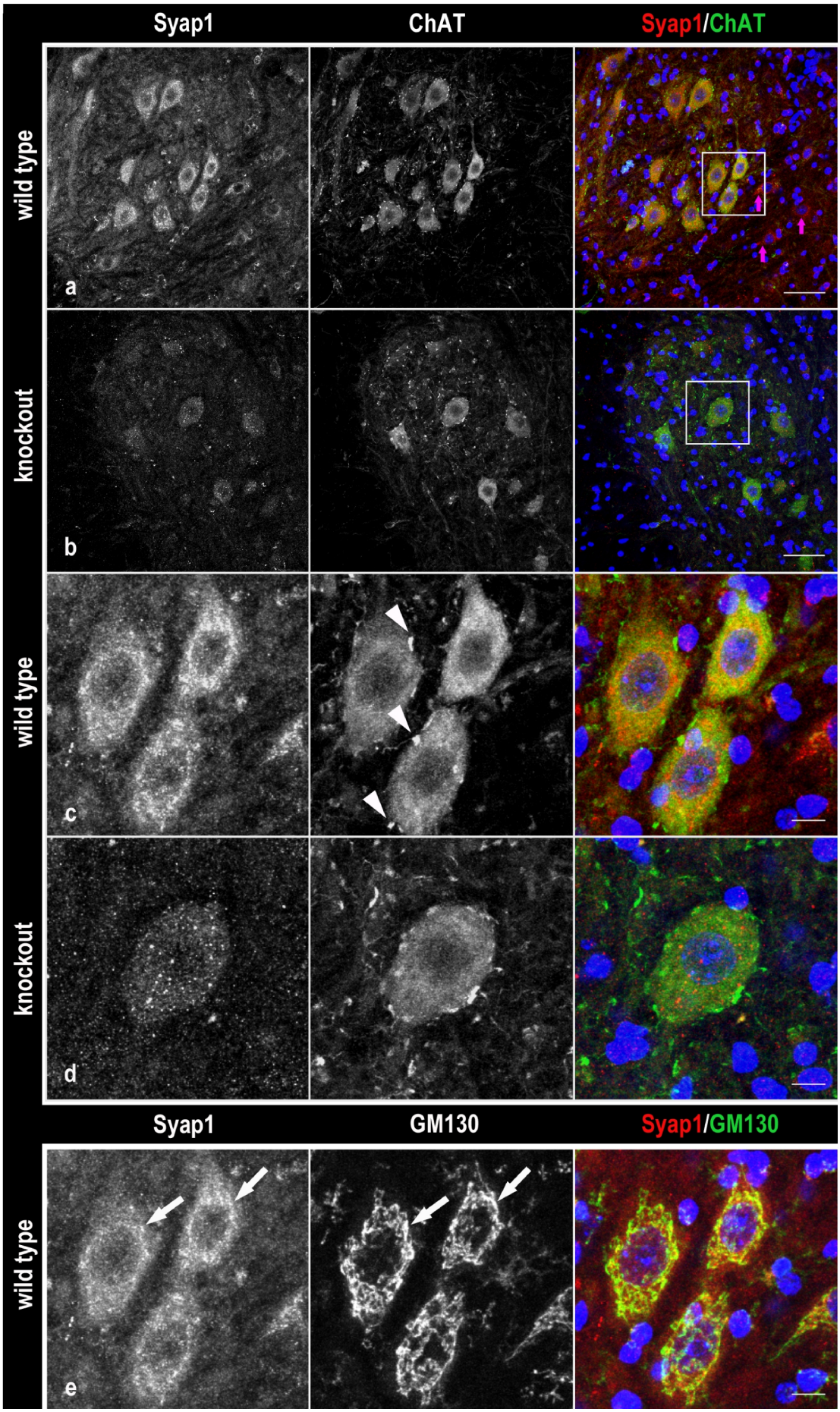

Figure 42: Syap1 distribution in the spinal cord

Syap1 immunofluorescence is especially observed in ChAT-positive motoneurons (a, c, d) but also in non-cholinergic cells (a, right image, magenta arrows) when compared with the knockout (b). Magnification (c and e) of the cells outlined in white display cholinergic boutons marked by white arrowheads in c do not show a clearly recognizable Syap1 accumulation. Again, some overlap with GM130 can be noticed (e, arrows). Scale bars: 50 µm (a, b), 10 µm (c, d, e)

Preliminary and reproducible stainings of neuromuscular junctions (NMJ) in gastrocnemius muscle preparations display similar low amounts of Syap1 at these specialized, cholinergic synapses as observed in the spinal cord (Figure 43). The surrounding muscle tissue apparently also contains low levels of Syap1, as indicated by comparison with knockout tissue, but needs to be verified with suitable co-markers.

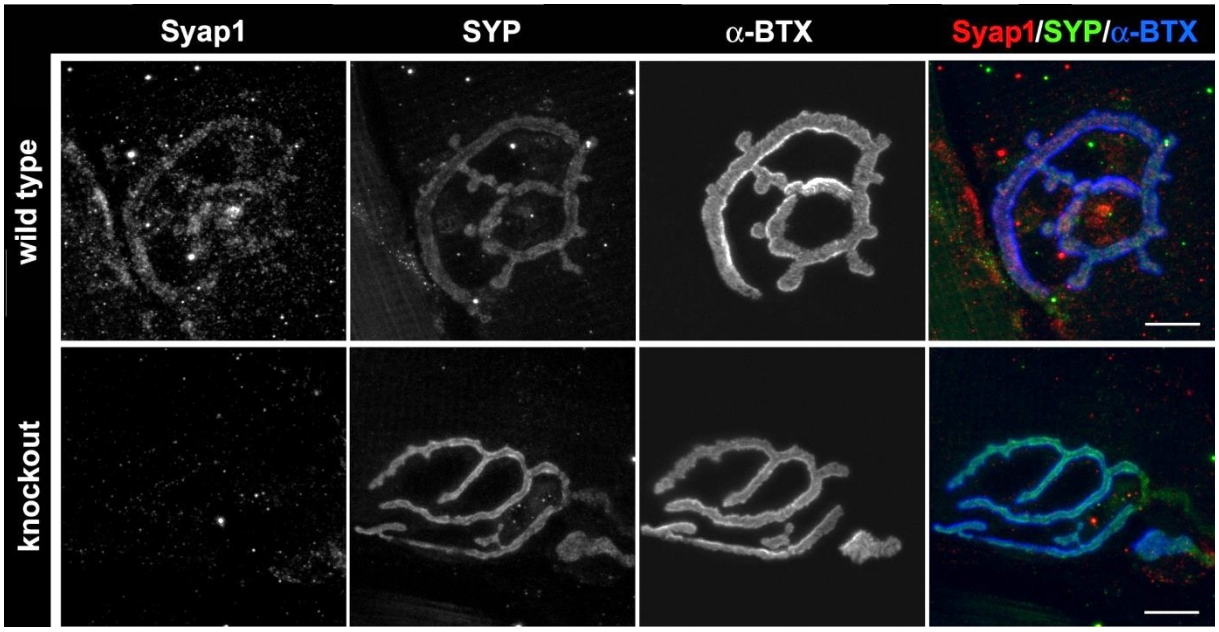

Figure 43: Syap1 localization at neuromuscular junctions

At neuromuscular junctions Syap1 is only sparsely labeled by the antibody showing its typical punctated distribution. Besides the localization in the synaptic region visualized by anti-Synaptophysin and α-bungarotoxin the protein can also be detected extra-synaptically in the muscle when compared with preparations from knockout animals. Scale bars: 10 µm

Since Syap1 was found to clearly accumulate perinuclearly in close proximity to the Golgi apparatus in almost every cell type (neuronal and non-neuronal), a possible influence on the morphology of the organelle was hypothesized. Therefore, detailed images from wild type and knockout stainings were compared and the Golgi morphology was investigated (Figure 44).

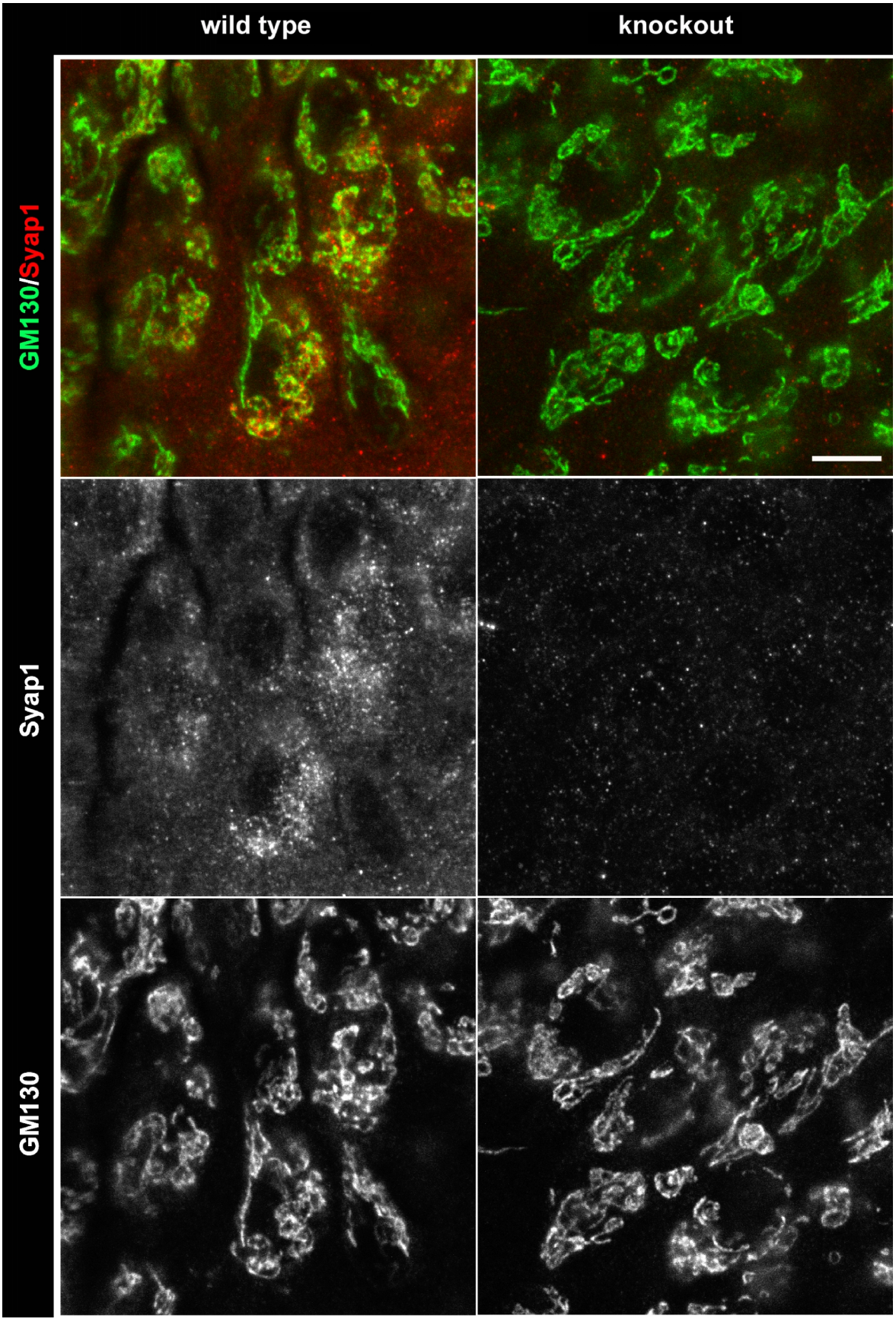

Figure 44: *Syap1* knockout does not influence the Golgi morphology

Syap1 knockout and wild type sections were stained against Syap1 and GM130 and perikarya in the hippocampal CA2 region imaged with high magnification. No obvious differences in the morphology of the Golgi apparatus - analyzed by GM130 labeling - were noticed by first visual inspections. Scale bar: 10 µm

First visual analysis of immunofluorescent images of the Golgi did not reveal obvious changes in its morphology after Syap1 depletion (Figure 44). Although the protein clearly accumulates near this organelle and shows a similar redistribution after BFA treatment (Figure 14), it seems not to be essential for the typical Golgi appearance. However, this does not preclude that Syap1 has an influence on the fine structure of the Golgi apparatus which failed to be detected by visual judgment of fluorescence staining in hippocampal area CA2.

3.8 Verification of *Syap1* knockdown data and functional analysis from isolated *Syap1*$^{-/-}$ motoneurons

3.8.1 Subcellular distribution of Syap1 protein in *Syap1*$^{-/-}$ motoneurons

Syap1 antibody specificity was already shown in chapter 3.1 by using lentiviral mediated knockdown of *Syap1* as evidence. Since the *Syap1* knockout mouse was available at later stages of this study some experiments were repeated with motoneurons isolated from *Syap1* knockout embryos to verify the results obtained before and/or to exclude possible off-target effects of the shRNA-mediated knockdown. Therefore, cultures obtained from single wild type and *Syap1* knockout embryos were investigated (as described in 2.2.1 followed by genotyping of each embryo) and experiments repeated under the identical conditions as for the knockdown experiments as an additional control for Syap1specificity of the staining.

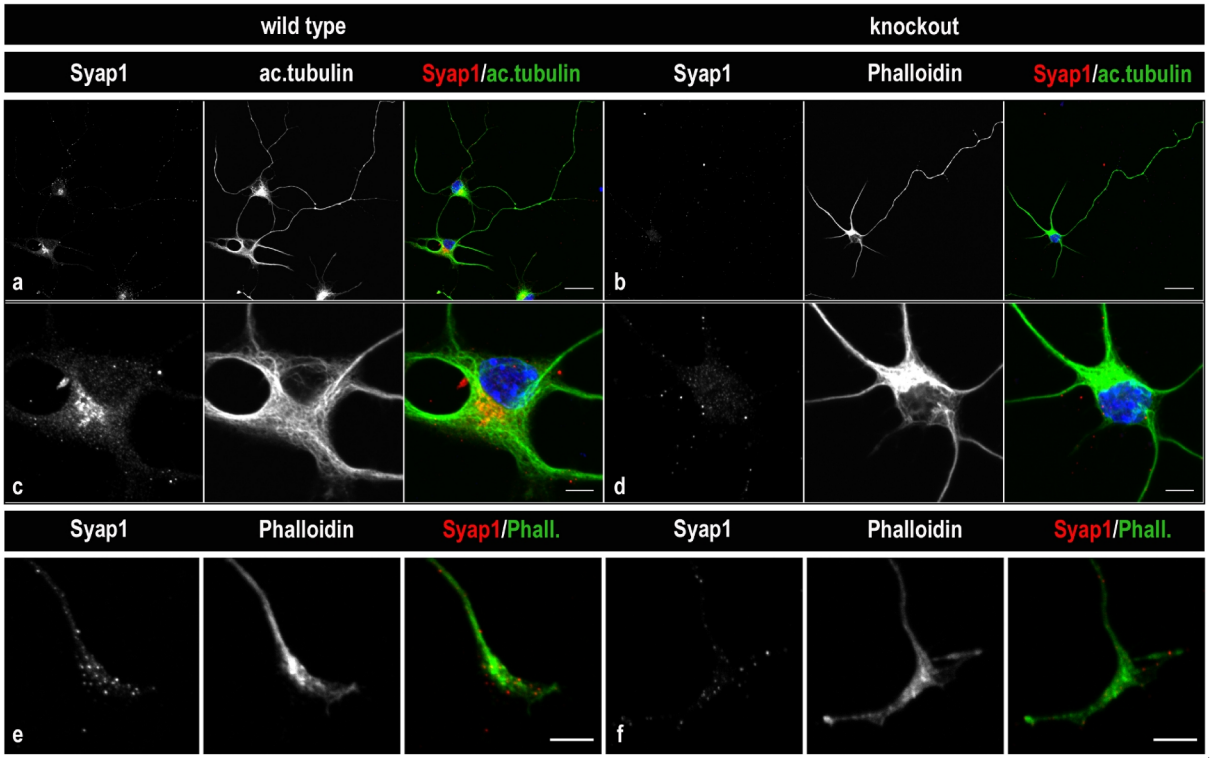

Figure 45: Syap1 distribution in wild type and *Syap1* knockout motoneurons

In confocal microscopy images of primary motoneurons, Syap1 immunofluorescence was strong in the cytoplasm next to the nucleus (a, c). Furthermore, it is found in dendrites, axon (a, c) and the growth cone (e). Images from *Syap1* knockout motoneurons served as control for signal specificity (b, d, f). Some Syap1 immunoreactivity was even detected in knockout cells resulting from unspecific cross-reactivity from the primary and/or secondary antibodies. Blue: DAPI staining. Scale bars: a, b: 25 µm; c, d, e, f: 5 µm

The comparison (Figure 45) revealed very similar results as those observed in Figure 6 and Figure 16. Here, the protein is also observed in a prominent perinuclear accumulation and distributes in a punctated manner throughout the cytoplasm, dendrites and axons (Figure 45a and c). Syap1 signals were also detected in the distal part of the axon and in the growth cone (Figure 45e). These signals were Syap1 specific by comparison to knockout cells (Fig. 45b, d, f). Nevertheless, some cross-reaction mainly caused by the primary antibody was observed since secondary antibody controls (not shown) did not display any considerable background. These results resemble the findings of what was observed when *Syap1* was knocked down and the stainings compared to uninfected motoneurons (Figure 6). Syap1 is distributed in a punctated manner throughout the perikarya, dendrites, axons and growth cones of primary motoneurons with a remarkable accumulation at the Golgi apparatus.

3.8.2 Morphological and functional analysis of Syap1 protein in *Syap1*$^{-/-}$ cultured motoneurons

Apart from the striking function of Syap1 in adipocyte differentiation (Yao et al. 2013), no other involvement of the protein was reported so far. Therefore, isolated primary motoneurons from wild type and *Syap1*$^{-/-}$ mice were cultured and analyzed concerning their functional aspects as partially already described in chapter 3.4 by comparison of uninfected mismatch, and Syap1 shRNA infected cells. As already observed for *Syap1* knockdown, there is no influence of the protein on motoneuron survival (Figure 46A) since no significant reduction in viability is observed after 7 DIV in the presence of the neurotrophic factor BDNF ($P > 0.3$). BDNF omission resulted in a drastic cell death - serving as a negative control ($P < 0.05$). Also, when axon growth was investigated no difference was observed between the genotypes (Figure 46B). This differs from the results obtained after lentiviral knockdown where a reduction in axon length after *Syap1* knockdown was observed. This could be indicative for a presumable off-target effect of the siRNA-sequence used (see 4.7). In order to further analyze the neurons concerning possible morphological differences, the number of primary dendrites was counted. No change in the number was observed after Syap1 depletion (Figure 46C).

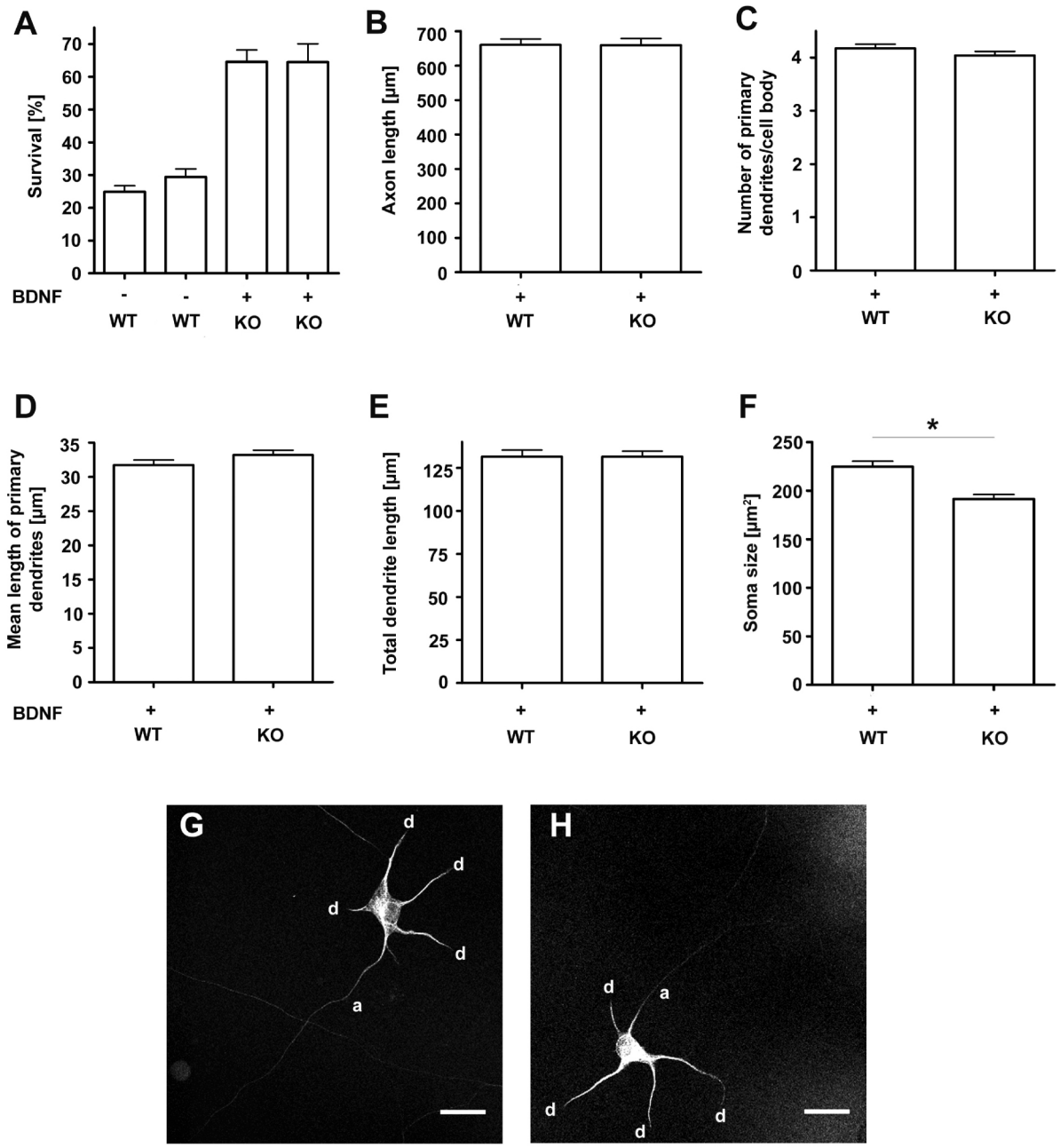

Figure 46: Influence of Syap1 on survival, axon length, dendritic outgrowth and soma size

Primary motoneurons from wild type and *Syap1* knockout mice were cultured for 7 DIV and analyzed for different functional and morphological aspects (A-F). No influence of Syap1 on the survival was observed when knockout motoneurons were compared to wild type neurons (A, two sample t-test; ns $P > 0.05$; wild type with BDNF: n= 17; 64.6 ± 3.6%; knockout with BDNF: n= 17; 64.5 ± 5.6%; wild type without BDNF: n= 7; 24.9 ± 1.9%; knockout without BDNF: n= 7; 29.4 ± 2.4%). Furthermore, several other morphological features like axon length (B; n=4; two sample t-test; ns $P > 0.05$; wild type: 660.5 ± 16.8 µm; knockout: 659.4 ± 19.3 µm), number of dendrites (C: n=4¸ two sample t-test; ns $P > 0.05$; wild type: N= 167; 4.1 ± 0.08; knockout: N= 168; 4.0 ± 0.08), mean (D; n= 4; two sample t-test wild type: N= 167; 31.74 ± 0.7 µm; knockout: N= 168; 33.2 ± 0.7 µm) and total length of dendrites (E; n= 4; two sample t-test; wild type: N= 167; 131.5 ± 3.8 µm; knockout: 131.5 ± 3.2 µm) were investigated but no difference compared to wild type can be noted when Syap1 is depleted. But the size of the soma is significantly smaller in *Syap1* knockout motoneurons (F, n= 4; two sample t-test; $P < 0.05$; wild type: N= 171; 224.7 ± 5.5 µm^2; knockout: N= 168; 191.4 ± 4.6 µm^2). Figures G and H show representative images of wild type (G) and *Syap1* knockout neurons (H). *: $P < 0.05$. a: axon, d: dendrite. Scale bars: 25 µm

In addition, no differences were observed when the mean or total length of dendrites was measured. This - together with the fact that axon outgrowth is also not affected by *Syap1* knockout - indicates that the protein itself does not have a critical function in neurite outgrowth or cell polarity. However, when the area of the somata was measured the size was significantly reduced in knockout motoneurons (Figure 46F).

3.8.3 Akt-phosphorylation is not altered in *Syap1*$^{-/-}$ motoneurons and *in vivo*

As already mentioned above Yao et al. (2013) showed an involvement of Syap1 in adipocyte differentiation by regulating Akt phosphorylation at Ser^{473} via mTORC2. *Syap1* knockdown and *Syap1* depleted embryonic stem cells revealed markedly reduced Akt^{Ser473} phosphorylation which is essential for adipocyte differentiation. In contrast, *Syap1* knockdown in cultured primary motoneurons did not noticeably affect Akt phosphorylation at Ser^{473} or Thr^{308} neither in Western blot analysis nor when different compartments were investigated (Figures 22 and 24). To exclude the possibility that phosphorylation is maintained by the low Syap1 protein levels remaining after shRNA mediated knockdown, the stimulation experiment was repeated with *Syap1* knockout motoneurons following the identical protocol as described in 2.2.19.

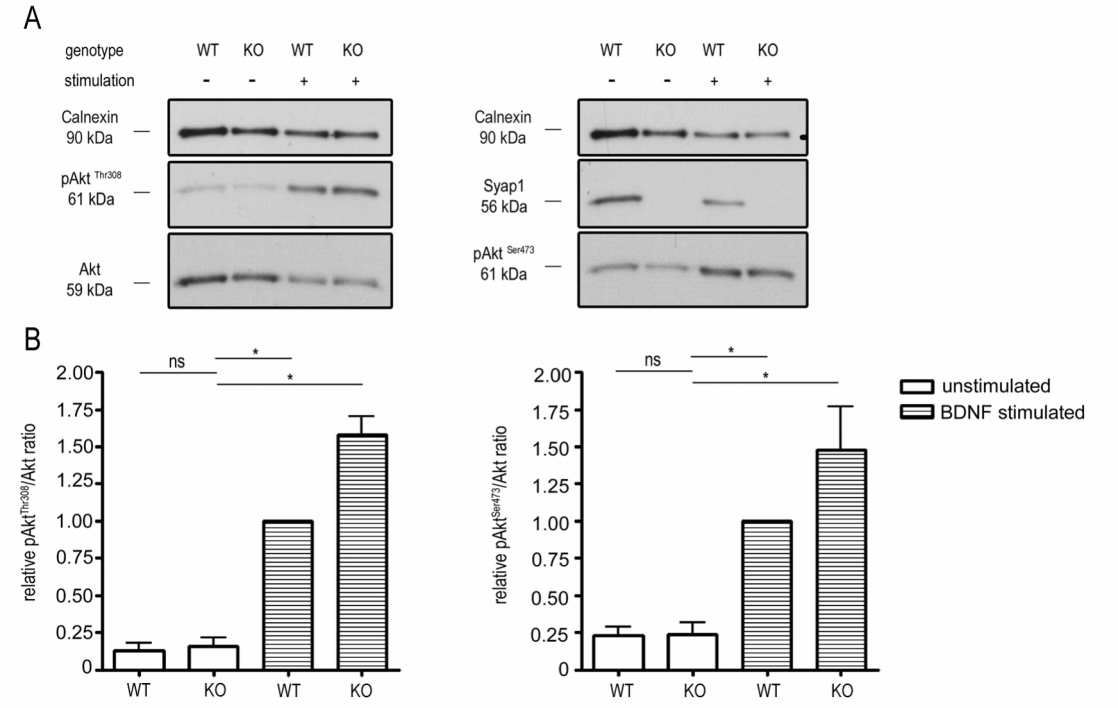

Figure 47: *Syap1* knockout does not decrease total Akt phosphorylation at Ser^{473} and Thr^{308}

Western blot of serum-starved and neurotrophic deprived wild type and *Syap1* knockout motoneurons stimulated with BDNF [20 ng/ml] for five minutes show no reduction in Akt phosphorylation at Thr^{308} (left blot) and Ser^{473} (right blot) after Syap1 depletion (A). Calnexin and pan-Akt served as loading controls. Densitometric quantification revealed a tendency for Akt phosphorylation to increase in *Syap1* knockout in motoneurons after BDNF stimulation (B, n = 3; values normalized to stimulated wild type; Thr^{308} (left): unstimulated, wild type 0.31 ± 0.06; unstimulated knockout: 0.15 ± 0.06; stimulated knockout: 1.58 ± 0.12; Ser^{473} (right): unstimulated wild type: 0.23 ± 0.06; unstimulated knockout: 0.24 ± 0.08; stimulated knockout: 1.48 ± 0.29). Bars shown represent means ± SEM. *: $P < 0.05$

As shown in Figure 47 densitometric quantification of Western blots revealed no reduction in Akt phosphorylation at Ser^{473} and Thr^{308} when signal values were normalized to the stimulated wild type condition. On the contrary, a tendency towards upregulation in the phosphorylation levels were observed in *Syap1* knockout motoneurons after BDNF stimulation. Unstimulated conditions did not differ between the genotypes. This is in accordance to the results obtained after *Syap1* knockdown (Figure 22) but is in contrast to the observations from Yao et al. in different cell types (2013).

Since the *Syap1* knockout mouse was available, the phosphorylation levels at Ser^{473} were investigated in different tissues in order to assess the levels *in vivo*. Therefore, tissues and organs were extracted, homogenized, subjected to Western blot analysis and densitometric signals were quantitatively evaluated. Figure 48 displays one representative blot and the corresponding quantification.

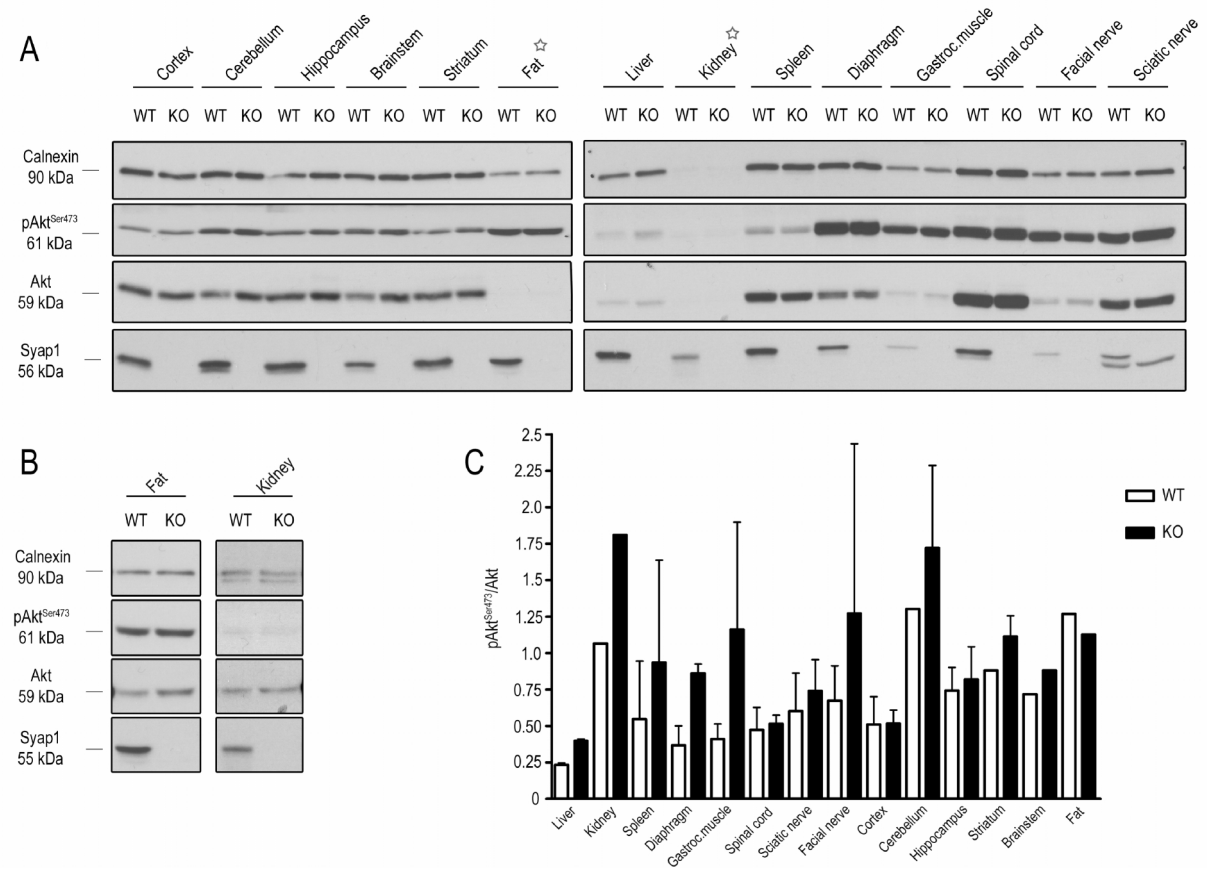

Figure 48: Akt^{Ser473} phosphorylation *in vivo* seems not to be affected by *Syap1* knockout

Several tissues of the central and peripheral nervous system from wild type and *Syap1* knockout mice were extracted, lysed in RIPA buffer and 20 µg per sample were subjected to Western blot analysis. The representative blot (A) does not show any obvious differences in Akt phosphorylation at Ser^{473} and was therefore densitometrically analyzed (C). In fat and liver tissue (marked with a star in A) some signals for proteins were not detectable with this exposure time and therefore longer exposures are depicted in B. Even with A higher exposure only very weak signals of pAkt^{Ser473} were achieved after extensive exposure. Therefore, for quantitative analysis higher amounts of protein need to be loaded. Probing for Calnexin and Akt served as loading controls, for Syap1 to prove the lack of Syap1 protein.

The results shown in Figure 48 support what was already observed for *in vitro* stimulation of motoneurons (Figure 47). No marked decrease in Akt^{Ser473} phosphorylation was detected in any of the investigated tissues after Syap1 depletion. In contrast, a tendency to an increased phosphorylation was observed. Nevertheless, since the results are only based on two independent experiments, no statistical analysis can be performed or a final conclusion drawn. Therefore, the experiment needs to be repeated several times.

4. Discussion

Although Syap1 is a highly conserved protein (Reichmuth et al. 1995), it is as yet poorly characterized. Only very few publications about its distribution and its possible function in mammalian cells (Yao et al. 2013) or about its homologue Sap47 in *Drosophila* (Saumweber et al. 2011; Funk et al. 2004; Kleber et al. 2016) are available so far. The presence of Sap47 in synaptic terminals in *Drosophila* larvae (Hofbauer et al. 2009) and the close proximity to synaptic vesicles (Saumweber et al. 2011) suggested a function especially in neuronal cells. Indeed, in 2011 Saumweber et al. observed an involvement of Sap47 in short-term plasticity at neuromuscular junctions as well as in maintaining normal levels of associative behavioral plasticity. However, results by Yao et al. (2013) suggest a function of Syap1 also in non-neuronal cells such as mouse embryonic fibroblasts, showing an implication in adipocyte differentiation. Recently, Kleber et al. (2016) reported modified Synapsin phosphorylation in Sap47 null mutant larvae.

4.1 Generation of the first *Syap1* knockout mouse

First information about a function of the Syap1 protein was based on *in vitro* experiments using mammalian cell lines (Yao et al. 2013). Since numerous questions remain to be answered such as its subcellular distribution and function in the nervous system and especially the *in vivo* consequences of the recently *in vitro* observed crucial role of Syap1 in Akt phosphorylation, a *Syap1* knockout mouse was produced in collaboration with the Institute of Laboratory Animal Science in Vienna. In 2010 Cox et al. already initiated the generation of a knockout mouse in a mutational screen of X-chromosomal genes studying prenatal developmental defects. As no obvious phenotypic developmental conspicuities were observed at E9.5, no further investigations were performed on that mouse. The available adult mice carrying the *tm1a* mutation did not express detectible levels of Syap1 protein. Even after increased protein loading and extensive exposure of the Western blot, no Syap1 signal was observed in tissue from *Syap1* knockout mouse although in the wild type tissue the protein was still detectable after a 1:100 dilution (Figure 32D). qRT-PCR experiments revealed a reduction of *Syap1* transcripts containing exon-3 and exon-4 (exon-8 and exon-9) to

approximately 6% (14%) in knockout brains when compared to wild type levels (Figure 32A-C). The difference in protein and transcript levels could possibly be explained by the short competing transcripts containing exon-1 to exon-3 and *En-2-lacZ* sequences for translation initiation with the residual intact *Syap1* transcripts. A partial RNA degradation or independent transcription initiation between exon-4 and exon-8 can be a reason for the discrepancy in the amount of transcripts containing exon-3 to exon-4 compared to those containing exon-8 and exon-9.

Initial phenotypic observation of the knockout animals did not reveal any gross conspicuities and differences in the general appearance, the size or the weight when compared to wild type littermates (Figure 31). As already observed for Sap47 in flies (Funk et al. 2004), the lack of Syap1 protein seems not to affect the fertility in mice whereas the number of female *Syap1*$^{-/-}$ animals obtained so far was reduced when genotypes of the F1 progeny were compared (Table 7). Nevertheless, more offspring of further crossings need to be compared for a final conclusion and profound statistical analysis. Together, the results generated in mice and flies might rather indicate a subtle function of this protein.

4.2 Syap1 antibody specificity

The biochemical, immunocytochemical and immunohistochemical study of Syap1 protein depends on a specific antibody. Since the MAB nc46 - detecting the Sap47 protein in *Drosophila melanogaster* - does not cross-react with murine Syap1, a characterization of several commercially available Syap1 antibodies was initiated. Only one of the tested antibodies (provided by Proteintech) raised against the human protein, detected only one single band at 55 kDa in human cells or at 56 kDa in lysates from mouse cell lines (Figure 5A). This small difference in electrophoretic mobility between the species corresponds to size difference as the murine protein is 17 aa longer than its human homologue. The observed bands at 55-56 kDa migrate significantly slower than the calculated weight of approximately 40 kDa (41.36 kDa in mouse, 39.94 kDa in human) would predict. A similar anomalous electrophoretic mobility was also reported by Yao et al. (2013) as their independently developed anti-Syap1 antibodies also detected a band of about 55 kDa. This observation had

also been described for Sap47 in *Drosophila* where bacterial expression of cDNA showed similar characteristics. This anomaly is not due to posttranslational modifications (Reichmuth et al. 1995). The specificity of the Proteintech antibody for biochemical assays was clearly proven by overexpression (Figure 5B) and knockdown experiments (Figure 5C-E) as well as in Western blots from *Syap1* knockout tissue (Figure 33A, B).

In order to gain first information about Syap1 localization *in vitro* and *in vivo*, the specificity of the commercial antibody was tested for immunocyto- and immunohistochemical analysis. Similar to the biochemical experiments, the results of Syap1 immunostainings in Figure 6A, B and Figures 33-43 provide profound evidence of the specificity of this antibody. After lentiviral knockdown or knockout, Syap1 signals - except some minor background signals - were almost abolished and therefore enabled the study of subcellular localization and tissue distribution of Syap1 within mammalian cells and mouse brain.

4.3 Subcellular distribution of Syap1 *in vitro*

Investigations of Syap1 localization and distribution were performed by immunocytochemistry in various cell types (HEK293 cells, NSC34 cells and primary motoneurons) using confocal and super-resolution microscopy. In all three studied cell types the basic distribution pattern was identical. The protein is found throughout the cytoplasm in a punctated manner with a strong accumulation in close proximity to the *cis/medial*-Golgi markers GM130 and γ-adaptin - one of the subunits of the AP-1 complex (Figures 6-13). Together with three other complexes (AP-2-4) which are present in mammalian cells AP-1 is implicated in operating of different trafficking pathways (Kirchhausen 1999; Robinson and Bonifacino 2001). AP-1 especially, is involved in the anterograde transport from the TGN to endosomes, but is also believed to act in recycling from endosomes to the TGN (Ahle et al. 1988; Robinson 1990; Meyer et al. 2000; Meyer et al. 2001). To examine the spatial correlation of Syap1 with the Golgi apparatus and the AP-1 complex, images obtained from super-resolution microscopy were analyzed (Figure 9G-J). The applied structured-illumination microscopy (SIM) allows a resolution beyond the 200 nm diffraction limit enabling a x-y-resolution in the range of 120 nm by using standard fluorescent probes as

immunocytochemical tags (Schermelleh et al. 2010). When results from confocal imaging and super-resolution microscopy were compared, it was noted that the overlap of signals of Syap1 and GM130 or AP-1 decreases, indicating that Syap1 apparently does not co-localize with GM130 or AP-1 (Figure 9C-J). Nevertheless, the accumulation at the Golgi apparatus is dependent on the intact structure of this organelle as it is lost after cells were treated with the toxic fungal metabolite BFA (Figure 14). This suggests, that Syap1 - although it does not directly co-localize with Golgi resident proteins - might either be linked to the Golgi via other proteins acting as an anchor or is possibly implicated in vesicular trafficking as BFA reversibly inhibits the ARF GEFs and thus disturbs COPI-mediated transport (Donaldson et al. 1992; Doms et al. 1989; Lippincott-Schwartz et al. 1989; Fujiwara et al. 1988). After BFA washout, Syap1 perinuclear accumulation was restored as observed for GM130 signals (Figure 14).

Moreover, crude subcellular fractionation using different buffers of increasing stringency revealed the presence of Syap1 protein in cytosolic as well as membranous fractions (Figure 15). This supports the hypothesis that Syap1 is somehow linked to the Golgi apparatus and/or to vesicular trafficking. In immunocytochemical stainings, low amounts of Syap1 were also detected in the nucleus (e.g. Figures 5 and 7); even in single plane images (Figure 8). Nevertheless, since this signal was also detected in knockdown (Figure 6B) and knockout cells (Figure 45d), it might be rather rated as unspecific cross-reaction. Furthermore, independent fractionation experiments, using different protocols, revealed no signal in the nuclear fraction in Western blot analysis (Figures 15 and 50). The slight band in the nuclear fraction P1 in Figure 17 likely resulted from a slight spill over from the first pocket; concluding that Syap1 levels in the nucleus are very low or the protein is completely absent from this organelle.

Besides the distribution pattern in the cytoplasm, Syap1 was also observed in dendrites, axons and axonal growth cones of neurons (Figure 9A, 16 and 45). In axonal growth cones, Syap1 signals appeared to be dense in Phalloidin-rich regions (Figure 16). The presence of Syap1 at synaptic terminals is in agreement with what was observed for Sap47 which is also observed in these structures (Saumweber et al. 2011). Furthermore, the isolation of synaptic vesicles by differential centrifugation also revealed Syap1 to be likely present in synapses (Figure 17), but

for a valid conclusion of an association with synaptic vesicles more experiments such as immunogold labeling and EM analysis need to be performed.

4.4 Syap1 expression

Syap1 was named after its homologue 'synapse-associated protein of 47 kDa' (Sap47) in *Drosophila* as it was first detected and described in synaptic terminals in immunohistochemical preparations (Reichmuth et al. 1995; Hofbauer 1991). However, initial experiments performed in this study already showed that Syap1 is not exclusively expressed in neuronal cell types or solely located at synapses. Biochemical and immunocytochemical studies with HEK293 showed that Syap1 is highly expressed in this non-neuronal cell type (Figure 1A and B). The protein was also detected in cell lysates from non-differentiated NSC34 cells or fibroblasts (Figure 1A, C and Figure 27A) which do not exhibit neurites or 'synapse-like' structures. To test the expression pattern of Syap1 in the mouse nervous system and also its occurrence in non-neuronal tissue, lysates from different brain areas and other organs were subjected to Western blot analysis, which revealed an equal expression levels within the investigated brain compartments (Figures 18, 33 and Figure 34A), similar to what was observed for MAB nc46 in *Drosophila* brain (Hofbauer 1991; Hofbauer et al. 2009). Likewise, the protein was detected in nerves (sciatic and facial nerve) supporting the immunocytochemical finding of Syap1 distribution in axons of primary motoneurons (Figure 9A, B and Figure 45a). The protein was also found in muscle tissue (diaphragm and gastocnemius muscle) and - as already assumed from cell lysates - in all of the tested non-neuronal organs like liver, spleen, fat and kidney (Figures 18, 33 and 48A, B). The results on Syap1 expression in non-neuronal cell types in this study are consistent with the findings of Yao and colleagues (2013) who also showed the presence of the protein in HEK293T cells and fibroblasts.

4.5 Syap1 distribution in the mouse nervous system

Since the results from biochemical analyses showed the expression of Syap1 in mouse brain (Figures 18, 33 and Figure 34A), and in view of the knowledge of Sap47 distribution in the neuropil, immunohistochemical studies were initiated to gain information about the distribution of Syap1 at the cellular and subcellular levels. The availability of a knockout-mouse now enabled the distinction of specific and unspecific immunofluorescence signals in the analyzed regions. The protein is found in all parts of the brain localizing preferentially in the gray matter (Figure 34). To see whether Syap1 can be found in presynaptic structures, localization of Syap1 was investigated in large mossy fiber synapses of the hippocampus and cerebellum. The data revealed relatively high levels of Syap1 in glutamatergic terminals of the mossy fiber pathway in the hippocampus (Kohara et al. 2014) (Figure 39) and in the molecular layer of the cerebellum (Figure 40 and 41). Interestingly, despite the fact of Syap1 being expressed in non-neuronal tissues such as the liver or spleen (Figure 18, 33 and 34A), the protein seems to be present only in low amounts in non-neuronal cells in the brain (Figure 38). In the olfactory bulb (Figure 36) high levels of Syap1 are found in the olfactory nerve layer and in the olfactory glomeruli which contain axons and glutamatergic nerve terminals, respectively (Ennis et al. 2006). In the dorso-medial cerebral cortex, Syap1 distribution is rather homogeneous and does not match soma density patterns observed by DAPI staining, indicating that Syap1 might preferentially be present in synapses (Figure 35). Furthermore, a large overlap with the vesicular transporter vGlut1, labeling the glutamatergic synaptic neuropil, was observed in the cerebellum (Figure 40a, c, e). There, detailed imaging revealed the presence of Syap1 in glutamatergic mossy fiber terminals but also in vGlut negative structures (Figure 41). In addition, immunohistochemical analysis showed for the cerebellar Purkinje cells the perinuclear accumulation of Syap1 as well as its localization in the large dendritic trees.

The strong selective perinuclear localization of Syap1 protein apparently seems to be restricted to distinct neuronal subtypes such as the large Purkinje cells in the cerebellum (Figure 40) and the hippocampal pyramidal cells in the CA2 region (Figure 39) as well as most of the neuronal somata in a thalamic subdomain (Figure 37). Syap1 distribution was also studied in spinal

cord where it was mainly detected in perinuclear accumulation of cholinergic motoneurons partially overlapping with GM130 (Figure 42e) but it does not aggregate in cholinergic synaptic boutons (Figure 42c). Likewise, at cholinergic neuromuscular junctions the protein seems to be present presynaptically only at low concentrations. However, Syap1 is found extrasynaptically also in muscle (Figure 43).

4.6 Syap1 and its interaction partners

An important hint on a possible function of any protein can be provided by information about its interaction partners. In a cyto-trap yeast-two-hybrid screen, TBCE-like protein was detected as a candidate interaction partner of Sap47 (N. Funk, unpublished data). TBCE-like protein is a regulator of microtubule stability being able to destabilize MTs (Bartolini et al. 2005). Therefore, TBCE-like counteracts TBCE, which promotes α-tubulin folding (Lewis et al. 1996; Tian et al. 1996). Based on these data and in view of the requirement of intact TBCE to prevent motoneuron degeneration, investigations of a possible interaction of TBCE and Syap1 were initiated. Co-immunoprecipitation studies using, due to the lack of an appropriate antibody, overexpressed HA-TBCE (generated by Dr. F. Bender) and FLAG-Syap1 (generated by Dr. N. Funk) in PC-12 and HEK293T cells, indicated an interaction between these two proteins. Interestingly, the interaction was reduced by the *TBCE*^{pmn}-mutation (unpublished data). Overexpression of proteins can lead to unphysiological interactions. Therefore, such results have to be substantiated by studies relying on endogenous expression. The newly characterized antibody specifically recognizing Syap1 protein and the available anti-TBCE antiserum, enabled the analysis of interactions of the two endogenous proteins. Therefore, immunoprecipitation analyses were performed using different cell lines, tissues and buffers in order to examine a possible TBCE-Syap1 interaction (Figure 26). Surprisingly, none of the immunoprecipitations (except one, data not shown as it was not reproducible) revealed an interaction. Since this could be due to a very weak or transient interaction, proteins were cross-linked prior to the experiment. Nonetheless, no interaction was observed (Figure 26D). This discrepancy with the results obtained from overexpression experiments can have different causes. Affinity tags and/or overexpression can produce artifacts leading to false

positive results which do not prove that the proteins are also interacting *in vivo* (Oeffinger 2012). Furthermore, it is possible that the homemade TBCE antiserum is not appropriate to detect very low amounts of the protein since it causes very strong background in Western blots and therefore could not be used to ascertain co-immunoprecipitated TBCE by longer exposure. Immunoprecipitations from endogenously expressed proteins are influenced by the native subcellular localization and post-translational modifications and require sufficient levels of both proteins of interest and highly specific antibodies. Therefore, it could well be that - although Syap1 and TBCE levels were detected in the input lanes - only very limited amounts of the proteins indeed interact after homogenization or that their interaction was transient with a short decay time and thus failed to be detected in the co-immunoprecipitate. Another explanation for the difference in the co-immunoprecipitation results obtained from overexpressed vs. endogenous proteins could be a competition of the Syap1 antibody with the interaction partner at the site of interaction. In this case, the antibody would be unable to precipitate the interaction partner. In conclusion, the endogenous interaction of Syap1 with TBCE remains still questionable and requires more investigations using more sensitive assays for analyzing the interaction such as mass spectrometry or immunoprecipitations with purified proteins. The latter would then also answer the question whether a possible interaction of both the proteins is direct or mediated by a third partner. Yet, besides the overexpression results, the localization of Syap1 is compatible with an interaction. As observed for Syap1, TBCE also accumulates at the Golgi apparatus with a striking overlap with GM130 and p115 - another *cis*-Golgi marker- as reported in 2007 by Schaefer and colleagues. There, TBCE exerts its function in a cross-talk together with ARF1 coordinating COPI formation and nucleation and polymerization of Golgi-derived microtubules (Bellouze et al. 2014). However, since a specific TBCE antibody for immunocytochemistry raised in a species other than rabbit was not available for this study, co-staining with Syap1 could not be performed.

Nevertheless, a screen reported by Havugimana et al. (2012), using human cell extracts for by an integrative global proteomic profiling approach for physical interactions did not support an interaction of these two proteins. When information on interactions of soluble proteins

isolated from HeLa S3 and HEK293 cells were evaluated, TBCE was not detected in one of the complexes with Syap1 but suggests other possible candidates such as β-actin, exportin, the hepatoma-derived growth factor or heat shock proteins which can be further investigated for an interaction.

Yao et al. (2013) report another interaction partner of Syap1. As mentioned above, the authors demonstrate a growth factor-dependent co-immunoprecipitation of Syap1 with Akt1 in 3T3-L1 cells and HEK293 cells (Yao et al. 2013). In order to investigate and to identify the molecular pathway by which Syap1 exerts its function in the nervous system, attempts were made to reproduce basic experiments of the Reddy group. Therefore, the protocol from Yao et al. (2013) was followed (as far as provided) and applied to the available cells. However, the reported results could not be reproduced here which might be due the different cell lines which were not identical. While Yao and colleagues used immortalized fibroblasts for their experiments, co-immunoprecipitations were performed with primary fibroblasts in our study (Figure 27A). This could be an explanation for the deviation in results since immortalization can influence the distribution as well as the expression of proteins (Pan et al. 2009). Hence, other cell types such as NSC34, HEK293T or neuronal stem cells were used and immunoprecipitation performed (Figure 27B, C and D). A slight interaction was observed in Figure 27B and C after EGF- or FCS-stimulation, respectively. In brain tissue, when Akt and Syap1 interaction was investigated a faint band was observed for the co-immunoprecipitate. However, the results did not show the apparent 1:1 stoichiometry as reported in the paper. In addition, in the screen from Havugimana et al. (2012), Akt was also not detected as one of the Syap1 interaction candidates. Therefore, the interaction between Syap1 and Akt might acutely depend on the cell type.

4.7 Functional analysis

In this study initial experiments were performed in order to analyze possible functions for Syap1 in the nervous system. Since an interaction with TBCE was hypothesized Syap1 deficient motoneurons were investigated in detail. Observations by Bommel et al. (2002) had shown that the *pmn*-mutation does not alter the survival of primary mutant motoneurons but

disrupts axon elongation resulting in shorter axons and an increased number of axonal swellings. Therefore, survival and morphological features such as growth cone (Figure 19E) and soma size (Figure 46F), number of filopodia (Figure 19F) axon length (Figure 19B, D and Figure 46) and dendritic length (Figure 46D and E) were investigated in *Syap1* knockdown (Figure 19) and/or knockout (Figure 46) motoneurons, respectively. The survival, growth cone size, number of filopodia and dendrites, as well as the dendritic lengths (total and mean) were not influenced by Syap1 reduction or depletion. However, axonal outgrowth was significantly reduced after 5 DIV and 7 DIV when primary motoneurons were infected with *Syap1* knockdown virus expressing a specific shRNA (Figure 19B-D). This shRNA (see 2.2.7) is 100% complementary to a sequence of the *Syap1* mRNA but due to its shortness it necessarily also shows significant complementarity to several other mouse mRNAs, as a nucleotide blast revealed. Thus given that motoneurons obtained from Syap1$^{-/-}$ embryos do not exhibit shorter axons after 7 DIV, it is likely that the observed result after the knockdown was caused by off-target effects of the shRNA (Jackson et al. 2003) (Figure 51). *Pmn*-mutant motoneurons exhibit shorter axons, presumably due to lower levels of stable, precipitable α-tubulin relative to soluble monomeric α-tubulin, without affecting total levels of α- or β_{III}-tubulin. This suggests that some α-tubulin was incorrectly folded and incompetent for polymerization (Schaefer et al. 2007). Therefore, microtubule-fractionation experiments (Figure 20) were performed using *Syap1*-knockdown motoneurons and corresponding controls to test if this could be the cause for the observed reduced axonal outgrowth. The results did not reveal any difference in soluble (tyrosinated tubulin), precipitable, stable (acetylated tubulin) or total α-tubulin levels which indicates that Syap1 does not play a role in microtubule assembly or posttranslational modifications. This finding supports the hypothesis of off target effects. However, another possible but more unlikely explanation for the difference in results obtained by (acute) knockdown and (permanent) knockout could be compensatory mechanisms effective during early embryogenesis making up for the lack of Syap1. Therefore, this phenotype demands further control experiments which could not be executed due to temporal limitations of the project. By designing additional Syap1 shRNAs and repeating the knockdown experiments the reproducibility of the axon length phenotype

could be tested. In case of consistent shRNA results, rescue experiments by overexpression of Syap1 using a cDNA with synonymous codons that disrupt shRNA complementarity could provide a final prove of the involvement of Syap1 in axonal outgrowth.

Interestingly, while other investigated morphological features of primary motoneurons remained unaffected by *Syap1* knockout or knockdown, a reduction in the soma size after depletion of the protein was observed (Figure 46F). In the nervous system, specific types of neurons exhibit a characteristic soma size. After growing to a particular size, the neurons exit from the cell cycle (McConnell 1988) indicating that neuronal growth plays a major role in neuronal differentiation which must be subject to a tight developmental regulation. Besides many other regulators, the mTOR-Akt pathway has been reported to be linked to the regulation of dendritic and somatic morphogenesis (Kumar et al. 2005; Jaworski and Sheng 2006). The recently reported involvement of Syap1 (BSTA) in Akt phosphorylation (Yao et al. 2013) could thus in principle explain the observed reduced soma size. However, as discussed below, the participation of Syap1 in the regulation of Akt phosphorylation seems to be unlikely in primary motoneurons (Figure 22) and most likely also *in vivo* (Figure 48). Therefore, the effect of a smaller soma size demands further investigations. Especially the determination of the size *in vivo* would be of high relevance since the lack of cell contacts and extracellular factors *in vitro* might lead to such a morphological phenotype.

In distinct non-neuronal cells Syap1 promotes mTORC2 mediated phosphorylation of Akt1 at Ser^{473} upon growth factor stimulation requiring the preceding interaction of the proteins. This step is crucial for the *in vitro* differentiation of adipocytes (Yao et al. 2013). In neurons, the Akt signaling pathway can be activated by neurotrophins such as BDNF (Huang and Reichardt 2003). Phosphorylation of Akt takes place at several amino acids. Immediately after translation, the protein is constitutively phosphorylated in the turn motif at Thr^{450} facilitating carboxyl-terminal folding and stabilizing the newly synthesized Akt (Facchinetti et al. 2008). A full activation of Akt activity is achieved by further phosphorylations at Thr^{308} and Ser^{473} (Jacinto et al. 2006; Alessi et al. 1996; Anderson et al. 1998; Sarbassov et al. 2005). In this study, the influence of Syap1 on the phosphorylation at Ser^{473} and Thr^{308} was investigated *in vitro* using primary motoneurons. After defining the kinetics of phosphorylation at these sites

knockdown and knockout motoneurons were stimulated with 20 ng/ml BDNF for two and five minutes (Figure 21). This stimulation paradigm seems to be optimal for the neuronal activation of Akt as it was also applied in studies with hippocampal neurons (Johnson-Farley et al. 2006; Johnson-Farley et al. 2007). Consistently, quantification of Western blots from motoneurons cell lysates and compartment specific analysis (soma, axon and growth cone) showed that phosphorylation at Ser^{473} and/or Thr^{308} is not influenced by *Syap1* knockdown or depletion (Figure 22, 24 and 47). As a reduction in Akt phosphorylation at these sites was not observed upon *Syap1* knockdown or knockout in BDNF-stimulated (Figures 22, 24 and 47) and unstimulated (Figure 23 and Figure 25) motoneurons, the hypothesis of a functionally important interaction of Syap1 and Akt was not confirmed. However, due to the high sequence similarity of the three different Akt isoforms, the phospho-specific antibodies used for analysis were not capable of discriminating between them. Akt3 is highly expressed in the nervous system (Tschopp et al. 2005; Easton et al. 2005). Hence, a possible Akt1 hypophosphorylation in the motoneurons might be undetected e.g. because of an Akt3 hyperphosphorylation. It is also conceivable that Syap1 plays a role in different molecular mechanisms depending on the cell type and/or developmental state as the effect of *Syap1* knockdown on Akt phosphorylation was shown in immortalized non-neuronal cell lines (Yao et al. 2013). Therefore, the deviation in the present results from those of Yao et al. are either attributed the use of postmitotic motoneurons or isoform-specific mechanisms in the nervous system which are operating to ensure constant levels of total Akt phosphorylation.

Independently from *in vitro* results, the generation of the first *Syap1* knockout mouse invites speculations on the role of Syap1 on Akt phosphorylation and adipocyte differentiation *in vivo*. Highly and ubiquitously expressed Akt1 was reported to be a critical determinant of adipocyte differentiation (Baudry et al. 2006), growth (Cho et al. 2001b; Chen et al. 2001). Therefore, if Syap1 was critical for Akt activity also *in vivo* one would expect that $Syap1^{-/-}$ mice show a defect in producing fat tissue and might thus be smaller or lighter in weight. Although further repetitions of these experiments need to be performed for statistical analysis, *Syap1* knockout animals did not show an obvious difference in size (Figure 31) or body weight when compared to littermates. In addition, when tissue homogenates of adult wild type and $Syap1^{-/-}$

mice were analyzed, no clear reduction in Akt phosphorylation levels at Ser^{473} due to Syap1 depletion was observed in any of the tested tissues, including fat (Figure 48B and C). These results support our *in vitro* data which also did not find a clear influence of Syap1 on Akt phosphorylation.

4.8 Conclusion

Taken together, the results of this initial characterization of the phylogenetically conserved Syap1 protein provide first information about expression, tissue localization and subcellular distribution in the mouse central nervous system and invite speculations on a possible molecular implication of the protein.

Since *Syap1* knockout mice are viable and the survival and axonal outgrowth of primary motoneurons from knockout mouse embryos are not affected, the function of the largely uncharacterized family of synapse-associated proteins seems to be more subtle. Mice lacking Syap1 do not show obvious morphological conspicuities in their general appearance or in the brain when compared to wild type littermates.

The widespread distribution of Syap1 was not only shown by Western blot analysis but also in brain sections and on a subcellular level by immunohistochemistry. Its close proximity to the Golgi apparatus and the vicinity of Sap47 to glutamatergic synaptic vesicles in *Drosophila* allows the speculation that Syap1/Sap47 may be involved in vesicular processing and/or trafficking in populations of cells, in particular neurons, and in distinct types of synapses.

As *Sap47* knockout flies show impairment in synaptic plasticity and olfactory associative learning, and in view of the present observation of strong Syap1 expression in the mouse central nervous system, the characterization of the behavioral as well as the motor phenotype of *Syap1*$^{-/-}$ mice as a model for studying Syap1 function in human is of high interest.

5. References

Aguilera Gomez A, Rabouille C (2015) Intra-Golgi Transport. In: Encyclopedia of Cell Biology. Academic Press, Waltham, pp 354-362. doi:http://dx.doi.org/10.1016/B978-0-12-394447-4.20034-5

Ahle S, Mann A, Eichelsbacher U, Ungewickell E (1988) Structural relationships between clathrin assembly proteins from the Golgi and the plasma membrane. The EMBO journal 7 (4):919-929

Ahle S, Ungewickell E (1989) Identification of a clathrin binding subunit in the HA2 adaptor protein complex. The Journal of biological chemistry 264 (33):20089-20093

Ahmed S (2011) Isolation and characterization of synaptic vesicles from mouse brain. phd, Georg-August-Universität, Göttingen

Akama KT, McEwen BS (2003) Estrogen stimulates postsynaptic density-95 rapid protein synthesis via the Akt/protein kinase B pathway. The Journal of neuroscience : the official journal of the Society for Neuroscience 23 (6):2333-2339

Al-Dhaheri MH, Shah YM, Basrur V, Pind S, Rowan BG (2006) Identification of novel proteins induced by estradiol, 4-hydroxytamoxifen and acolbifene in T47D breast cancer cells. Steroids 71 (11-12):966-978. doi:10.1016/j.steroids.2006.07.006

Alessi DR, Andjelkovic M, Caudwell B, Cron P, Morrice N, Cohen P, Hemmings BA (1996) Mechanism of activation of protein kinase B by insulin and IGF-1. The EMBO journal 15 (23):6541-6551

Anderson KE, Coadwell J, Stephens LR, Hawkins PT (1998) Translocation of PDK-1 to the plasma membrane is important in allowing PDK-1 to activate protein kinase B. Current biology : CB 8 (12):684-691

Arakawa Y, Sendtner M, Thoenen H (1990) Survival effect of ciliary neurotrophic factor (CNTF) on chick embryonic motoneurons in culture: comparison with other neurotrophic factors and cytokines. The Journal of neuroscience : the official journal of the Society for Neuroscience 10 (11):3507-3515

Arce CA, Rodriguez JA, Barra HS, Caputo R (1975) Incorporation of L-tyrosine, L-phenylalanine and L-3,4-dihydroxyphenylalanine as single units into rat brain tubulin. Eur J Biochem 59 (1):145-149

Aridor M, Bannykh SI, Rowe T, Balch WE (1995) Sequential coupling between COPII and COPI vesicle coats in endoplasmic reticulum to Golgi transport. The Journal of cell biology 131 (4):875-893

Arikkath J, Reichardt LF (2008) Cadherins and catenins at synapses: roles in synaptogenesis and synaptic plasticity. Trends Neurosci 31 (9):487-494. doi:10.1016/j.tins.2008.07.001

Auguin D, Barthe P, Auge-Senegas MT, Stern MH, Noguchi M, Roumestand C (2004) Solution structure and backbone dynamics of the pleckstrin homology domain of the human protein kinase B (PKB/Akt). Interaction with inositol phosphates. Journal of biomolecular NMR 28 (2):137-155. doi:10.1023/B:JNMR.0000013836.62154.c2

Baas PW, Black MM (1990) Individual microtubules in the axon consist of domains that differ in both composition and stability. The Journal of cell biology 111 (2):495-509

Bannykh SI, Rowe T, Balch WE (1996) The organization of endoplasmic reticulum export complexes. The Journal of cell biology 135 (1):19-35

Barlowe C (2003) Signals for COPII-dependent export from the ER: what's the ticket out? Trends in cell biology 13 (6):295-300

Barlowe C, Orci L, Yeung T, Hosobuchi M, Hamamoto S, Salama N, Rexach MF, Ravazzola M, Amherdt M, Schekman R (1994) COPII: a membrane coat formed by Sec proteins that drive vesicle budding from the endoplasmic reticulum. Cell 77 (6):895-907

Bartolini F, Tian G, Piehl M, Cassimeris L, Lewis SA, Cowan NJ (2005) Identification of a novel tubulin-destabilizing protein related to the chaperone cofactor E. Journal of cell science 118 (Pt 6):1197-1207. doi:10.1242/jcs.01719

Baskaran N, Kandpal RP, Bhargava AK, Glynn MW, Bale A, Weissman SM (1996) Uniform amplification of a mixture of deoxyribonucleic acids with varying GC content. Genome research 6 (7):633-638

Baudry A, Yang ZZ, Hemmings BA (2006) PKBalpha is required for adipose differentiation of mouse embryonic fibroblasts. Journal of cell science 119 (Pt 5):889-897. doi:10.1242/jcs.02792

Baumert M, Maycox PR, Navone F, De Camilli P, Jahn R (1989) Synaptobrevin: an integral membrane protein of 18,000 daltons present in small synaptic vesicles of rat brain. The EMBO journal 8 (2):379-384

Bellouze S, Schafer MK, Buttigieg D, Baillat G, Rabouille C, Haase G (2014) Golgi fragmentation in pmn mice is due to a defective ARF1/TBCE cross-talk that coordinates COPI vesicle formation and tubulin polymerization. Human molecular genetics 23 (22):5961-5975. doi:10.1093/hmg/ddu320

Belnoue L, Grosjean N, Abrous DN, Koehl M (2011) A critical time window for the recruitment of bulbar newborn neurons by olfactory discrimination learning. The Journal of neuroscience : the official journal of the Society for Neuroscience 31 (3):1010-1016. doi:10.1523/JNEUROSCI.3941-10.2011

Bhamidipati A, Lewis SA, Cowan NJ (2000) ADP ribosylation factor-like protein 2 (Arl2) regulates the interaction of tubulin-folding cofactor D with native tubulin. The Journal of cell biology 149 (5):1087-1096

Bi X, Mancias JD, Goldberg J (2007) Insights into COPII coat nucleation from the structure of Sec23.Sar1 complexed with the active fragment of Sec31. Dev Cell 13 (5):635-645. doi:10.1016/j.devcel.2007.10.006

Blum R, Pfeiffer F, Feick P, Nastainczyk W, Kohler B, Schafer KH, Schulz I (1999) Intracellular localization and in vivo trafficking of p24A and p23. Journal of cell science 112 (Pt 4):537-548

Bommel H, Xie G, Rossoll W, Wiese S, Jablonka S, Boehm T, Sendtner M (2002) Missense mutation in the tubulin-specific chaperone E (Tbce) gene in the mouse mutant progressive motor neuronopathy, a model of human motoneuron disease. The Journal of cell biology 159 (4):563-569. doi:10.1083/jcb.200208001

Bonanomi D, Fornasiero EF, Valdez G, Halegoua S, Benfenati F, Menegon A, Valtorta F (2008) Identification of a developmentally regulated pathway of membrane retrieval in neuronal growth cones. Journal of cell science 121 (Pt 22):3757-3769. doi:10.1242/jcs.033803

Bonifacino JS, Glick BS (2004) The mechanisms of vesicle budding and fusion. Cell 116 (2):153-166

Bonifacino JS, Rojas R (2006) Retrograde transport from endosomes to the trans-Golgi network. Nat Rev Mol Cell Biol 7 (8):568-579

Briese M, Saal L, Appenzeller S, Moradi M, Baluapuri A, Sendtner M (2016) Whole transcriptome profiling reveals the RNA content of motor axons. Nucleic acids research 44 (4):e33. doi:10.1093/nar/gkv1027

Brodbeck D, Cron P, Hemmings BA (1999) A human protein kinase Bgamma with regulatory phosphorylation sites in the activation loop and in the C-terminal hydrophobic domain. The Journal of biological chemistry 274 (14):9133-9136

Brunet A, Bonni A, Zigmond MJ, Lin MZ, Juo P, Hu LS, Anderson MJ, Arden KC, Blenis J, Greenberg ME (1999) Akt promotes cell survival by phosphorylating and inhibiting a Forkhead transcription factor. Cell 96 (6):857-868

Bulinski JC, Richards JE, Piperno G (1988) Posttranslational modifications of alpha tubulin: detyrosination and acetylation differentiate populations of interphase microtubules in cultured cells. The Journal of cell biology 106 (4):1213-1220

Calof AL, Reichardt LF (1984) Motoneurons purified by cell sorting respond to two distinct activities in myotube-conditioned medium. Developmental biology 106 (1):194-210

Cashman NR, Durham HD, Blusztajn JK, Oda K, Tabira T, Shaw IT, Dahrouge S, Antel JP (1992) Neuroblastoma x spinal cord (NSC) hybrid cell lines resemble developing motor neurons. Developmental dynamics : an official publication of the American Association of Anatomists 194 (3):209-221. doi:10.1002/aja.1001940306

Chang YC, Yu YL, Wang N, Xu YH (2001) [Cloning and characterization of syap1, a down regulated gene in human hepatocellular carcinoma]. Shi yan sheng wu xue bao 34 (4):319-322

Chen WS, Xu PZ, Gottlob K, Chen ML, Sokol K, Shiyanova T, Roninson I, Weng W, Suzuki R, Tobe K, Kadowaki T, Hay N (2001) Growth retardation and increased apoptosis in mice with homozygous disruption of the Akt1 gene. Genes Dev 15 (17):2203-2208. doi:10.1101/gad.913901

Cheng JQ, Godwin AK, Bellacosa A, Taguchi T, Franke TF, Hamilton TC, Tsichlis PN, Testa JR (1992) AKT2, a putative oncogene encoding a member of a subfamily of protein-serine/threonine kinases, is amplified in human ovarian carcinomas. Proceedings of the National Academy of Sciences of the United States of America 89 (19):9267-9271

Cho H, Mu J, Kim JK, Thorvaldsen JL, Chu Q, Crenshaw EB, 3rd, Kaestner KH, Bartolomei MS, Shulman GI, Birnbaum MJ (2001a) Insulin resistance and a diabetes mellitus-like syndrome in mice lacking the protein kinase Akt2 (PKB beta). Science 292 (5522):1728-1731. doi:10.1126/science.292.5522.1728

Cho H, Thorvaldsen JL, Chu Q, Feng F, Birnbaum MJ (2001b) Akt1/PKBalpha is required for normal growth but dispensable for maintenance of glucose homeostasis in mice. The Journal of biological chemistry 276 (42):38349-38352. doi:10.1074/jbc.C100462200

Cosson P, Amherdt M, Rothman JE, Orci L (2002) A resident Golgi protein is excluded from peri-Golgi vesicles in NRK cells. Proceedings of the National Academy of Sciences 99 (20):12831-12834. doi:10.1073/pnas.192460999

Cox BJ, Vollmer M, Tamplin O, Lu M, Biechele S, Gertsenstein M, van Campenhout C, Floss T, Kuhn R, Wurst W, Lickert H, Rossant J (2010) Phenotypic annotation of the mouse X chromosome. Genome research 20 (8):1154-1164. doi:10.1101/gr.105106.110

Datta SR, Dudek H, Tao X, Masters S, Fu H, Gotoh Y, Greenberg ME (1997) Akt phosphorylation of BAD couples survival signals to the cell-intrinsic death machinery. Cell 91 (2):231-241

De Matteis MA, Luini A (2008) Exiting the Golgi complex. Nat Rev Mol Cell Biol 9 (4):273-284. doi:10.1038/nrm2378

Diez H, Garrido JJ, Wandosell F (2012) Specific roles of Akt iso forms in apoptosis and axon growth regulation in neurons. PloS one 7 (4):e32715. doi:10.1371/journal.pone.0032715

Doerks T, Huber S, Buchner E, Bork P (2002) BSD: a novel domain in transcription factors and synapse-associated proteins. Trends in biochemical sciences 27 (4):168-170

Doms RW, Russ G, Yewdell JW (1989) Brefeldin A redistributes resident and itinerant Golgi proteins to the endoplasmic reticulum. The Journal of cell biology 109 (1):61-72

Donaldson JG, Finazzi D, Klausner RD (1992) Brefeldin A inhibits Golgi membrane-catalysed exchange of guanine nucleotide onto ARF protein. Nature 360 (6402):350-352. doi:10.1038/360350a0

Dull T, Zufferey R, Kelly M, Mandel RJ, Nguyen M, Trono D, Naldini L (1998) A third-generation lentivirus vector with a conditional packaging system. J Virol 72 (11):8463-8471

Dummler B, Hemmings BA (2007) Physiological roles of PKB/Akt isoforms in development and disease. Biochem Soc Trans 35 (Pt 2):231-235. doi:10.1042/BST0350231

Dunphy WG, Rothman JE (1985) Compartmental organization of the Golgi stack. Cell 42 (1):13-21

Easton RM, Cho H, Roovers K, Shineman DW, Mizrahi M, Forman MS, Lee VM, Szabolcs M, de Jong R, Oltersdorf T, Ludwig T, Efstratiadis A, Birnbaum MJ (2005) Role for Akt3/protein kinase Bgamma in attainment of normal brain size. Molecular and cellular biology 25 (5):1869-1878. doi:10.1128/MCB.25.5.1869-1878.2005

Emr S, Glick BS, Linstedt AD, Lippincott-Schwartz J, Luini A, Malhotra V, Marsh BJ, Nakano A, Pfeffer SR, Rabouille C, Rothman JE, Warren G, Wieland FT (2009) Journeys through the Golgi--taking stock in a new era. The Journal of cell biology 187 (4):449-453. doi:10.1083/jcb.200909011

Eng LF, Vanderhaeghen JJ, Bignami A, Gerstl B (1971) An acidic protein isolated from fibrous astrocytes. Brain research 28 (2):351-354

Ennis M, Zhu M, Heinbockel T, Hayar A (2006) Olfactory nerve-evoked, metabotropic glutamate receptor-mediated synaptic responses in rat olfactory bulb mitral cells. Journal of neurophysiology 95 (4):2233-2241. doi:10.1152/jn.01150.2005

Eugster A, Frigerio G, Dale M, Duden R (2000) COP I domains required for coatomer integrity, and novel interactions with ARF and ARF-GAP. The EMBO journal 19 (15):3905-3917. doi:10.1093/emboj/19.15.3905

Facchinetti V, Ouyang W, Wei H, Soto N, Lazorchak A, Gould C, Lowry C, Newton AC, Mao Y, Miao RQ, Sessa WC, Qin J, Zhang P, Su B, Jacinto E (2008) The mammalian target of rapamycin complex 2 controls folding and stability of Akt and protein kinase C. The EMBO journal 27 (14):1932-1943. doi:10.1038/emboj.2008.120

Farquhar MG, Hauri H-P (1997) Protein sorting and vesicular traffic in the Golgi apparatus. In: Berger EG, Roth J (eds) The Golgi Apparatus. Birkhäuser Basel, Basel, pp 63-129. doi:10.1007/978-3-0348-8876-9_3

Figueres-Onate M, Gutierrez Y, Lopez-Mascaraque L (2014) Unraveling Cajal's view of the olfactory system. Front Neuroanat 8:55. doi:10.3389/fnana.2014.00055

Forscher P, Smith SJ (1988) Actions of cytochalasins on the organization of actin filaments and microtubules in a neuronal growth cone. The Journal of cell biology 107 (4):1505-1516

Fujiwara T, Oda K, Yokota S, Takatsuki A, Ikehara Y (1988) Brefeldin A causes disassembly of the Golgi complex and accumulation of secretory proteins in the endoplasmic reticulum. The Journal of biological chemistry 263 (34):18545-18552

Funk N, Becker S, Huber S, Brunner M, Buchner E (2004) Targeted mutagenesis of the Sap47 gene of Drosophila: flies lacking the synapse associated protein of 47 kDa are viable and fertile. BMC neuroscience 5:16. doi:10.1186/1471-2202-5-16

Gao Y, Thomas JO, Chow RL, Lee GH, Cowan NJ (1992) A cytoplasmic chaperonin that catalyzes beta-actin folding. Cell 69 (6):1043-1050

Gao Y, Vainberg IE, Chow RL, Cowan NJ (1993) Two cofactors and cytoplasmic chaperonin are required for the folding of alpha- and beta-tubulin. Molecular and cellular biology 13 (4):2478-2485

Garofalo RS, Orena SJ, Rafidi K, Torchia AJ, Stock JL, Hildebrandt AL, Coskran T, Black SC, Brees DJ, Wicks JR, McNeish JD, Coleman KG (2003) Severe diabetes, age-dependent loss of adipose tissue, and mild growth deficiency in mice lacking Akt2/PKB beta. J Clin Invest 112 (2):197-208. doi:10.1172/JCI16885

Gonzalez E, McGraw TE (2009) The Akt kinases: isoform specificity in metabolism and cancer. Cell Cycle 8 (16):2502-2508

Gotz R, Wiese S, Takayama S, Camarero GC, Rossoll W, Schweizer U, Troppmair J, Jablonka S, Holtmann B, Reed JC, Rapp UR, Sendtner M (2005) Bag1 is essential for differentiation and survival of hematopoietic and neuronal cells. Nature neuroscience 8 (9):1169-1178. doi:10.1038/nn1524

Gould E, Beylin A, Tanapat P, Reeves A, Shors TJ (1999) Learning enhances adult neurogenesis in the hippocampal formation. Nature neuroscience 2 (3):260-265. doi:10.1038/6365

Griffiths G, Simons K (1986) The trans Golgi network: sorting at the exit site of the Golgi complex. Science 234 (4775):438-443

Haase G, Rabouille C (2015) Golgi Fragmentation in ALS Motor Neurons. New Mechanisms Targeting Microtubules, Tethers, and Transport Vesicles. Front Neurosci 9:448. doi:10.3389/fnins.2015.00448

Hadjivassiliou G, Martinian L, Squier W, Blumcke I, Aronica E, Sisodiya SM, Thom M (2010) The application of cortical layer markers in the evaluation of cortical dysplasias in epilepsy. Acta Neuropathol 120 (4):517-528. doi:10.1007/s00401-010-0686-x

Havugimana PC, Hart GT, Nepusz T, Yang H, Turinsky AL, Li Z, Wang PI, Boutz DR, Fong V, Phanse S, Babu M, Craig SA, Hu P, Wan C, Vlasblom J, Dar VU, Bezginov A, Clark GW, Wu GC, Wodak SJ, Tillier ER, Paccanaro A, Marcotte EM, Emili A (2012) A census of human soluble protein complexes. Cell 150 (5):1068-1081. doi:10.1016/j.cell.2012.08.011

Heilker R, Spiess M, Crottet P (1999) Recognition of sorting signals by clathrin adaptors. BioEssays : news and reviews in molecular, cellular and developmental biology 21 (7):558-567. doi:10.1002/(SICI)1521-1878(199907)21:7<558::AID-BIES4>3.0.CO;2-R

Hell JW, Jahn R (2006) Chapter 12 - Preparation of Synaptic Vesicles from Mammalian Brain A2 - Celis, Julio E. In: Cell Biology (Third Edition). Academic Press, Burlington, pp 85-90. doi:http://dx.doi.org/10.1016/B978-012164730-8/50084-8

Hofbauer A (1991) Eine Bibliothek monoklonaler Antikörper gegen das Gehirn von

Drosophila melanogaster. Universität Würzburg, Wuerzburg

Hofbauer A, Ebel T, Waltenspiel B, Oswald P, Chen YC, Halder P, Biskup S, Lewandrowski U, Winkler C, Sickmann A, Buchner S, Buchner E (2009) The Wuerzburg hybridoma library against Drosophila brain. Journal of neurogenetics 23 (1-2):78-91. doi:10.1080/01677060802471627

Holden P, Horton WA (2009) Crude subcellular fractionation of cultured mammalian cell lines. BMC Res Notes 2:243. doi:10.1186/1756-0500-2-243

Horton AC, Ehlers MD (2003) Neuronal polarity and trafficking. Neuron 40 (2):277-295

Huang EJ, Reichardt LF (2003) Trk receptors: roles in neuronal signal transduction. Annual review of biochemistry 72:609-642. doi:10.1146/annurev.biochem.72.121801.161629

Huber S (2003) Charakterisierung von SAP47 in Drosophila melanogaster und der dazugehörigen Proteinfamilie

Characterization of SAP47 in Drosophila melanogaster and its protein familiy.

Irie HY, Pearline RV, Grueneberg D, Hsia M, Ravichandran P, Kothari N, Natesan S, Brugge JS (2005) Distinct roles of Akt1 and Akt2 in regulating cell migration and epithelial-mesenchymal transition. The Journal of cell biology 171 (6):1023-1034. doi:10.1083/jcb.200505087

Itakura M, Tsujimura J, Yamamori S, Ohkido T, Takahashi M (2013) NMDA receptor-dependent recruitment of Calnexin to the neuronal plasma membrane. Neuroscience letters 550:173-178. doi:10.1016/j.neulet.2013.06.064

Jablonka S, Beck M, Lechner BD, Mayer C, Sendtner M (2007) Defective Ca2+ channel clustering in axon terminals disturbs excitability in motoneurons in spinal muscular atrophy. The Journal of cell biology 179 (1):139-149. doi:10.1083/jcb.200703187

Jacinto E, Facchinetti V, Liu D, Soto N, Wei S, Jung SY, Huang Q, Qin J, Su B (2006) SIN1/MIP1 maintains rictor-mTOR complex integrity and regulates Akt phosphorylation and substrate specificity. Cell 127 (1):125-137. doi:10.1016/j.cell.2006.08.033

Jackson AL, Bartz SR, Schelter J, Kobayashi SV, Burchard J, Mao M, Li B, Cavet G, Linsley PS (2003) Expression profiling reveals off-target gene regulation by RNAi. Nat Biotechnol 21 (6):635-637. doi:10.1038/nbt831

Janke C, Bulinski JC (2011) Post-translational regulation of the microtubule cytoskeleton: mechanisms and functions. Nat Rev Mol Cell Biol 12 (12):773-786. doi:10.1038/nrm3227

Jaworski J, Sheng M (2006) The growing role of mTOR in neuronal development and plasticity. Mol Neurobiol 34 (3):205-219. doi:10.1385/MN:34:3:205

Jin S, Pan L, Liu Z, Wang Q, Xu Z, Zhang YQ (2009) Drosophila Tubulin-specific chaperone E functions at neuromuscular synapses and is required for microtubule network formation. Development 136 (9):1571-1581. doi:10.1242/dev.029983

Johnson-Farley NN, Patel K, Kim D, Cowen DS (2007) Interaction of FGF-2 with IGF-1 and BDNF in stimulating Akt, ERK, and neuronal survival in hippocampal cultures. Brain research 1154:40-49. doi:10.1016/j.brainres.2007.04.026

Johnson-Farley NN, Travkina T, Cowen DS (2006) Cumulative activation of akt and consequent inhibition of glycogen synthase kinase-3 by brain-derived neurotrophic factor and insulin-like growth factor-1 in cultured hippocampal neurons. The Journal of pharmacology and experimental therapeutics 316 (3):1062-1069. doi:10.1124/jpet.105.094433

Jones PF, Jakubowicz T, Hemmings BA (1991) Molecular cloning of a second form of rac protein kinase. Cell Regul 2 (12):1001-1009

Kane LP, Shapiro VS, Stokoe D, Weiss A (1999) Induction of NF-kappaB by the Akt/PKB kinase. Current biology : CB 9 (11):601-604

Kirchhausen T (1999) Adaptors for clathrin-mediated traffic. Annual review of cell and developmental biology 15:705-732. doi:10.1146/annurev.cellbio.15.1.705

Kleber J, Chen YC, Michels B, Saumweber T, Schleyer M, Kahne T, Buchner E, Gerber B (2016) Synapsin is required to "boost" memory strength for highly salient events. Learning & memory (Cold Spring Harbor, NY) 23 (1):9-20. doi:10.1101/lm.039685.115

Klumperman J (2011) Architecture of the mammalian Golgi. Cold Spring Harbor perspectives in biology 3 (7). doi:10.1101/cshperspect.a005181

Kohara K, Pignatelli M, Rivest AJ, Jung HY, Kitamura T, Suh J, Frank D, Kajikawa K, Mise N, Obata Y, Wickersham IR, Tonegawa S (2014) Cell type-specific genetic and optogenetic tools reveal hippocampal CA2 circuits. Nature neuroscience 17 (2):269-279. doi:10.1038/nn.3614

Kumar V, Zhang MX, Swank MW, Kunz J, Wu GY (2005) Regulation of dendritic morphogenesis by Ras-PI3K-Akt-mTOR and Ras-MAPK signaling pathways. The Journal of neuroscience : the official journal of the Society for Neuroscience 25 (49):11288-11299. doi:10.1523/JNEUROSCI.2284-05.2005

L'Hernault SW, Rosenbaum JL (1985) Chlamydomonas alpha-tubulin is posttranslationally modified by acetylation on the epsilon-amino group of a lysine. Biochemistry 24 (2):473-478

Ladinsky MS, Mastronarde DN, McIntosh JR, Howell KE, Staehelin LA (1999) Golgi structure in three dimensions: functional insights from the normal rat kidney cell. The Journal of cell biology 144 (6):1135-1149

Lasiecka ZM, Winckler B (2011) Mechanisms of polarized membrane trafficking in neurons -- focusing in on endosomes. Mol Cell Neurosci 48 (4):278-287. doi:10.1016/j.mcn.2011.06.013

Lee WK, Vargas A, Barnes J, Root AW (1983) The Kenny-Caffey syndrome: growth retardation and hypocalcemia in a young boy. Am J Med Genet 14 (4):773-782. doi:10.1002/ajmg.1320140419

Letourneur F, Gaynor EC, Hennecke S, Demolliere C, Duden R, Emr SD, Riezman H, Cosson P (1994) Coatomer is essential for retrieval of dilysine-tagged proteins to the endoplasmic reticulum. Cell 79 (7):1199-1207

Leuner B, Gould E, Shors TJ (2006) Is there a link between adult neurogenesis and learning? Hippocampus 16 (3):216-224. doi:10.1002/hipo.20153

Lewis SA, Tian G, Cowan NJ (1997) The alpha- and beta-tubulin folding pathways. Trends in cell biology 7 (12):479-484. doi:10.1016/S0962-8924(97)01168-9

Lewis SA, Tian G, Vainberg IE, Cowan NJ (1996) Chaperonin-mediated folding of actin and tubulin. The Journal of cell biology 132 (1-2):1-4

Lippincott-Schwartz J, Yuan LC, Bonifacino JS, Klausner RD (1989) Rapid redistribution of Golgi proteins into the ER in cells treated with brefeldin A: evidence for membrane cycling from Golgi to ER. Cell 56 (5):801-813

Manning BD, Cantley LC (2007) AKT/PKB signaling: navigating downstream. Cell 129 (7):1261-1274. doi:10.1016/j.cell.2007.06.009

Marcos S, Moreau J, Backer S, Job D, Andrieux A, Bloch-Gallego E (2009) Tubulin tyrosination is required for the proper organization and pathfinding of the growth cone. PloS one 4 (4):e5405. doi:10.1371/journal.pone.0005405

Martin N, Jaubert J, Gounon P, Salido E, Haase G, Szatanik M, Guenet JL (2002) A missense mutation in Tbce causes progressive motor neuronopathy in mice. Nature genetics 32 (3):443-447. doi:10.1038/ng1016

Martinez-Menarguez JA, Geuze HJ, Slot JW, Klumperman J (1999) Vesicular tubular clusters between the ER and Golgi mediate concentration of soluble secretory proteins by exclusion from COPI-coated vesicles. Cell 98 (1):81-90. doi:10.1016/S0092-8674(00)80608-X

Martínez-Menárguez JA, Prekeris R, Oorschot VMJ, Scheller R, Slot JW, Geuze HJ, Klumperman J (2001) Peri-Golgi vesicles contain retrograde but not anterograde proteins consistent with the cisternal progression model of intra-Golgi transport. The Journal of cell biology 155 (7):1213-1224. doi:10.1083/jcb.200108029

Martinou JC, Falls DL, Fischbach GD, Merlie JP (1991) Acetylcholine receptor-inducing activity stimulates expression of the epsilon-subunit gene of the muscle acetylcholine receptor. Proceedings of the National Academy of Sciences of the United States of America 88 (17):7669-7673

McConnell SK (1988) Development and decision-making in the mammalian cerebral cortex. Brain research 472 (1):1-23

Melchior WB, Jr., Von Hippel PH (1973) Alteration of the relative stability of dA-dT and dG-dC base pairs in DNA. Proceedings of the National Academy of Sciences of the United States of America 70 (2):298-302

Mellman I, Simons K (1992) The Golgi complex: in vitro veritas? Cell 68 (5):829-840

Meyer C, Eskelinen EL, Guruprasad MR, von Figura K, Schu P (2001) Mu 1A deficiency induces a profound increase in MPR300/IGF-II receptor internalization rate. Journal of cell science 114 (Pt 24):4469-4476

Meyer C, Zizioli D, Lausmann S, Eskelinen EL, Hamann J, Saftig P, von Figura K, Schu P (2000) mu1A-adaptin-deficient mice: lethality, loss of AP-1 binding and rerouting of mannose 6-phosphate receptors. The EMBO journal 19 (10):2193-2203. doi:10.1093/emboj/19.10.2193

Milburn CC, Deak M, Kelly SM, Price NC, Alessi DR, Van Aalten DM (2003) Binding of phosphatidylinositol 3,4,5-trisphosphate to the pleckstrin homology domain of protein kinase B induces a conformational change. The Biochemical journal 375 (Pt 3):531-538. doi:10.1042/bj20031229

Mitchell KJ, Pinson KI, Kelly OG, Brennan J, Zupicich J, Scherz P, Leighton PA, Goodrich LV, Lu X, Avery BJ, Tate P, Dill K, Pangilinan E, Wakenight P, Tessier-Lavigne M, Skarnes WC (2001)

Functional analysis of secreted and transmembrane proteins critical to mouse development. Nature genetics 28 (3):241-249. doi:10.1038/90074

Mourelatos Z, Gonatas NK, Stieber A, Gurney ME, Dal Canto MC (1996) The Golgi apparatus of spinal cord motor neurons in transgenic mice expressing mutant Cu,Zn superoxide dismutase becomes fragmented in early, preclinical stages of the disease. Proceedings of the National Academy of Sciences of the United States of America 93 (11):5472-5477

Mullen RJ, Buck CR, Smith AM (1992) NeuN, a neuronal specific nuclear protein in vertebrates. Development 116 (1):201-211

Nakamura N, Rabouille C, Watson R, Nilsson T, Hui N, Slusarewicz P, Kreis TE, Warren G (1995) Characterization of a cis-Golgi matrix protein, GM130. The Journal of cell biology 131 (6 Pt 2):1715-1726

Naldini L, Blomer U, Gallay P, Ory D, Mulligan R, Gage FH, Verma IM, Trono D (1996) In vivo gene delivery and stable transduction of nondividing cells by a lentiviral vector. Science 272 (5259):263-267

Nickel W, Malsam J, Gorgas K, Ravazzola M, Jenne N, Helms JB, Wieland FT (1998) Uptake by COPI-coated vesicles of both anterograde and retrograde cargo is inhibited by GTPgammaS in vitro. Journal of cell science 111 (20):3081-3090

Oeffinger M (2012) Two steps forward--one step back: advances in affinity purification mass spectrometry of macromolecular complexes. Proteomics 12 (10):1591-1608. doi:10.1002/pmic.201100509

Onishi K, Higuchi M, Asakura T, Masuyama N, Gotoh Y (2007) The PI3K-Akt pathway promotes microtubule stabilization in migrating fibroblasts. Genes to cells : devoted to molecular & cellular mechanisms 12 (4):535-546. doi:10.1111/j.1365-2443.2007.01071.x

Oprins A, Duden R, Kreis TE, Geuze HJ, Slot JW (1993) Beta-COP localizes mainly to the cis-Golgi side in exocrine pancreas. The Journal of cell biology 121 (1):49-59

Orci L, Glick BS, Rothman JE (1986) A new type of coated vesicular carrier that appears not to contain clathrin: Its possible role in protein transport within the Golgi stack. Cell 46 (2):171-184. doi:10.1016/0092-8674(86)90734-8

Orci L, Stamnes M, Ravazzola M, Amherdt M, Perrelet A, Sollner TH, Rothman JE (1997) Bidirectional transport by distinct populations of COPI-coated vesicles. Cell 90 (2):335-349

Ori-McKenney KM, Jan LY, Jan YN (2012) Golgi outposts shape dendrite morphology by functioning as sites of acentrosomal microtubule nucleation in neurons. Neuron 76 (5):921-930. doi:10.1016/j.neuron.2012.10.008

Paglini G, Pigino G, Kunda P, Morfini G, Maccioni R, Quiroga S, Ferreira A, Caceres A (1998) Evidence for the participation of the neuron-specific CDK5 activator P35 during laminin-enhanced axonal growth. The Journal of neuroscience : the official journal of the Society for Neuroscience 18 (23):9858-9869

Pan C, Kumar C, Bohl S, Klingmueller U, Mann M (2009) Comparative proteomic phenotyping of cell lines and primary cells to assess preservation of cell type-specific functions. Molecular & cellular proteomics : MCP 8 (3):443-450. doi:10.1074/mcp.M800258-MCP200

Park JH, Lee SB, Lee KH, Ahn JY (2012) Nuclear Akt promotes neurite outgrowth in the early stage of neuritogenesis. BMB reports 45 (9):521-525

Parvari R, Diaz GA, Hershkovitz E (2007) Parathyroid development and the role of tubulin chaperone E. Horm Res 67 (1):12-21. doi:10.1159/000095944

Parvari R, Hershkovitz E, Grossman N, Gorodischer R, Loeys B, Zecic A, Mortier G, Gregory S, Sharony R, Kambouris M, Sakati N, Meyer BF, Al Aqeel AI, Al Humaidan AK, Al Zanhrani F, Al Swaid A, Al Othman J, Diaz GA, Weiner R, Khan KT, Gordon R, Gelb BD, Consortium HRARK-CS (2002) Mutation of TBCE causes hypoparathyroidism-retardation-dysmorphism and autosomal recessive Kenny-Caffey syndrome. Nature genetics 32 (3):448-452. doi:10.1038/ng1012

Pearse BM (1975) Coated vesicles from pig brain: purification and biochemical characterization. J Mol Biol 97 (1):93-98

Pearse BM (1976) Clathrin: a unique protein associated with intracellular transfer of membrane by coated vesicles. Proceedings of the National Academy of Sciences of the United States of America 73 (4):1255-1259

Pearse BM, Robinson MS (1990) Clathrin, adaptors, and sorting. Annu Rev Cell Biol 6:151-171. doi:10.1146/annurev.cb.06.110190.001055

Presley JF, Cole NB, Schroer TA, Hirschberg K, Zaal KJ, Lippincott-Schwartz J (1997) ER-to-Golgi transport visualized in living cells. Nature 389 (6646):81-85. doi:10.1038/38001

Qi XJ, Wildey GM, Howe PH (2006) Evidence that Ser87 of BimEL is phosphorylated by Akt and regulates BimEL apoptotic function. The Journal of biological chemistry 281 (2):813-823. doi:10.1074/jbc.M505546200

Ramirez OA, Couve A (2011) The endoplasmic reticulum and protein trafficking in dendrites and axons. Trends in cell biology 21 (4):219-227. doi:10.1016/j.tcb.2010.12.003

Read DE, Gorman AM (2009) Involvement of Akt in neurite outgrowth. Cellular and molecular life sciences : CMLS 66 (18):2975-2984. doi:10.1007/s00018-009-0057-8

Rees WA, Yager TD, Korte J, von Hippel PH (1993) Betaine can eliminate the base pair composition dependence of DNA melting. Biochemistry 32 (1):137-144

Reichmuth C, Becker S, Benz M, Debel K, Reisch D, Heimbeck G, Hofbauer A, Klagges B, Pflugfelder GO, Buchner E (1995) The sap47 gene of Drosophila melanogaster codes for a novel conserved neuronal protein associated with synaptic terminals. Brain research Molecular brain research 32 (1):45-54

Reisch N (2003) Das Cysteine-String-Protein in Drosophila melanogaster: Molekulare und funktionelle Analyse verschiedener CSP-Mutanten; Ein Modell zur räumlich und zeitlich kontrollierten CSP-Expression

The cysteine string protein in Drosophila melanogaster: Molecular and functional analysis of different CSP-mutants; A model for spatial and temporal controlled CSP-expression.

Richardson RJ, Kirk JM (1990) Short stature, mental retardation, and hypoparathyroidism: a new syndrome. Archives of disease in childhood 65 (10):1113-1117

Robinson MS (1990) Cloning and expression of gamma-adaptin, a component of clathrin-coated vesicles associated with the Golgi apparatus. The Journal of cell biology 111 (6 Pt 1):2319-2326

Robinson MS, Bonifacino JS (2001) Adaptor-related proteins. Current opinion in cell biology 13 (4):444-453

Rochlin MW, Wickline KM, Bridgman PC (1996) Microtubule stability decreases axon elongation but not axoplasm production. The Journal of neuroscience : the official journal of the Society for Neuroscience 16 (10):3236-3246

Romashkova JA, Makarov SS (1999) NF-kappaB is a target of AKT in anti-apoptotic PDGF signalling. Nature 401 (6748):86-90. doi:10.1038/43474

Rossoll W, Jablonka S, Andreassi C, Kroning AK, Karle K, Monani UR, Sendtner M (2003) Smn, the spinal muscular atrophy-determining gene product, modulates axon growth and localization of beta-actin mRNA in growth cones of motoneurons. The Journal of cell biology 163 (4):801-812. doi:10.1083/jcb.200304128

Sabry MA, Zaki M, Shaltout A (1998) Genotypic/phenotypic heterogeneity of Kenny-Caffey syndrome. Journal of medical genetics 35 (12):1054-1055

Sanes JR, Lichtman JW (1999) Development of the vertebrate neuromuscular junction. Annual review of neuroscience 22:389-442. doi:10.1146/annurev.neuro.22.1.389

Santi SA, Lee H (2010) The Akt isoforms are present at distinct subcellular locations. American journal of physiology Cell physiology 298 (3):C580-591. doi:10.1152/ajpcell.00375.2009

Sarbassov DD, Guertin DA, Ali SM, Sabatini DM (2005) Phosphorylation and regulation of Akt/PKB by the rictor-mTOR complex. Science 307 (5712):1098-1101. doi:10.1126/science.1106148

Sarkar G, Kapelner S, Sommer SS (1990) Formamide can dramatically improve the specificity of PCR. Nucleic acids research 18 (24):7465

Saumweber T, Weyhersmuller A, Hallermann S, Diegelmann S, Michels B, Bucher D, Funk N, Reisch D, Krohne G, Wegener S, Buchner E, Gerber B (2011) Behavioral and synaptic plasticity are impaired upon lack of the synaptic protein SAP47. The Journal of neuroscience : the official journal of the Society for Neuroscience 31 (9):3508-3518. doi:10.1523/JNEUROSCI.2646-10.2011

Scales SJ, Pepperkok R, Kreis TE (1997) Visualization of ER-to-Golgi transport in living cells reveals a sequential mode of action for COPII and COPI. Cell 90 (6):1137-1148

Scales TM, Lin S, Kraus M, Goold RG, Gordon-Weeks PR (2009) Nonprimed and DYRK1A-primed GSK3 beta-phosphorylation sites on MAP1B regulate microtubule dynamics in growing axons. Journal of cell science 122 (Pt 14):2424-2435. doi:10.1242/jcs.040162

Schaefer MK, Schmalbruch H, Buhler E, Lopez C, Martin N, Guenet JL, Haase G (2007) Progressive motor neuronopathy: a critical role of the tubulin chaperone TBCE in axonal tubulin routing from the Golgi apparatus. The Journal of neuroscience : the official journal of the Society for Neuroscience 27 (33):8779-8789. doi:10.1523/JNEUROSCI.1599-07.2007

Schermelleh L, Heintzmann R, Leonhardt H (2010) A guide to super-resolution fluorescence microscopy. The Journal of cell biology 190 (2):165-175. doi:10.1083/jcb.201002018

Schmalbruch H, Jensen HJ, Bjaerg M, Kamieniecka Z, Kurland L (1991) A new mouse mutant with progressive motor neuronopathy. J Neuropathol Exp Neurol 50 (3):192-204

Schneider CA, Rasband WS, Eliceiri KW (2012) NIH Image to ImageJ: 25 years of image analysis. Nature methods 9 (7):671-675

Schrimpf SP, Meskenaite V, Brunner E, Rutishauser D, Walther P, Eng J, Aebersold R, Sonderegger P (2005) Proteomic analysis of synaptosomes using isotope-coded affinity tags and mass spectrometry. Proteomics 5 (10):2531-2541. doi:10.1002/pmic.200401198

Sellin ME, Holmfeldt P, Stenmark S, Gullberg M (2008) Op18/Stathmin counteracts the activity of overexpressed tubulin-disrupting proteins in a human leukemia cell line. Exp Cell Res 314 (6):1367-1377. doi:10.1016/j.yexcr.2007.12.018

Selvaraj BT, Frank N, Bender FL, Asan E, Sendtner M (2012) Local axonal function of STAT3 rescues axon degeneration in the pmn model of motoneuron disease. The Journal of cell biology 199 (3):437-451. doi:10.1083/jcb.201203109

Sendtner M, Arakawa Y, Stockli KA, Kreutzberg GW, Thoenen H (1991) Effect of ciliary neurotrophic factor (CNTF) on motoneuron survival. J Cell Sci Suppl 15:103-109

Sendtner M, Pei G, Beck M, Schweizer U, Wiese S (2000) Developmental motoneuron cell death and neurotrophic factors. Cell and tissue research 301 (1):71-84

Shih W, Gallusser A, Kirchhausen T (1995) A clathrin-binding site in the hinge of the beta 2 chain of mammalian AP-2 complexes. The Journal of biological chemistry 270 (52):31083-31090

Skarnes WC (2015) Is mouse embryonic stem cell technology obsolete? Genome Biol 16:109. doi:10.1186/s13059-015-0673-6

Skarnes WC, Auerbach BA, Joyner AL (1992) A gene trap approach in mouse embryonic stem cells: the lacZ reported is activated by splicing, reflects endogenous gene expression, and is mutagenic in mice. Genes Dev 6 (6):903-918

Skarnes WC, Rosen B, West AP, Koutsourakis M, Bushell W, Iyer V, Mujica AO, Thomas M, Harrow J, Cox T, Jackson D, Severin J, Biggs P, Fu J, Nefedov M, de Jong PJ, Stewart AF, Bradley A (2011) A conditional knockout resource for the genome-wide study of mouse gene function. Nature 474 (7351):337-342. doi:10.1038/nature10163

Song Y, Brady ST (2015) Post-translational modifications of tubulin: pathways to functional diversity of microtubules. Trends in cell biology 25 (3):125-136. doi:10.1016/j.tcb.2014.10.004

St Pierre SE, Ponting L, Stefancsik R, McQuilton P, FlyBase C (2014) FlyBase 102--advanced approaches to interrogating FlyBase. Nucleic acids research 42 (Database issue):D780-788. doi:10.1093/nar/gkt1092

Stambolic V, Woodgett JR (2006) Functional distinctions of protein kinase B/Akt isoforms defined by their influence on cell migration. Trends in cell biology 16 (9):461-466. doi:10.1016/j.tcb.2006.07.001

Stephens DJ, Lin-Marq N, Pagano A, Pepperkok R, Paccaud JP (2000) COPI-coated ER-to-Golgi transport complexes segregate from COPII in close proximity to ER exit sites. Journal of cell science 113 (Pt 12):2177-2185

Subramanian N, Wetzel A, Dombert B, Yadav P, Havlicek S, Jablonka S, Nassar MA, Blum R, Sendtner M (2012) Role of Na(v)1.9 in activity-dependent axon growth in motoneurons. Human molecular genetics 21 (16):3655-3667. doi:10.1093/hmg/dds195

Takamori S, Rhee JS, Rosenmund C, Jahn R (2000) Identification of a vesicular glutamate transporter that defines a glutamatergic phenotype in neurons. Nature 407 (6801):189-194. doi:10.1038/35025070

Thiel G (1993) Synapsin I, Synapsin II, and Synaptophysin: marker proteins of synaptic vesicles. Brain Pathol 3 (1):87-95

Thomas CC, Dowler S, Deak M, Alessi DR, van Aalten DM (2001) Crystal structure of the phosphatidylinositol 3,4-bisphosphate-binding pleckstrin homology (PH) domain of tandem

PH-domain-containing protein 1 (TAPP1): molecular basis of lipid specificity. The Biochemical journal 358 (Pt 2):287-294

Tian G, Huang MC, Parvari R, Diaz GA, Cowan NJ (2006) Cryptic out-of-frame translational initiation of TBCE rescues tubulin formation in compound heterozygous HRD. Proceedings of the National Academy of Sciences of the United States of America 103 (36):13491-13496. doi:10.1073/pnas.0602798103

Tian G, Huang Y, Rommelaere H, Vandekerckhove J, Ampe C, Cowan NJ (1996) Pathway leading to correctly folded beta-tubulin. Cell 86 (2):287-296

Tian G, Lewis SA, Feierbach B, Stearns T, Rommelaere H, Ampe C, Cowan NJ (1997) Tubulin subunits exist in an activated conformational state generated and maintained by protein cofactors. The Journal of cell biology 138 (4):821-832

Toker A (2012) Achieving specificity in Akt signaling in cancer. Adv Biol Regul 52 (1):78-87. doi:10.1016/j.advenzreg.2011.09.020

Toker A, Marmiroli S (2014) Signaling specificity in the Akt pathway in biology and disease. Adv Biol Regul 55:28-38. doi:10.1016/j.jbior.2014.04.001

Tong J, Huang C, Bi F, Wu Q, Huang B, Zhou H (2012) XBP1 depletion precedes ubiquitin aggregation and Golgi fragmentation in TDP-43 transgenic rats. Journal of neurochemistry 123 (3):406-416. doi:10.1111/jnc.12014

Traub LM, Kornfeld S (1997) The trans-Golgi network: a late secretory sorting station. Current opinion in cell biology 9 (4):527-533

Tschopp O, Yang ZZ, Brodbeck D, Dummler BA, Hemmings-Mieszczak M, Watanabe T, Michaelis T, Frahm J, Hemmings BA (2005) Essential role of protein kinase B gamma (PKB gamma/Akt3) in postnatal brain development but not in glucose homeostasis. Development 132 (13):2943-2954. doi:10.1242/dev.01864

van Dis V, Kuijpers M, Haasdijk ED, Teuling E, Oakes SA, Hoogenraad CC, Jaarsma D (2014) Golgi fragmentation precedes neuromuscular denervation and is associated with endosome abnormalities in SOD1-ALS mouse motor neurons. Acta neuropathologica communications 2:38. doi:10.1186/2051-5960-2-38

Varadaraj K, Skinner DM (1994) Denaturants or cosolvents improve the specificity of PCR amplification of a G + C-rich DNA using genetically engineered DNA polymerases. Gene 140 (1):1-5

Vlug AS, Teuling E, Haasdijk ED, French P, Hoogenraad CC, Jaarsma D (2005) ATF3 expression precedes death of spinal motoneurons in amyotrophic lateral sclerosis-SOD1 transgenic mice and correlates with c-Jun phosphorylation, CHOP expression, somato-dendritic ubiquitination and Golgi fragmentation. The European journal of neuroscience 22 (8):1881-1894. doi:10.1111/j.1460-9568.2005.04389.x

Wang Q, Liu L, Pei L, Ju W, Ahmadian G, Lu J, Wang Y, Liu F, Wang YT (2003) Control of synaptic strength, a novel function of Akt. Neuron 38 (6):915-928

Wang X, Huang T, Bu G, Xu H (2014) Dysregulation of protein trafficking in neurodegeneration. Mol Neurodegener 9:31. doi:10.1186/1750-1326-9-31

Webster DR, Gundersen GG, Bulinski JC, Borisy GG (1987) Assembly and turnover of detyrosinated tubulin in vivo. The Journal of cell biology 105 (1):265-276

Wiedenmann B, Franke WW (1985) Identification and localization of Synaptophysin, an integral membrane glycoprotein of Mr 38,000 characteristic of presynaptic vesicles. Cell 41 (3):1017-1028

Wiese S, Herrmann T, Drepper C, Jablonka S, Funk N, Klausmeyer A, Rogers ML, Rush R, Sendtner M (2010) Isolation and enrichment of embryonic mouse motoneurons from the lumbar spinal cord of individual mouse embryos. Nature protocols 5 (1):31-38. doi:10.1038/nprot.2009.193

Yamada KM, Spooner BS, Wessells NK (1970) Axon growth: roles of microfilaments and microtubules. Proceedings of the National Academy of Sciences of the United States of America 66 (4):1206-1212

Yang L, Zhang H, Bruce JE (2009) Optimizing the detergent concentration conditions for immunoprecipitation (IP) coupled with LC-MS/MS identification of interacting proteins. Analyst 134 (4):755-762. doi:10.1039/b813335b

Yao Y, Suraokar M, Darnay BG, Hollier BG, Shaiken TE, Asano T, Chen CH, Chang BH, Lu Y, Mills GB, Sarbassov D, Mani SA, Abbruzzese JL, Reddy SA (2013) BSTA promotes mTORC2-mediated phosphorylation of Akt1 to suppress expression of FoxC2 and stimulate adipocyte differentiation. Science signaling 6 (257):ra2. doi:10.1126/scisignal.2003295

Yoshihisa T, Barlowe C, Schekman R (1993) Requirement for a GTPase-activating protein in vesicle budding from the endoplasmic reticulum. Science 259 (5100):1466-1468

Zhou H, Li X, Wu Q, Li F, Fu Z, Liu C, Liang Z, Chu T, Wang T, Lu L, Ning G, Kong X, Feng S (2015) shRNA against PTEN promotes neurite outgrowth of cortical neurons and functional recovery in spinal cord contusion rats. Regenerative medicine 10 (4):411-429. doi:10.2217/rme.14.88

Zlatic SA, Ryder PV, Salazar G, Faundez V (2010) Isolation of labile multi-protein complexes by in vivo controlled cellular cross-linking and immuno-magnetic affinity chromatography. J Vis Exp (37). doi:10.3791/1855

Znamensky V, Akama KT, McEwen BS, Milner TA (2003) Estrogen levels regulate the subcellular distribution of phosphorylated Akt in hippocampal CA1 dendrites. The Journal of neuroscience : the official journal of the Society for Neuroscience 23 (6):2340-2347

6. Appendix

6.1 Syap1 overexpression vector

N-terminally FLAG-tagged Syap1 was cloned into the pGJ3 overexpression vector under the SFFV promoter.

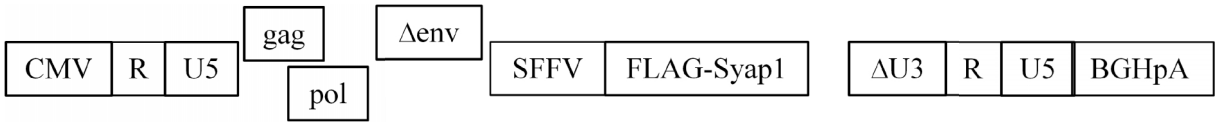

Figure 49: FLAG-Syap1 pGJ3 overexpression vector

6.2 Genotyping and qRT-PCR primer sequences

Gene	Forward primer	Reverse primer
gapdh	GCAAATTCAACGGCACA	CACCAGTAGACTCCACGAC
Syap1 (Exon 3-4)	GATGTACCCTGTTGCCCTGG	GCTTAATCAGGGAGATTCGGTAGA
Syap1 (Exon 3-4)	GATGTACCCTGTTGCCCTGG	GCTTAATCAGGGAGATTCGGTAGA
Syap1 (Exon 8-9)	CGATACGTGCAGCTTAAATCA	TGTAGCTCCTTTTCCCAATCA
Syap1 wild type	ACATACACACATGTGTACCACTTT	ACAAGACCACAATTGCAATTTACC
Syap1 knockout	ACATACACACATGTGTACCACTTT	GTCCCCCTTCCTATGTAACC

Table 8: Genotyping and qRT-PCR primer sequences

6.3 Nuclear/cytosolic fractionation of NSC34 cells

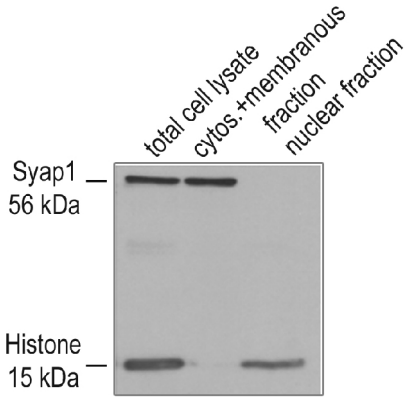

Figure 50: Crude nuclear/cytosolic fractionation of NSC34 cells

NSC34 cells were subjected to a fast and easy fractionation in order to study the presence of Syap1 in the nucleus. Therefore, the cells were washed once with PBS and lysed in 50 mM Tris-HCl (pH 7.5), 0.5% Triton X-100, 137.5 mM NaCl, 10% Glycerol and protease inhibitors (Protease inhibitor cocktail tablet, Roche, 04693159001) followed by one centrifugation step at 1,000 rcf for 10 minutes at 4°C. The supernatant, containing cytosolic and membranous proteins, was transferred to a new tube. The pellet was resuspendet in the same amount of lysis buffer than the obtained supernatant. Equal amounts of Laemmli buffer were added to both fractions and samples subjected to Western blot analysis. This experiment showed, that Syap1 is found in the fraction containing cytosolic and membranous proteins but not in the nuclear fraction (indicated by Histone).

6.4 sh-Syap1 sequence BLAST

Sequences producing significant alignments:

Select: All None Selected:0

Alignments Download GenBank Graphics Distance tree of results

Description	Max score	Total score	Query cover	E value	Ident	Accession
Transcripts						
Mus musculus synapse associated protein 1 (Syap1), mRNA	38.2	38.2	100%	0.028	100%	NM_025932.2
Mus musculus DCN1, defective in cullin neddylation 1, domain containing 3 (S. cerevisiae) (Dcun1d3), transcript variant 2, mRNA	28.2	28.2	73%	27	100%	NM_001163703.1
Mus musculus DCN1, defective in cullin neddylation 1, domain containing 3 (S. cerevisiae) (Dcun1d3), transcript variant 1, mRNA	28.2	28.2	73%	27	100%	NM_173408.3
Mus musculus platelet derived growth factor receptor, alpha polypeptide (Pdgfra), transcript variant 1, mRNA	28.2	28.2	94%	27	94%	NM_011058.2
Mus musculus platelet derived growth factor receptor, alpha polypeptide (Pdgfra), transcript variant 2, mRNA	28.2	28.2	94%	27	94%	NM_001083316.1
Mus musculus WD repeat domain 77 (Wdr77), mRNA	28.2	28.2	73%	27	100%	NM_027432.3
Mus musculus adaptor-related protein complex 3, sigma 2 subunit (Ap3s2), mRNA	28.2	28.2	73%	27	100%	NM_009682.3
Mus musculus predicted gene 12925 (Gm12925), long non-coding RNA	26.3	26.3	68%	108	100%	NR_136925.1
Mus musculus tudor domain containing 5 (Tdrd5), transcript variant 2, mRNA	26.3	26.3	68%	108	100%	NM_001277730.1
Mus musculus maltase-glucoamylase (Mgam), mRNA	26.3	26.3	68%	108	100%	NM_001171003.1
Mus musculus PTPRF interacting protein, binding protein 1 (liprin beta 1) (Ppfibp1), transcript variant 1, mRNA	26.3	26.3	68%	108	100%	NM_001170433.1
Mus musculus PTPRF interacting protein, binding protein 1 (liprin beta 1) (Ppfibp1), transcript variant 2, mRNA	26.3	26.3	68%	108	100%	NM_026221.2
Mus musculus RIKEN cDNA 4931428F04 gene (4931428F04Rik), transcript variant 2, mRNA	26.3	26.3	89%	108	94%	NM_001166394.1
Mus musculus RIKEN cDNA 4931428F04 gene (4931428F04Rik), transcript variant 1, mRNA	26.3	26.3	89%	108	94%	NM_028888.2
Mus musculus Src-like-adaptor 2 (Sla2), mRNA	26.3	26.3	68%	108	100%	NM_029983.5
Mus musculus centrosomal protein 83, opposite strand (Cep83os), long non-coding RNA	26.3	26.3	68%	108	100%	NR_015524.1
Mus musculus integrin beta 6 (Itgb6), transcript variant 1, mRNA	26.3	26.3	68%	108	100%	NM_001159564.1
Mus musculus integrin beta 6 (Itgb6), transcript variant 2, mRNA	26.3	26.3	68%	108	100%	NM_021359.3
Mus musculus mex3 RNA binding family member B (Mex3b), mRNA	26.3	26.3	68%	108	100%	NM_175366.3
Mus musculus La ribonucleoprotein domain family, member 1 (Larp1), mRNA	26.3	26.3	89%	108	94%	NM_028451.1
Mus musculus RIKEN cDNA 1110008F13 gene (1110008F13Rik), mRNA	26.3	26.3	68%	108	100%	NM_026124.3
Mus musculus tudor domain containing 5 (Tdrd5), transcript variant 1, mRNA	26.3	26.3	68%	108	100%	NM_001134741.1
Mus musculus diacylglycerol kinase, gamma (Dgkg), mRNA	26.3	26.3	68%	108	100%	NM_138650.2
Mus musculus kinesin family member 4 (Kif4), mRNA	26.3	26.3	68%	108	100%	NM_008446.2
Mus musculus tetratricopeptide repeat domain 12 (Ttc12), mRNA	26.3	26.3	68%	108	100%	NM_172770.3
Mus musculus nucleolar protein 3 (apoptosis repressor with CARD domain) (Nol3), mRNA	26.3	26.3	89%	108	94%	NM_030152.4
Mus musculus zinc finger protein 335 (Zfp335), mRNA	26.3	26.3	68%	108	100%	NM_199027.2
Mus musculus PARK2 co-regulated-like (Pacrgl), mRNA	26.3	26.3	68%	108	100%	NM_025755.3
Mus musculus proteasome (prosome, macropain) activator subunit 4 (Psme4), mRNA	26.3	26.3	68%	108	100%	NM_134013.3

Figure 51: Nucleotide BLAST of sh-Syap1 sequence
sh-Syap1 sequence (GAG ACA ATT CAA CAG CAG A)

Affidavit

I hereby confirm that my thesis entitled "Initial characterization of mouse Syap1 in the nervous system: Search for interaction partners, effects of gene knockdown and knockout, and tissue distribution with focus on the adult brain" is the result of my own work. I did not receive any help or support from commercial consultants. All sources and / or materials applied are listed and specified in the thesis.

Furthermore, I confirm that this thesis has not yet been submitted as part of another examination process neither in identical nor in similar form.

Würzburg, _____ _____

Place, Date Signature

Eidesstattliche Erklärung

Hiermit erkläre ich an Eides statt, die Dissertation mit dem Titel "Erste Charakterisierung des Maus-Syap1 im Nervensystem: Suche nach Interaktionspartnern, Auswirkungen von Gen -Knockdown und -Knockout sowie Untersuchungen über die Verteilung im Gewebe mit Fokus auf das adulte Gehirn" eigenständig, d.h. insbesondere selbständig und ohne Hilfe eines kommerziellen Promotionsberaters, angefertigt und keine anderen als die von mir angegebenen Quellen und Hilfsmittel verwendet zu haben.

Ich erkläre außerdem, dass die Dissertation weder in gleicher noch in ähnlicher Form bereits in einem anderen Prüfungsverfahren vorgelegen hat.

Würzburg, _____ _____

Ort, Datum Unterschrift

Curriculum vitae

Publication:

Schmitt, D., Funk, N., Blum, R. Asan A., Andersen L., Rülicke T., Sendtner M., Buchner E., Histochem Cell Biol (2016) Initial characterization of a *Syap1* knock-out mouse and distribution of Syap1 in mouse brain and cultured motoneurons, 146: 489. doi:10.1007/s00418-016-1457-0

Poster presentations:

Schmitt D., Sevaraj BT., Funk N., Buchner E., Sendtner M., (2012) Characterization of murine Synapse-associated protein 1 - homologue of *Drosophila* SAP47. 7. Internationales Symposium der Graduiertenschule im Bereich Biowissenschaften (Life Sciences)

Schmitt D., Sevaraj BT., Funk N., Buchner E., Sendtner M., (2013) Tubulin-specific chaperone E (TBCE) interacts with synapse-associated protein 1 (Syap1): Potential relevance for motoneuron disease. 8. Internationales Symposium der Graduiertenschule im Bereich Biowissenschaften (Life Sciences)

Schmitt D., Buchner E., Sendtner M., (20143) Initial characterization and localization of Syap1 protein in primary motoneurons and the mouse nervous system. 9. Internationales Symposium der Graduiertenschule im Bereich Biowissenschaften (Life Sciences)

Acknowledgements